Graphene and carbon nanotube biosensors for detection of human chorionic gonadotropin.

Teixeira, Sofia

Graphene and Carbon Nanotube biosensors for detection of human chorionic gonadotropin

Sofia Teixeira

Submitted to Swansea University in fulfilment of the requirements for the degree of Doctor of Philosophy

Swansea University, 2014

To my parents and my lovely sister

Acknowledgments

I would like to express the most sincere gratitude to my supervisor, Doctor Owen Guy, for giving me this opportunity to further my education and for the valuable lessons passed down over the last few years.

A special thanks to Doctor Steve Conlan for being so kind, professional and helpful.

I would like to thank all of the students and staff at Swansea University that have made this PhD not only possible, but so enjoyable.

I would like to express my sincere and full gratitude to all people that direct or indirectly helped me in the course of this PhD, you know who you are!

A special thanks to Doctor Deya Gonzalez for being so kind, professional and helpful.

A special thanks to Chris Williams from IgInnovations.

I would like to gratefully acknowledge Doctor Goreti Sales for the opportunity she gave me to do research, for all her guidance, support, pertinent advices, endless encouragement, and for all interesting scientific discussions and constructive suggestions that allowed me to see science in a better way. It was a great privilege and honour for me to learn from her great scientific knowledge.

A special thank goes to my colleagues and friends for their many valuable discussions, support and mainly for your constant willingness and hilarious moments in coffee breaks.

To all the BioMark people, for their support, friendship, help and the fun moments shared.

I would like to acknowledge CNH, BioMark and Swansea University for the facilities to support this work, without this research would not be possible.

Finally, I would like to express my gratitude to all my friends and family, for their great support, advice, motivation, encouragement, understanding, unconditional friendship and specially for believing in me. I am truly thankful for all their prompt help whenever I needed it, and without which I would not have come this far.

This work is part-funded by the European Social Fund (ESF) through the European Union's Convergence programme administered by the Welsh Government.

THANK YOU ALL!

Abstract

Graphene is essentially a monolayer of sp^2 bonded carbon atoms, arranged in a honeycomb lattice. Graphene has in recent years attracted phenomenal interest from researchers in materials science, condensed matter physics, and electronics since its first demonstration in 2004. The importance of graphene research was epitomised by the Nobel prize for physics being awarded to pioneers of the field in 2010.

The main topic of this research was the development of epitaxial graphene on silicon carbide (SiC) substrates. The substrate inferred processability of epitaxial graphene enables graphene devices to be fabricated on full wafers using standard semiconductor processing techniques.

Biosensor research is a rapidly expanding field. The major driver comes from the healthcare industry but there are also applications for biosensors in the food quality appraisal and environmental monitoring industries. The key advantages of electrochemical biosensors over competing sensor technologies are the low cost of mass production, and ability to make sensors into small compact systems. Smaller, portable sensors allow for the development of point-of-care medical devices, which can be crucial in fast diagnosis and long-term monitoring of diseases.

Graphene channel resistor devices have been fabricated using electron beam lithography and a successfully developed contact metallisation scheme – using Titanium / Gold contacts. The metal-graphene contacts have been characterised using XPS and electrical current-voltage measurements.

The graphene channel device has been used as the basis of an electrochemical sensor for human chorionic gonadotropin (hCG), an indicator of pregnancy – which has also been linked to increased risk of several cancers.

The immunosensor developed is a promising tool for point-of-care detection of hCG, due to its excellent detection capability, simplicity of fabrication, low-cost, high sensitivity and selectivity.

Keywords

Immunosensor; Graphene; Carbon Nanotube; Antibody; human chorionic gonadotropin.

"To know, is to know that you know nothing.

That is the meaning of true knowledge"

Socrates

Table of Contents

List of Figures

List of Tables

Symbols

C_{dl}	Capacitance of the double layer
R_{ct}	Charge transfer resistance
R_s	Resistance of the solution phase
W	Warburg diffusion element
Z`	Imaginary component of impedance
Z``	Warburg impedance
Λ	Quantitative measure of the reversibility
ω	Angular frequency
ϕ	Phase angle

Abbreviations

AMP	Amperometry
Ab	Antibody
AFM	Atomic Force Microscopy
ATR	Attenuated Total Reflectance
AOPs	Advanced oxidation processes
AuNPs	Gold nanoparticles
AP	Alkaline phosphatase
APS	Aminopropylsilane
APTES	3-aminopropyltrimethoxy-silane
BSA	Bovine Serum Albumin
CAP	Capacitance
CNTs	Carbon nanotubes
CS	Chitosan
CV	Cyclic voltammetry
DPV	Differential pulse voltammetry
dsDNA	Double stranded DNA
EDC/EDAC	N-(3-dimethylaminopropyl)-N'-ethylcarbodiimide

ELISA	Enzyme-linked immunosorbent assay
EIS	Electrochemical Impedance Spectroscopy
EBL	Electron beam lithography
E-LUM	Electrochemiluminescence
F_c	Fragment crystallisable region
F_{ab}	Fragment antigen-binding
FRA	Frequency Response Analysis
FSH	Follicle stimulating hormone
FTIR	Fourier transform infrared spectroscopy
GA	Glutaraldehyde
GCE	Glassy carbon electrode
G-FET	Graphene Field-Effect Transistor
GPMS	Glycidoxypropyltrimethoxysilane
hCG	Human chorionic gonadotrophin
HRP	Horseradish peroxidase
HF	Hydrochloric acid
Hb	Hemoglobin
HQ	Hydroquinone
ITO	Indium Tin Oxide

IRMA	Immunoradiometric assays
LOD	Limit of detection
LUM	Chemiluminescence
MIBK	Methyl isobutyl ketone
MWCNT	Multiwall carbon nanotubes
MLG	Multilayer graphene
NHS	N-hydroxysuccinimide
NPG	Nanoporous gold
NPs	Nanoparticles
PANI	Polyaniline
POC	Point-of-Care
PB	Prussian blue
PBS	Phosphate Buffered Saline
PDA	*o*-phenylenediamine
PDDA	Poly(diallyldimethylammonium chloride)
PDMS	Poly(dimethylsiloxane)
PMMA	Polymethyl methacrylate
PEG	Polyethylene glycol
PPy-Ppa	Copolymer of pyrrole and pyrole-2-carboxylic acid

PVD	Physical Vapour Deposition
QCM	Quartz-crystal microbalance
QD	Quantum dot
RCA	Standard clean
RIE	Reactive Ion etching
RTA	Rapid Thermal Annealing
Ru(bpy)3	Tris(bipyridine)ruthenium(II)
SEM	Scanning Electron Microscopy
SiNW	Silicon nanowires
SiC	Silicon carbide
SPD	Diffraction of surface plasmon
SPE	Screen-Printed Electrode
SPDP	Succinimidyl-6-[3'-(2-pyridyldithio)-propionamido] hexanoate
SPTE	(3-Mercaptopropyl)-trimethoxysilane silane
SWV	Square-wave voltammetry
SWSV	Square-wave stripping voltammetry
TB	Toluidine blue
t-BOC	Di-tert-butyl dicarbonate
TEOS	Tetraethyoxysilane

TFA	Trifluoroacetic acid
TH	Thionine
TPA	Triproprylamine
UV	Ultraviolet
XPS	X-ray photoelectron spectroscopy

CHAPTER 1

"Education is the most powerful weapon
which you can use to change the world."
Nelson Mandela (1918-2013), South African Politician

Framework

1.1 Motivation

Nanotechnology has become an increasingly popular buzzword over the past 15 years or so, a trend that has been fueled by a global set of publicly funded nanotechnology initiatives. Even as researchers have been struggling to demonstrate some of the most fundamental and simple aspects of this field, the term nanotechnology has entered into the public consciousness through articles in the popular press and popular fiction. As a consequence, the expectations of the public are high for nanotechnology, even while the actual public definition of nanotechnology remains a bit fuzzy.

Nanotechnology is the ability to manipulate individual atoms and molecules to produce nanostructured materials and submicron objects that have applications in the real world. Nanotechnology involves the production and application of physical, chemical and biological systems at scales ranging from individual atoms or molecules to about 100 nm, as well as the integration of the resulting nanostructures into larger systems. Nanotechnology is likely to have a profound impact on our economy and society in the early 21st century, perhaps comparable to that of information technology or cellular and molecular biology. Science and engineering research in nanotechnology promises breakthroughs in areas such as materials and manufacturing, electronics, medicine and healthcare, energy and the environment, biotechnology, information technology and national security. Clinical trials are already underway for nanomaterials that offer the promise of cures for certain cancers. It is widely felt that nanotechnology will be the next industrial revolution.

1.2 Structure of the thesis

This thesis is organized in eight chapters.

Chapter 1 outlines the motivation of this work, describes the structure and the framework of the thesis, and lists of publications and communications associated with the PhD.

Chapter 2 presents a literature review about the principal concepts of this work.

Chapter 3 presents the experimental methods of the production and characterization techniques used during the research work of this dissertation, highlighting the graphene growth, the characterization techniques for the nanofabrication of the devices and electrochemical characterization of the devices.

Chapters 4 to 7, present the development, characterization and application of electrochemical assays detection of the hormone biomarker hCG.

Chapter 4 describes the use of lithographic techniques to pattern epitaxial graphene devices, whose dimensions are scalable and suitable for wafer scale production. Epitaxial graphene devices have been functionalized using (3-Aminopropyl)triethoxysilane (APTES), to achieve an amine terminated graphene surface. Antibodies targeted against hCG have been bound to the amine-terminated graphene. This sensor was operational but improvement of the electrochemistry became necessary for enhanced sensor performance.

Chapter 5, an immunosensor with a Chitosan layer incorporating gold nanoparticles, able to be functionalized with the anti-hCG for subsequent detection of hCG is described.

Chapter 6 a new impedimetric biosensor for hCG fabricated, based on antibody–antigen binding to a PANI-modified screen-printed graphene electrode, was developed. It was shown that polyaniline was successfully deposited on a graphene-SPE. The simple approach for antibody binding, enabled attachment of the antibody to the sensing layer, and provided excellent reproducibility and stability in the sensor. The sensor's electrode impedance, increased linearly with increasing hCG protein concentration and was not significantly affected by interference from chemical components present in synthetic urine.

Chapter 7, an immunosensor set-up, where the antibody has been directly attached to a CNT amine-modified layer, on a screen-printed electrode, was developed and investigated using electrochemical impedance spectroscopy (EIS) label-free measurements. This sensor had a clinically relevant limit of detection of 0.01ng/mL.

Chapter 8 summarizes the main results obtained and presents guidelines for future research work.

1.3 List of Publications

The main results obtained during this dissertation were presented in some international conferences and published in peer-reviewed publications.

1.3.1 Papers published in international scientific journals

1. Sofia Teixeira, G. Burwell, A. Castaing, D. Gonzalez, R.S. Conlan, O.J. Guy, Epitaxial graphene immunosensor for human chorionic gonadotropin, Sensors and Actuators B, 2014, 190, 723–729.

2. Sofia Teixeira, Robert Steven Conlan, O. J. Guy, M. Goreti F. Sales, Label-free human chorionic gonadotropin detection at picogram levels using oriented antibodies bound to graphene screen printed electrodes, Journal of Materials Chemistry B, 2014, 2,1852-1865.

3. Gregory Burwell, Sofia Teixeira, Ambroise Castaing, Owen Guy, Synthesis and characterization of (3-aminopropyl)triethoxysilanemodified epitaxial graphene, Proceedings of Hetero-SIC-WASMPE13, accepted.

4. Sofia Teixeira, Robert Steven Conlan, O. J. Guy, M. Goreti F. Sales, SWCNT Screen-printed electrode as an immunosensor for human chorionic gonadotropin, Electrochimica Acta, submitted on February 2014.

1.3.2. Communications presented in international scientific conferences

1. Teixeira, S., Burwell, G., Castaing, A., Conlan, R. S., Guy, O.J., "Graphene biosensor for hCG pregnancy biomarker", oral communication presented at the 5th International workshop on biosensors for food safety and environmental monitoring, Ouarzazate, Morocco, 2011.

2. Teixeira, S., Burwell, G., Castaing, A., Conlan, R. S., Guy, O.J., "Development of nano-channel devices for antibody detection", poster presentation at Multidisciplinary Nanotechnology Centre (MNC), Swansea, UK, 2012.

3. Teixeira, S., "Graphene biosensors for detection of diseases biomarkers", oral communication presented at the 6th International meeting on development in materials, processes and applications of emerging technologies (MPA 2012), Alvor, Portugal, 2012.

4. Teixeira, S., Burwell, G., Castaing, A., Conlan, R. S., Guy, O.J., "Graphene biosensor for detection of hCG biomarker", poster presentation at NanoPT 2013 International conference, Porto, Portugal, 2013.

5. Teixeira, S., Castaing, A., Burwell, G., Conlan, R.S., Guy. O.J., "Graphene biosensor for detection of hCG biomarker" oral communication presented at Imaginenano2013, Bilbao, Spain, 2013.

6. Owen Guy, Sofia Teixeira, Gregory Burwell, "Synthesis and characterization of (3-aminopropyl)triethoxysilane- modified epitaxial graphene" oral communication presented at HeteroSiC-WASMPE, Nice, France, 2013.

CHAPTER 2

"Anybody who has been seriously engaged in scientific work of any kind realizes that over the entrance to the gates of the temple of science are written the words: We must have faith. It is a quality which the scientist cannot dispense with."

Max Planck (1858-1947), German Theoretical Physicist

Literature Review

In this chapter a fundamental background regarding the functioning principles of biosensors, field effect based devices and electrochemical sensors are provided. A brief overview of graphene and CNT materials are given.

To set the context for this research, it is important to understand the application for the biosensors being developed.

Detection of the biomarker hCG is important in establishing whether a woman is pregnant. hCG is also becoming increasingly important as a marker for several cancers. Both pregnancy and cancer, and the role of hCG in these conditions, are discussed at the outset of this chapter.

2.1 Pregnancy and hCG

Pregnancy is the fertilization and development of one or more offspring, known as an embryo or fetus, in a woman's uterus. In a pregnancy, there can be multiple gestations, as in the case of twins or triplets. Childbirth usually occurs about 38 weeks after conception; in women who have a menstrual cycle length of four weeks, this is approximately 40 weeks from the start of the last normal menstrual period (LNMP). Human pregnancy is the most studied of all mammalian pregnancies. Conception can be achieved through sexual intercourse or assisted reproductive technology.

human chorionic gonadotropin (hCG) has always been thought of as one molecule, a hormone which promotes progesterone production. The last 20 years has seen big changes in this concept: hCG has been shown to comprise 3 independent molecules and not one. All 3 have a common β-subunit peptide structure (has a highly glycosylated carboxyl terminal peptide (CTP) extension, rich in serine and proline, which confers the immunological and biological specificity to the whole hCG) and the name hCG has remained attached to all three molecules. These are: (i) hCG, which has been shown to have multiple functions extending way beyond promoting progesterone production by corpus luteal cells [1]; (ii) hyperglycosylated hCG (hCG-H), a major glycosylation variant of hCG which has a different 3 dimensional structure and is also produced by placenta. hCG-H has critical functions in invasion and growth of choriocarcinoma cells and implantation of pregnancy [1]. (iii) hCG free β-subunit is produced by most human cancers. It promotes cancer cell growth and malignancy.

Human chorionic gonadotropin (hCG) is a kind of glycoprotein hormone with a molecular mass of about 37 kDa, secreted by the trophoblastic cells of the placenta chorionic vesicle [2]. In healthy human serum and urine, the concentration of hCG is extremely low. The increased level of hCG in serum and urine is associated with the trophoblastic cancer and many diseases related to pregnancy [3]. Levels can first be detected by a blood test about 11 days after conception and about 12 - 14 days after conception by a urine test. In general the hCG levels will double every 72 hours. The level will reach its peak in the first 8 – 11 weeks of pregnancy and then will decline and level off for the remainder of the pregnancy. There is really no single "normal" hCG level in early pregnancy and there is a very wide range of hCG values as pregnancy progresses.

The hCG hormone is measured in milli-international units per milliliter (mIU/ml).

Table 2.1 - hCG levels in weeks from last menstrual period.

Weeks	Level of hCG (mIU/mL)	Level of hCG (ng/mL)
3	5 - 50	1 - 10
4	5 - 426	1 – 85.2
5	18 - 7.340	3.6 - 1468
6	1.080 - 56.500	216 - 11300
7 - 8	7.650 - 229.000	1530 - 45800
9 - 12	25.700 - 288.000	5140 - 57600
13 - 16	13.300 - 254.000	2660 - 50800
17 - 24	4.060 - 165.400	812 - 33080
25 - 40	3.640 - 117.000	728 – 23400
Non-pregnant females	< 5.0	<1
Postmenopausal females	< 9.5	<1.9

Thus, it is necessary to measure hCG in all modern immunological pregnancy tests and even early monitoring of trophoblastic diseases [4-6]. Amperometric immunosensors seem to be excellent candidates for the quantification of immunological moieties in clinical samples, displaying a low detection limit and high sensitivity, and employing the innate amplification properties of enzymes. Recently, several amperometric immunosensors for hCG have been reported [7,8]. In the amperometric immunosensor, since most antibody and antigen are intrinsically unable to act as redox partners, the entrapment of an enzyme mediator onto the electrode has been used to improve the sensitivity of the immunoassay [9-11].

Immunosensors for hCG presented in literature are summarised in the following Tables. Table 2.1 presents graphene-based immunosensors; Table 2.2 presents labelled-free immunosensors and Table 2.3 presents immunosensors employing chemical labels, the most complex processes presented in the literature. Antibody binding type is also presented. Almost all previous works give no importance to binding the antibody randomly [12]. Some other studies use an amine function for this purpose, which means that the antibody in linked upside-down [13]. Only a few reports use specific proteins that show special affinity to the fragment crystallisable region (F_c) terminal antibody sites ensuring that suitable orientation is achieved [14].

Table 2.2 - Graphene-based immunosensors for hCG.

Electrode support	Immunosensor design	Additional nanomaterial	Detection		Response to hCG Concentration	Antibody Binding	Ref.
			Sequential process	Technique			
Glassy carbon	GCE sequentially modified with graphene, MWCNTs and Au-NPs and after bound to anti-HCG by physical adsorption. BSA blocked non-specific binding.	Mesoporous silica NPs (MCM-41) decorated with TH, AuNPs, and finally HRP-labeled anti-hCG	1) incubation in hCG 2) incubation in nanomaterial 3) solution of H_2O_2	DPV	*LR:* 0.005–500 mIU/mL *LOD:* 0.0026 mIU/mL	Random	15
	A GCE was modified by casting a mixture of TH/graphene solution and binding anti-hCG through GA reaction. BSA blocked non-specific binding.	Amined mesoporous silica NPs were modified with Pt. HRP and anti-hCG were bound next by GA linking.	1) incubation in hCG 2) incubation in nanomaterial 3) solution of H_2O_2	AMP	LR: 0.01–12 ng/mL LOD: 7.50 pg/mL	Random	16
	GCE modified by casting (1) sulfonated graphene mixed with TH acting as electron transfer mediator and (2) mesoporous silica (SBA-15) modified by amination with APTES, then added of Pd and finally bound to anti-hCG by GA linking.	—	1) incubation in hCG 2) PBS solution	AMP	*LR:* 0.01–16.00 ng/mL *LOD:* 8.60 pg/mL	Random	17
	A GCE was modified with graphene oxide and NPG foils. Anti-hCG was added and immobilized by physical adsorption. BSA blocked non-specific binding.	—	1) incubation in hCG 2) coating with Nafion 3) PBS solution	AMP	LR: 0.5–40.00 ng/mL LOD: 0.034 ng/mL	Random	18
Graphene	Graphene was casted with polyaniline film (by electropolymerization) and added to anti-hCG modified by EDAC/NHS chemistry. BSA blocked non-specific binding.	—	1) incubation in hCG 2) Iron redox probe	EIS	LR: 0.001–50 ng/mL LOD: 0.286 pg/mL	Via -COOH	19

AMP: amperometry; AP: alkaline phosphatase; APTES: 3-aminopropyltrimethoxy-silane; DPV: Differential pulse voltammetry; EDAC: N-(3-dimethylaminopropyl)-N'-ethylcarbodiimide; EIS: Electrochemical Impedance Spectroscopy; EIS: Electrochemical Impedance Spectroscopy; GA: glutaraldehyde; GCE: glassy carbon electrode; GPMS: glycidoxypropyltrimethoxysilane; HRP: horseradish peroxidase; MWCNT: multiwall carbon nanotubes; NHS: N-hydroxysuccinimide; NPG: nanoporous gold; NPs: nanoparticles; NPs: nanoparticles; SPDP: succinimidyl-6-[3'-(2-pyridyldithio)-propionamido] hexanoate; TH: thionine.

Table 2.3 – Label-free immunosensors for hCG.

Electrode support	Immunosensor design	Detection		Response to hCG Concentration	Antibody Binding	Ref.
		Sequential process	Technique			
Glassy carbon	A GCE was modified by electrodeposition of a composite of MWCNTs and CS. Then TH was bound via GA linkage and the free amino groups of the composite were used to adsorb AuNPs–TiO_2 that was previously linked to anti-hCG. BSA blocked non-specific binding.	1) incubation in hCG 2) PBS solution	AMP	LR: 0.2–300 mIU/mL LOD: 0.08 mIU/mL	Random	20
	Anti-hCG was casted on a GCE. This layer was in contact with saturated titanium isopropoxide vapor to allow the slow formation of a titania sol–gel membrane.	1) HRP labeled 2) PBS solution	AMP	LR: 2.5–12.5 mIU/mL LOD: 1.4 mIU/mL	Random	21
	A GCE was modified with a composite of poly-(2,6-pyridinediamine) and MWNTs. Au-NPs were bound to this film and the anti-hCG was added next. BSA blocked non-specific binding.	1) incubation in hCG 2) PBS solution	AMP	LR: 1.0–10.0 mIU/mL or 10.0–160.0 mIU/mL LOD: 0.3 mIU/mL	Random	22
	A composite of Ag, CS and TiO_2 was prepared and casted over a GCE. Pt hollow nanospheres were casted over the composite layer. Anti-hCG was incubated on this. BSA blocked non-specific binding.	1) incubation in hCG 2) PBS solution	AMP	LR: 0.5–250 mIU/mL LOD: 0.26 mIU/mL	Random	23
	dsDNA was dispersed in MWCNTs was after casted onto a GCE. MB and Au-NPs were adsorbed to this surface and anti/hCG was bound next to the gold surface.	1) incubation in hCG 2) —	AMP	LR: 0.1–10.0 mIU/mL or 10.0–125.0 mIU/mL LOD: 0.04 mIU/mL	Random	24
	GCE was modified with thioureia by electrodeposition. Then *n* replicates of (Au-NPs / MB) monolayers were formed by alternated casting. Finally, anti-hCG was bound by adsorption and non-specific binding blocked by BSA.	1) incubation in hCG 2) PBS solution	CV	LR: 1–100 mIU/mL LOD: 0.3 mIU/mL	Random	25
	GCE was subsequently modified with **boiled** HNO_3 and GPMS. This was followed by **anti-hCG covalent binding via an amine group**. Non-specific binding was blocked with BSA.	1) incubation in hCG 2) PBS solution	CAP	LR: **18–450 mIU/mL** LOD: 5 mIU/mL	Via -NH_2	26
	Anti-hCG labelled with HRP was absorbed on Au-NPs and casted on a GCE. The surface was then encapsulated in sol-gel membrane by contact with titanium isopropoxide. Non-specific binding was blocked with BSA.	1) incubation in hCG 2) PBS solution	DPV	LR: 0.5 to 5.0 mIU/mL or 5.0 to 30 mIU/mL	Random	27

				LOD: 0.3 mIU/mL		
	A GCE electrode was modified by layer-by-layer technology, applying successively MWNT-CS, Hb, TB, nanogold, anti-hCG. Hb blocked non-specific binding.	1) incubation in hCG 2) solution of H_2O_2	AMP	LR: 0.8–500 mIU/mL LOD: 0.3 mIU/mL	Random	28
	Pt–Au alloy nanotubes was produced on a polycarbonate support and casted over a GCE electrode. Anti-hCG was bound to this by adsorption. BSA blocked non-specific binding.	1) incubation in hCG 2) solution of H_2O_2	AMP	LR: 25–400 mIU/mL LOD: 12 mIU/mL	Random	29
Carbon ink	Carbon ink was casted of carboxylated PPy–PPa copolymer that was modified next by EDAC/NHS chemistry. Anti-hCG was bound next to this layer. BSA blocked non-specific binding.	1) incubation in hCG 2) Iron redox probe	EIS	LR: 2–40 ng/mL or up to 1000 pg/mL LOD: 2.3 pg/mL	Via -NH_2	30
	Carbon ink with 1-pyrenebutanoic acid succinimidyl ester for further reaction with amine groups of the anti-hCG. BSA blocked non-specific binding.	1) incubation in hCG 2) Iron redox probe	EIS	LR: 1–70 ng/mL LOD: 33 pg/mL	Via -NH_2	31
Carbon paste	The carbon paste was electrochemically oxidized, modified by EDAC/NHS chemistry, covalently bound to protein A through lysine residues, added of anti-hCG, and finally of etanolamine.	1) incubation in hCG 2) PBS solution	SWSV	LR: 15-300 mIU/mL LOD: 14 mIU/mL 20 mIU/mL	Via Fc, -COOH	32
Graphite	The graphite electrode was modified by casting a mixture of Ormosil (sol-gel matrix prepared by hydrolyzing TEOS and APTES in weak alkali solution) and anti-hCG that was previously HRP labelled.	1) incubation in hCG 2) PBS solution	DPV	LR: 0.5–50 mIU/mL LOD: 0.3 mIU/mL	Random	33
Gold	A PDMS stamp was prepared with a periodicity of 100 μm and a width of the embossing strip 42 μm, let interact with biotin/spacer thiol and later with a 50 nm gold film freshly evaporated onto a high-refractive-index substrate. The streptavidin was bond to biotin and a biotinylated Fab fragement of an anti-hCG	1) incubation in hCG 2) —	SPD	LR: — LOD: ~200 pmol/L	—	34
	Sulfo-LC-SPDP cross-linking Au (via sulphur binding after DTT treatment) to anti-hCG (through its succinimidyl terminal).	1) incubation in hCG and reading	QCM	LR: 2.5–500 mIU/mL LOD: —	Via -NH_2	35
	A gold electrode was sequentiallu modified with cysteine, nanosized PB bilayer films, Au-NPs and anti-hCG, using layer-by-layer technology. Hb was applied next to block non-specific binding.	1) incubation in hCG 2) H_2O_2 solution	AMP	LR: 0.5–10 mIU/mL or 10–200 mIU/mL	Random	36

				LOD: 0.2 mIU/mL		
Cellulose membrane	Anti-hCG was immobilized on cellulose acetate membrane and membrane potentials varied with the electrolyte and hCG concentrations.	—	Potential	LR: 50-2500 mIU/mL LOD: —	Random	37

AMP: amperometry; AP: alkaline phosphatase; APTES: 3-aminopropyltrimethoxysilane; CAP: capacitance; CS: chitosan; CV: Cyclic voltammetry; DPV: Differential pulse voltammetry; dsDNA: double stranded DNA; EDAC: N-(3-dimethylaminopropyl)-N`-ethylcarbodiimide; EIS: Electrochemical Impedance Spectroscopy; E-LUM: Electrochemiluminescence; FSH: Follicle stimulating hormone; GA: glutaraldehyde; GCE: glassy carbon electrode; GPMS: glycidoxypropyltrimethoxysilane; Hb: hemoglobin; HQ: hydroquinone; HRP: horseradish peroxidase; ITO: Indium Tin Oxide; LUM: Chemiluminescence; MWCNT: multiwall carbon nanotubes; NHS: N-hydroxysuccinimide; NPG: nanoporous gold; NPs: nanoparticles; PB: Prussian blue; PDDA: poly (diallyldimethylammonium chloride); PDMS: poly(dimethylsiloxane); PEG: polyethylene glycol; PPy-Ppa: copolymer of pyrrole and pyrole-2-carboxylic acid; QCM: quartz-crystal microbalance; QD: Quantum dot; Ru(bpy)3: Tris(bipyridine)ruthenium(II); SPD: Diffraction of surface plasmon; SPDP: succinimidyl-6-[3'-(2-pyridyldithio)-propionamido] hexanoate; SPTES: (3-Mercaptopropyl)-trimethoxysilane silane; Sulfo-LC-SPDP: a sulfosuccinimidyl 6-[3-(2-pyridyldithio) propionamido] hexanoate; SWSV: Square-wave stripping voltammetry; SWV: Square-wave voltammetry; TB: toluidine blue; TEOS: tetraethyoxysilane; TH: thionine.

Table 2.4 - Immunosensors for hCG employing chemical labels.

Electrode support	Immunosensor design	Additional nanomaterial	Detection		Response to hCG Concentration	Antibody Binding	Ref.
			Sequential process	Technique			
Glassy carbon	A GCE was electrochemically oxidized and incubated in Mos-butyrylCS and acetic acid to create a cross-linked matrix. The surface was soaked in Au-NPs. hCG was drop-casted on this.	HRP labelled anti-hCG.	1) incubation in hCG and nanomaterial in the sensor 2) solution of H_2O_2 and PDA	AMP	LR: up to 30 mIU/mL LOD: 0.26 mIU/mL	Random	38
	A GCE was modified with a composite of TiO_2 and Cs. Anti-hCG was covalently bound to CS by means of GA. BSA blocked non-specific binding.	MWCNTs that were sequentially modified with PB, CS, Au-NPs and HRP labelled anti-hCG.	1) incubation in hCG 2) incubation in nanomaterial 3) solution of H_2O_2	DPV	LR: 0.05–150 mIU/mL LOD: 0.023 mIU/mL	Random	39
	Au-NPs and CS were mixed and casted on a GCE and followed electrochemical deposition. Anti-hCG was bound next by adsorption. Glycine was used to block non-specific binding.	HRP labelled anti-hCG.	1) incubation in hCG 2) incubation in nanomaterial 3) solution of H_2O_2	AMP	LR: 0.2–100 mIU/mL LOD: 0.1 mIU/mL	Random	40
	A GCE was electrochemically oxidized and incubated SPTES to create a cross-linked sol-gel matrix. Au-NPs were bound to this layer via–SH groups. hCG was drop-casted on this.	HRP labelled anti-hCG.	1) incubation in hCG and nanomaterial in the sensor 2) solution of H_2O_2 and PDA	AMP	LR: 5-30 mIU/mL LOD: 1.4 ng/mL	Random	41
	A GCE was electrochemically treated and modified with EDAC. Anti-hCG as bound next by covalent binding. Ethanolamine was employed to deactivate un-reacted sites.	Ferrocenecarboxylic acid was modified by EDAC/NHS chemistry and bound covalently to anti-hCG	1) incubation in hCG 2) incubation in nanomaterial 3) PBS solution	CV	LR: Up to 1500 mIU/mL or Up to 3200 mIU/mL LOD: 2.2 mIU/mL	Via $-NH_2$	42
	A GCE was modified by drop casting Nafion solution. After drying, anti-hCG solution was casted on this. An additional coat of Nafion was placed on top of this to assist in maintaining the antibody	HRP labelled anti-hCG	1) incubation in hCG in BSA 2) incubation in nanomaterial in BSA	AMP	LR: ~10-200 mIU/mL LOD: 11.2	Random	43

	on the electrode surface.		3) H_2O_2 and HQ solutions		mIU/mL		
Graphite	A composite of polysulfone and MWCNTs was casted on the graphite electrode and precipitated by adding water. The resulting surface was incubated in hCG.	HRP labelled anti-hCG	1) incubation in hCG in BSA + nanomaterial in the sensor 2) solution of H_2O_2	AMP	LR: Up to 600 mIU/mL LOD: 14.6 mIU/mL	Random	44
Carbon	Anti-FSH was bound by adsorption to the carbon electrode. BSA was used to block non-specific binding.	Anti-hCG was incubated with Ag-NPs. Non-specific binding was blocked with BSA and PEG	1) incubation in hCG 2) incubation in nanomaterial 3)Ag-NPs underwent pre-oxidation and pre-reduction stages prior to DPV	DPV	LR: 0.01-1 ng/mL LOD: 7.2 pg/mL	Random	45
	Anti-FSH was bound by adsorption to the carbon electrode. BSA was used to block non-specific binding.	Anti-hCG was incubated with Au-NPs. Non-specific binding was blocked with BSA and PEG	1) incubation in hCG 2) incubation in nanomaterial 3)Au-NPs underwent pre-oxidation prior to DPV	DPV	LR: Up to 2 ng/mL LOD: 36 pg/mL	Random	46
Carbon Paste	A Graphite–methacrylate matrix was added of anti-hCG and the resulting paste was packed in a PVC tube.	HRP labelled anti-hCG	1) incubation in hCG and BSA 2) incubation in nanomaterial and BSA 3) H_2O_2 and HQ solutions	AMP	LR: ~20-98 mIU/mL LOD: 2.6 mIU/mL	Random	47
Gold	Au-NPs were electrodeposited on the gold electrode and anti-hCG attached to these. Non-specific binding was blocked with BSA.	Anti-hCG was bound a Nafion layer deposited over TiO_2 and after labelled with $Ru(bpy)_3$ and blocked with BSA	1) incubation in hCG 2) incubation in nanomaterial 3) PBS solution with TPA	LUM	LR: 0.02 to 25 mIU/mL LOD: 0.007 mIU/mL	Random	48
	Protein G was thiolated with SPDP and bound to gold. Anti-hCG was bound next. Human IgG was added to remove unbound antibody. Non-specific binding was blocked with BSA.	Anti-hCG modified with an AP by cross-link with SPDP or the biotin-streptavidin	1) incubation in hCG 2) incubation in nanomaterial 3) solution of 4-Aminophenyl	AMP	LR: Up to 5000 mIU/mL LOD: 175 mIU/mL	Via Fc, -COOH	49

			phosphate.				
	Protein G was thiolated with SPDP and bound to gold. Anti-hCG was bound next. Non-specific binding was blocked with BSA	Anti-hCG modified with an AP by cross-link with SPDP or the biotin-streptavidin	1) incubation in hCG 2) incubation in nanomaterial 3) solution of 4-Aminophenyl phosphate.	SWV	LR: Up to 2000 mIU/mL or Up to 4000 mIU/mL LOD: 216 mIU/mL or 240 mIU/ML	Via Fc, -COOH	50
Iridium oxide	hCG was bound to an iridium oxide support and "Seablock" was used as blocking buffer	Anti-IgG labelled with AP	1) incubation of hCG with anti-hCG solutions 2) casting this in the sensor 3) HQ solution	AMP	LR: 12.5-100 ng/mL LOD: 1.8 ng/mL	—	51
Si substrate	SWCNT grown in Si substrate and modified with 1-pyrenebutanoic acid succinimidyl ester for binding covalently anti-FSH. BSA blocked non-specific binding	Anti-hCG was bound to Au-NPs. Non-specific binding was blocked with PEG and BSA	1) incubation in hCG 2) incubation in nanomaterial 3) pre-oxidation of Au-NPs followed by DPV	DPV	*LR:* 10–2000 pg/mL *LOD:* 2.4 pg/mL or 0.024 mIU/mL	Via $-NH_2$	52
ITO	A composite of Iron oxide NPs/CS was prepared and modified with GA. Anti-hCG was added next by covalent bond. BSA was used to block non-specific binding. This composite was kept in ITO by a magnet placed in the back-side.	PtRu alloy was modified with water-soluble CdTe QDs. This was made react with a mixture of EDAC/NHS and anti-hCG.	1) incubation in hCG 2) incubation in nanomaterial 3) $K_2S_2O_8$ in PBS	E-LUM	LR: 0.005-50 ng/mL LOD: 0.8 pg/mL	Random	53

AMP: amperometry; AP: alkaline phosphatise; APTES: 3-aminopropyltrimethoxysilane; CAP: capacitance; CS: chitosan; QCM: quartz-crystal microbalance; CV: Cyclic voltammetry; PEG: polyethylene glycol; DPV: Differential pulse voltammetry; dsDNA: double stranded; EDAC: N-(3-dimethylaminopropyl)-N'-ethylcarbodiimide or similar compound; EIS: Electrochemical Impedance Spectroscopy; E-LUM: Electrochemiluminescence; FSH: Follicle stimulating hormone; GA: glutaraldehyde; GCE: glassy carbon electrode; GPMS: glycidoxypropyltrimethoxysilane; Hb: hemoglobin; HQ: hydroquinone; NPG: nanoporous gold; HRP: horseradish peroxidase; ITO: Indium Tin Oxide; LUM: Chemiluminescence; MWCNT: multiwall carbon nanotubes; NHS: N-hydroxysuccinimide; NPs: nanoparticles; PB: Prussian blue; PDA: *o*-phenylenediamine; PDDA: poly (diallyldimethylammonium chloride); PDMS: poly(dimethylsiloxane); PPy-Ppa: copolymer of pyrrole and pyrole-2-carboxylic acid; QD: Quantum dot; Ru(bpy)3: Tris(bipyridine)ruthenium(II); SPD: Diffraction of surface plasmon; SPDP: succinimidyl-6-[3'-(2-pyridyldithio)-propionamido]hexanoate; SPTES: (3-Mercaptopropyl)-trimethoxysilane silane; Sulfo-LC-SPDP: sulfosuccinimidyl 6-[3-(2-pyridyldithio) propionamido]hexanoate; SWSV: Square-wave stripping voltammetry; SWV: Square-wave voltammetry; TB: toluidine blue; TEOS: tetraethyoxysilane; TH: thionine; TPA: triproprylamine.

2.2 Conventional methods for detection of hCG

2.2.1 ELISA

Enzyme-linked immunosorbent assays (ELISAs) are plate-based assays designed for detecting and quantifying substances such as peptides, proteins, antibodies and hormones. Other names, such as enzyme immunoassay (EIA), are also used to describe the same technology. In an ELISA, an antigen must be immobilized to a solid surface and then complexed with an antibody that is linked to an enzyme. Detection is accomplished by assessing the conjugated enzyme activity via incubation with a substrate to produce a measureable signal. The most crucial element of the detection strategy is a highly specific antibody-antigen interaction.

ELISAs are typically performed in 96-well (or 384-well) polystyrene plates, which will bind antibodies and proteins. It is this binding and immobilization of reagents that makes ELISAs so easy to design and perform. Having the reactants of the ELISA immobilized to the microplate surface makes it easy to separate bound from nonbound material during the assay. This ability to wash away nonspecifically bound materials makes the ELISA a powerful tool for measuring specific analytes within a crude preparation.

A detection enzyme or other tag can be linked directly to the primary antibody or introduced through a secondary antibody that recognizes the primary antibody. It also can be linked to a protein such as streptavidin if the primary antibody is biotin labeled. The most commonly used enzyme labels are horseradish peroxidase (HRP) and alkaline phosphatase (AP). Other enzymes have been used as well, but they have not gained widespread acceptance because of limited substrate options. These other enzymes include β-galactosidase, acetylcholinesterase and catalase. A large selection of substrates is available for performing the ELISA with an HRP or AP conjugate. The choice of substrate depends upon the required assay sensitivity and the instrumentation available for signal-detection (spectrophotometer, fluorometer or luminometer).

ELISAs can be performed with a number of modifications to the basic procedure. The key step, immobilization of the antigen of interest, can be accomplished by direct adsorption to the assay plate or indirectly via a capture antibody that has been attached to the plate. The antigen is then detected either directly (labeled primary antibody) or indirectly (labeled secondary antibody). The most powerful ELISA assay format is the sandwich assay (Figure 2.1). This type of capture assay is called a "sandwich" assay because the analyte to be measured is bound between two primary antibodies – the capture antibody and the detection antibody. The sandwich format is used because it is sensitive and robust.

An ELISA can also be performed as a competitive assay (Figure 2.1). This is common when the antigen is small and has only one epitope, or antibody binding site. One variation of this method consists of labeling purified antigen instead of the antibody. Unlabeled antigen from samples and the labeled antigen compete for binding to the capture antibody. A decrease in signal from purified antigen indicates the presence of the unlabelled antigen in samples when compared to assay wells with labeled antigen alone.

Fluorescent tags and other alternatives to enzyme-based detection can be used for plate-based assays. Despite not involving reporter-enzymes, these methods are also generally referred to as a type of ELISA. Likewise, wherever detectable probes and specific protein binding interactions can be used in a plate-based method, these assays are often called ELISAs despite not involving antibodies.

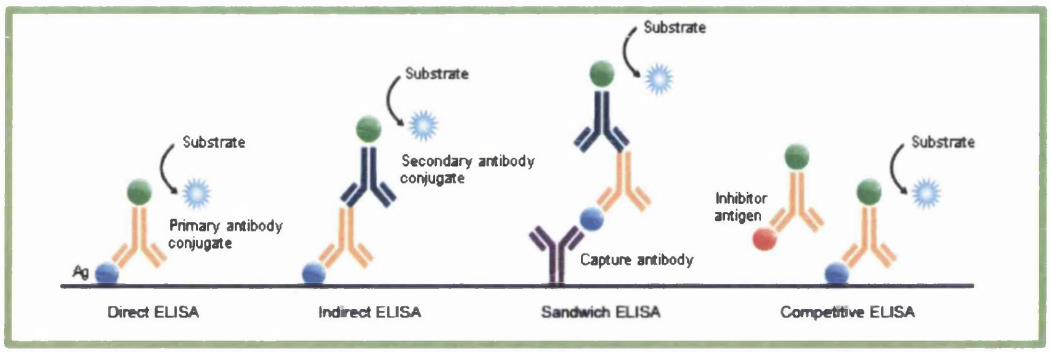

Figure 2.1 - Common ELISA formats. In the assay, the antigen of interest is immobilized by direct adsorption to the assay plate or by first attaching a capture antibody to the plate surface.

The direct detection method uses a labeled primary antibody that reacts directly with the antigen. Direct detection can be performed with antigen that is directly immobilized on the assay plate or with the capture assay format. Direct detection is not widely used in ELISA but is quite common for immunohistochemical staining of tissues and cells.

The indirect detection method uses a labeled secondary antibody for detection and is the most popular format for ELISA. The secondary antibody has specificity for the primary antibody. In a sandwich ELISA, it is critical that the secondary antibody be specific for the detection primary antibody only (and not the capture antibody) or the assay will not be specific for the antigen. Generally, this is achieved by using capture and primary antibodies from different host species (e.g., mouse IgG and rabbit IgG, respectively).

Table 2.5 - Comparison of direct and indirect ELISA tests

Comparison of Direct and Indirect ELISA Detection Methods	
Direct ELISA Detection	
Advantages	• Quick because only one antibody and fewer steps are used. • Cross-reactivity of secondary antibody is eliminated.
Disadvantages	• Immunoreactivity of the primary antibody might be adversely affected by labeling with enzymes or tags. • Labeling primary antibodies for each specific ELISA system is time-consuming and expensive. • No flexibility in choice of primary antibody label from one experiment to another. • Minimal signal amplification.
Indirect ELISA Detection	
Advantages	• A wide variety of labeled secondary antibodies are available commercially. • Versatile because many primary antibodies can be made in one species and the same labeled secondary antibody can be used for detection. • Maximum immunoreactivity of the primary antibody is retained because it is not labeled. • Sensitivity is increased because each primary antibody contains several epitopes that can be bound by the labeled secondary antibody, allowing for signal amplification. • Different visualization markers can be used with the same primary antibody.
Disadvantages	• Cross-reactivity might occur with the secondary antibody, resulting in nonspecific signal. • An extra incubation step is required in the procedure.

Either monoclonal or polyclonal antibodies can be used as the capture and detection antibodies in sandwich ELISA systems. Monoclonals (made by identical immune cells that are all clones of a unique parent cell) have an inherent monospecificity toward a single epitope that allows specific detection and quantitation of small differences in antigen. A polyclonal (made from several different immune cells) is often used as the capture antibody to pull down as much of the antigen as possible. Then a monoclonal is used as the detecting antibody in the sandwich assay to provide improved specificity.

An important consideration in designing a sandwich ELISA is that the capture and detection antibodies must recognize two different non-overlapping epitopes. When the antigen binds to the capture antibody, the epitope recognized by the detection antibody must not be obscured or altered. Capture and detection antibodies that do not interfere with one another and can bind simultaneously are called "matched pairs" and are suitable for developing a sandwich ELISA. Many primary antibody suppliers provide information about epitopes and indicate pairs of antibodies that have been validated in ELISA as matched pairs.

2.2.2 Pregnancy Test Strip

A pregnancy test attempts to determine whether a woman is pregnant (Figure 2.2). Markers that indicate pregnancy are found in both urine and blood, and pregnancy tests require sampling one of these substances. The first of pregnancy marker to be discovered, human chorionic gonadotropin (hCG), was discovered in 1930 to be produced by the trophoblast cells of the fertilised ova (eggs). While hCG is a reliable marker of pregnancy, it cannot be detected until after implantation (movement of the fertilized egg through the fallopian tube to the uterus). This results in false negatives if the test is performed during the very early stages of pregnancy. Obstetric ultrasonography may also be used to detect pregnancy. Obstetric ultrasonography was first practiced in the 1960s; the first home test kit for hCG was invented in 1968 by Margaret Crane in New York. She was granted two U.S. patents: 3,579,306 and 215,774. The kits went on the market in the United States and Europe in the mid-1970s.

Figure 2.2 - Pregnancy strip.

There are two basic types of home pregnancy tests:

- The most common types of home pregnancy tests use a test strip or dipstick that is hold in the urine stream or dipped into a sample of urine. An area on the end of the dipstick or test strip changes color if hCG is present, meaning pregnancy.
- A second type uses a urine collection cup with a test device. To use this type of test, several drops of urine may be placed into a well in the test device or the test device is immersed into urine collected in a cup. An area of the device changes color if hCG is present, meaning pregnancy.

The first urine of the morning (collected in the bladder overnight) yields the most accurate test results.

A typical test strip consists of the following components (Figure 2.3):

- Sample pad – an adsorbent pad onto which the test sample is applied;
- Conjugate or reagent pad – this contains antibodies specific to the target analyte conjugated to coloured particles (usually colloidal gold particles, or latex microspheres);
- Reaction membrane – typically hydrophobic nitrocellulose or cellulose acetate membrane onto which anti-target analyte antibodies are immobilized in a line that crosses the membrane to act as a capture zone or test line. A control zone will also be present, containing antibodies specific for the conjugate antibodies;
- Wick or waste reservoir – a further absorbent pad designed to draw the sample across the reaction membrane by capillary action and collect it.

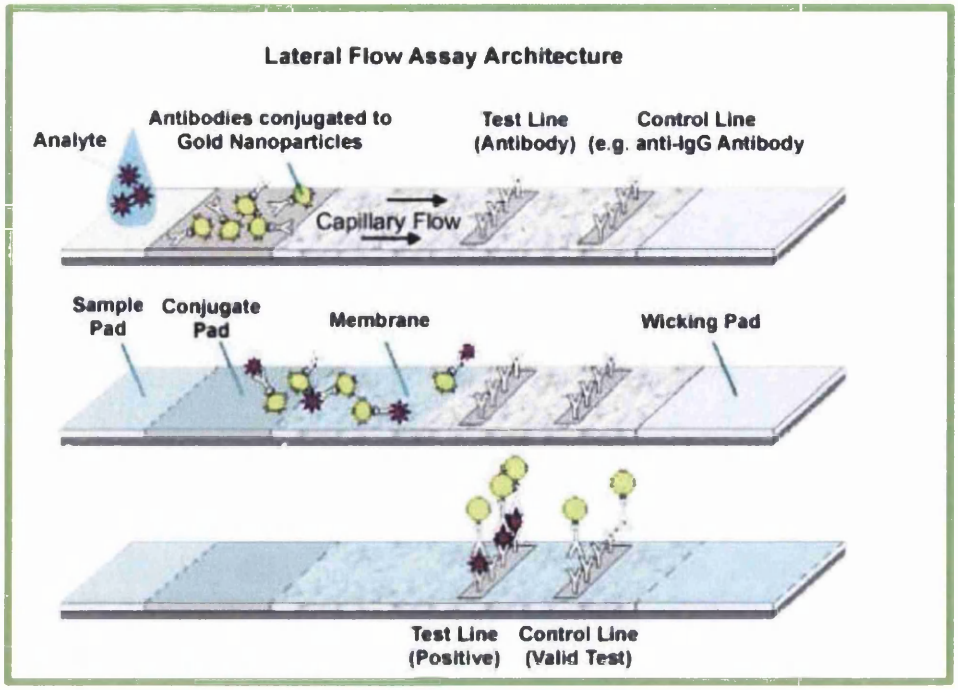

Figure 2.3 - Detection mechanism of a pregnancy strip.

2.3 Biosensors

According to a IUPAC document [54] a biosensor is defined as a specific type of chemical sensor comprising a biological recognition element and a physico-chemical transducer. The biological element is capable of recognizing the presence, activity or concentration of a specific analyte in solution. The recognition may be either a binding process (affinity ligand-based biosensor, when the recognition element is, for example, an antibody, DNA segment or cell receptor) or a biocatalytic reaction (enzyme-based biosensor). The interaction of the recognition element with a target analyte results in a measurable change in a solution property, such as formation of a product (Figure 2.4).

The transducer converts the change in solution property into a quantifiable electrical signal. The mode of transduction may be one of several approaches, including electrochemical, optical and the measurement of mass or heat.

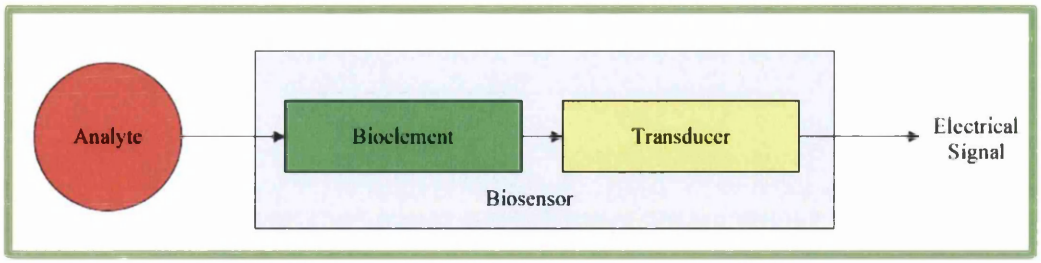

Figure 2.4 - Schematic Representation of Biosensors.

Biosensors should ideally demonstrate stability during operation and over time; reversibility of the recognition event; a linear or well-defined range of operation; defined detection limit and reproducibility of sensor response.

Biosensors can be classified according to the nature of the signal that occurs from the physical-chemical interaction between the analyte and the sensitive layer. These can be optical (fluorescence, luminescence, refractive index), thermal, acoustic, magnetic, piezoelectric or electrochemical. Electrochemical sensors, in turn, can be divided into potentiometric, amperometric, conductometric and field effect-based according to the measurement type.

Historically the first biosensor was reported in 1962 [55]. It was an electrochemical biosensor where an enzyme (glucose-oxidase) containing membrane was combined with an oxygen electrode to yield the well-known glucose sensor. The interest and development of biosensors has been growing ever since due to the inumerable possibilities of applications of such devices. The demands in process control and monitoring of complex biochemical reactions both *in-vitro* and *in-vivo* and the constant progress in biotechnology (genomics, proteomics and pharmaceuticals) have been some of the driving forces behind the increased development of this new generation of analytical devices.

2.3.1 Enzyme-based biosensors

2.3.1.1 Immunosensors

Biosensors which monitor antigen–antibody interactions are referred to as immunosensors [57]. Either an antigen or antibody is immobilized on a solid-state surface and participates in a biospecific interaction with the other component, allowing detection and quantification of an analyte of interest. The specific interaction is followed by a measuring device (transducer) capable of sensing a change in a physical property resulting from the antigen–antibody interaction.

The sensors may operate either as direct sensors, i.e., the change in property is produced directly by the antigen–antibody-binding reaction and detected in real time, with or without a label, or as indirect sensors, requiring a label on one of the biomolecules, a separation step and a secondary reaction to produce a change in the property to be measured. The latter method is commonly used in a competitive binding approach and results in more sensitive and versatile detection modes when incorporated into immunosensors [58]. These direct and indirect modes of sensing are often referred as homogeneous and heterogeneous immunosensors, respectively.

The sensitivity and specificity of an immunosensor are governed by the specificity and affinity of the antigen–antibody interaction and the noise and selectivity of the transducer. In the ideal sense, an immunosensor would be a multiuse device, using the reversibility of the antigen–antibody interaction to regenerate the immobilized component. However, in practice, adequate analytical sensitivity can only be achieved if antibodies with increased affinity are used [59]. Therefore, a high-affinity constant and a labile immobilized antibody, sensitive to the harsh conditions often required, make regeneration of the surface difficult to realize in practice, limiting practical application of immunosensors to single-use devices [60].

2.3.1.1.1 Amperometric immunosensors

Biosensors based on electrochemical transducers are the most commonly used for clinical analyses and the most frequently cited in the literature after ELISA tests [61]. Amperometry is the electrochemical technique usually applied in commercially available biosensors for clinical analysis. Amperometry is a specific electrochemical technique taking advantage of the fact that certain chemical species are oxidized or reduced (redox reactions) at inert metal electrodes, driven at a constant applied potential. These chemical species are known as electroactive substances. Two or three electrodes may comprise an electrochemical cell: the working electrode (WE), the reference electrode (RE) and the counter electrode (CE) (Figure 2.5).

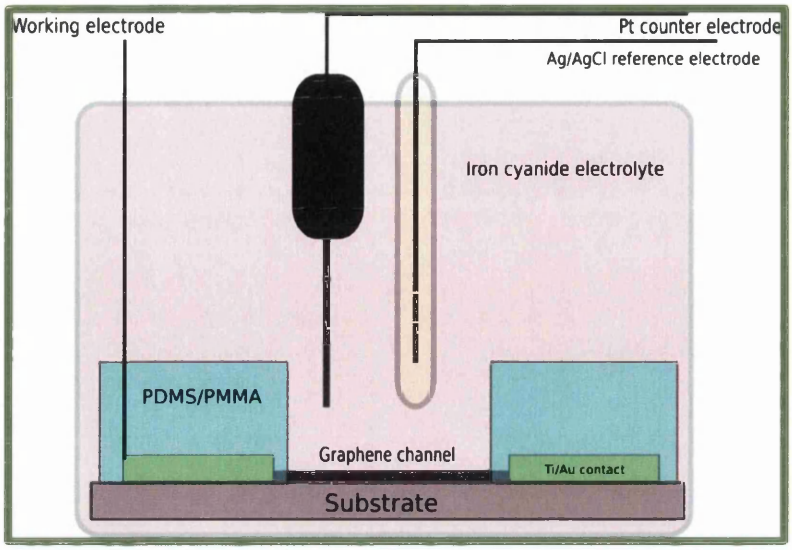

Figure 2.5 - Schematic of an electrode electrochemical cell. WE is the graphene channel, CE is the Platinum electrode and the RE is the Ag/AgCL electrode.

The working electrode is usually constructed from a metal such as platinum or gold.

A reference electrode, usually Ag/AgCl, provides a fixed potential against which the potential applied to the working electrode is measured and controlled.

A third electrode, the counter (or second) electrode is sometimes included. The counter electrode can be any material which conducts easily and will not react excessively with the bulk electrolyte solution. The most common materials that can be used as counter electrodes are platinum or silver wire electrodes. Platinum is often used because of its inert nature. The counter electrode supplies current to the working electrode, and its size should be larger than that of the working electrode. Reactions occurring at the counter electrode surface are unimportant as long as it continues to conduct current well. To maintain a constant current between the counter electrode and the working electrode, the counter electrode will often oxidize or reduce the solvent or bulk electrolyte.

There is a small current flow between the counter electrode and reference electrode and for this reason the potential of the reference electrode does not change. If the working electrode is driven to a positive potential, relative to the reference electrode, an oxidation reaction is supported at the working electrode, and it is referred to as the anode of the electrochemical cell. When applied to biosensors, the anode monitors formation of a product or depletion of a reactant resulting from a bioreaction (e.g., an enzyme-catalyzed reaction) involving an analyte of interest, near the surface of the electrode.

The species to be monitored diffuses to the surface of the electrode, where it undergoes a redox reaction. The measured cell current (diffusion current) is a quantitative measure of the analyte of interest.

Coupling of immunological reactions to amperometric electrodes has been demonstrated as a versatile technique for measurement of many analytes of clinical interest. Most analytes (e.g., proteins, hormones) are not electrochemically active and cannot participate directly in redox reactions. An immunoreaction is used as a selective recognition mechanism for an analyte of interest. Coupling of the immunoreaction to an amperometric transducer usually involves use of a labelled immunoagent. Enzymes, when used as labels, facilitate production of electroactive species, which can be determined electrochemically. A major advantage of electrochemical detection of the label is that it can be used in turbid media, unlike optical detection. Solid supports for labeled immunoagents for amperometric immunosensors can be made of large surface materials area to increase sensitivity, and the support is not required to be optically transparent. The first report of an amperometric immunosensor adapted an ELISA assay for human chorionic gonadotropin (hCG) to an amperometric measurement [62].

In amperometric electrodes a capture antibody is usually bound to a solid support. This antibody binds antigen (analyte) from the sample. After a rinsing step to separate free from bound antigen, a second labeled antibody is added, which binds to a different epitope on the antigen. After incubation and rinsing steps, substrate is added. The rate of formation of electroactive product is proportional to the amount of labeled antibody bound to the support, which is proportional to the concentration of antigen in the sample. This type of noncompetitive, heterogeneous sandwich assay generally shows better sensitivity and specificity for measurement of protein analytes [63].

As an example, a heterogeneous, sandwich-type amperometric immunosensor for apolipoprotein E (apo E)[1] in serum has been demonstrated [64]. In this assay, a monoclonal capture antibody for apo E is attached to the surface of a disposable, activated cellulose membrane and placed over a carbon working electrode. Bound apo E was determined using a polyclonal antibody labeled with alkaline phosphatase and p-aminophenyl phosphate was used as the substrate. Enzymatically generated p-aminophenol was monitored amperometrically. The sensitivity of this type of approach is evidenced by a linear response to a lower limit of 50ng/ml apo E.

[1] This protein combines with fats (lipids) in the body to form molecules called lipoproteins. Lipoproteins are responsible for packaging cholesterol and other fats and carrying them through the bloodstream. Apolipoprotein E is a major component of a specific type of lipoprotein called very low-density lipoproteins (VLDLs)

2.4 Biofunctionalization

2.4.1 Antibody

In addition to the sensor electrode, the Ab is also a critical component of an immunosensor.

Antibodies (often abbreviated Ab) also known as immunoglobulin (Ig), are proteins produced by an organism's immune system to provide a response against foreign substances, such as microbes.

It is a natural produced protein, composed of four chains: two identical "heavy" and two identical "light" polypeptide chains, which together form a "Y-shaped" conformation (Figure 2.6). The arms of the Y-shaped molecule are the antigen binding fragments (F_{ab}), and the vertical portion is called the fragment crystallisable (F_c) region.

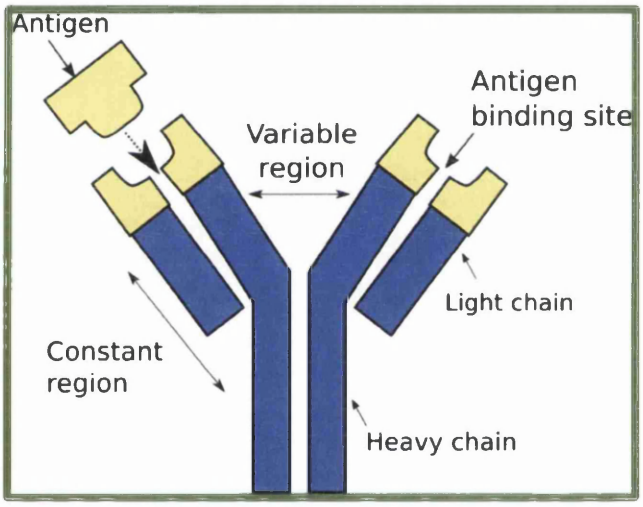

Figure 2.6 - A schematic representation of an IgG molecule.

When an Ab is randomly attached to a conductive support, it may adopt four possible orientations: F_c attached to the support, F_{ab} attached to the support, one F_c and one F_{ab} attached to the support, or all three fragments attached to the support [65]. The actual orientation of the antibodies on the surface may indeed comprise of a combination of these four 4 positions (Figure 2.7). As the active sites of the antibody are on the F_{ab} segment, the ideal orientation of the immobilized antibody is when the F_c fragment binds to the adsorbent substrate surface and the F_{ab} is oriented so that it is exposed to the analyte solution [65]. Thus, this oriented Ab immobilization is expected to yield an analytical improvement of the final immunosensor.

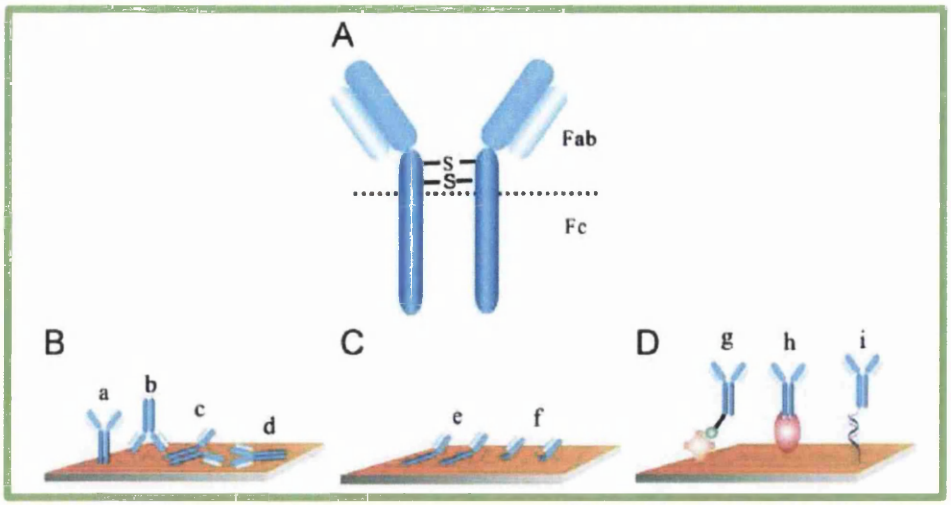

Figure 2.7 - Illustration of **(A)** main structure of antibody; **(B)** different orientation of randomly immobilized antibodies: (a) end-on, (b) head-on, (c) sideways-on,(d) flat-on; **(C)** oriented immobilization of antibody fragments: (e) half-antibody, and (f) Fab; **(D)** immobilization of antibodies through different bio-affinity systems:(g) avidin–biotin, (h) protein A,G or L, and (i) DNA-directed immobilization.

There are few reported strategies related to the oriented immobilization of antibodies to solid supports. Feng *et al.* reported an affinity ligand fused to the N/C-terminus of chimeric antigen for site-oriented immobilization, which resulted in significant enhancement of analytic signal [66]. Rosales-Rivera *et al.* reported the oriented immobilization of antibodies on surfaces of gold, achieved using a carboxylic-terminated bipodal alkanethiol that is covalently linked with amino groups of the antibody's F_{ab} fragments [67]. The most common approach includes attaching protein A or protein G to the biosensing surface prior to Ab binding. These proteins bind specifically to the F_c region of the antibodies, providing a suitable orientation of the antibodies all over the surface. However, this additional step in the surface modification process decreases the order and organization on the biosensing surface, simply because the proteins are also randomly attached to the surface. Other approaches employ the reduction of disulphide bonds between the peptide chains present in the same Ab, using the resulting thiol side chains as reactive sites for conjugation to gold or maleimide functionalized surfaces [68]. The simplest process for Ab orientation modifies its F_c region in order to facilitate its chemical binding to an amine layer under mild conditions. This is achieved by carboxylic activation at the F_c terminal via carbodiimide chemistry [68].

2.4.1.1 EDC/NHS Reaction Chemistry

Cross-linking refers to the formation of covalent bonds between molecules. A cross-linking agent is a compound with two reactive ends that can react with special functionalized groups (such as amino groups) on proteins.

For coupling of proteins and peptides a diversity of chemical methods exist. The standard amine coupling includes a three-step reaction with EDC/NHS chemistry (Figure 2.8). Many small molecules like drugs can be chemically modified to include amine or aldehyde functionality. A few exceptions to these coupling procedures exist: neutral molecules and highly negatively charged molecules.

Proteins vary in composition and structure, but only four functional groups of proteins are typically used in cross-linking: primary amines (-NH2), carboxyls (-COOH), thiols (-SH), and carbonyls (-CHO). For each protein functional group, there are one to several types of reactive group capable of targeting and binding to them. The most commonly used cross-linkers have two functional groups.

Carbodiimide compounds are used for cross-linking carboxylic acid to proteins [69]. The conjugation between carboxyls and amines is often performed using 1-Ethyl-3-(e-dimethylamino-propyl) carbodiimide hydrochloride (EDC, sometimes written EDAC) and N-Hydroxysuccinimide (NHS). EDC acts to dehydrate the carboxylate groups into an active o-acylisourea intermediate. This is quickly displaced by nucleophilic attack from a primary amine. NHS reacts with the o-acylisourea intermediate to form a semi-stable NHS-ester, which favours conjugation with amines. As the EDC/NHS facilitates the conjugation of the carboxyl group to amines without becoming part of the final linkages between molecules, the process is referred to as a zero-length cross linker [70]. This process is commonly used to attach proteins or peptides to a carboxyl/ amine modified surface.

An overview of the cross-linking process with EDC and NHS is shown in Figure 2.8.

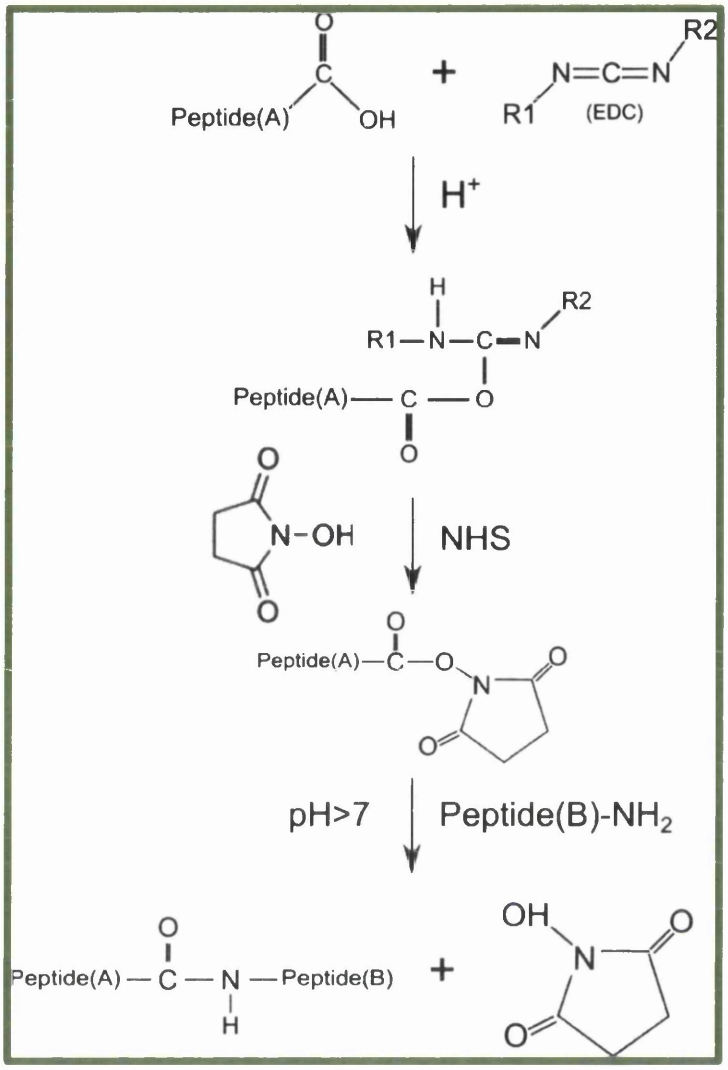

Figure 2.8 - Carbodiimide crosslinking reaction scheme.

2.4.1.2 Bovine Serum Albumin (BSA)

Protein–surface and protein–protein interactions are essential for a wide variety of biological applications in biotechnology, food processing, biomedical implant fixation, and many industrial processes [71–75]. Limitations such as low sensitivity or selectivity in biosensors or immunoassays, are often a result of non-specific protein–surface and protein–protein interactions [76,77]. In order to reduce such non-specific interactions, blocking reagents are employed.

Bovine serum albumin (BSA) is typically used at a 0.5 to 3% concentration. BSA is inexpensive and can be stored dry or as a sterile solution at 4°C. The use of BSA as a blocking reagent is documented and has been proven to be a good blocker of non-specific protein-surface binding on medium and high binding surfaces, as well as many of the pre-activated covalent surfaces. Disadvantages associated with BSA include:

- lot-to-lot variability — primarily related to the fatty acid content (BSA used as a blocking reagent should be fatty acid free),
- cross-reactions with antibodies prepared against BSA-hapten conjugates (BSA is typically linked to small haptens that lack the ability to elicit an immune response as individual molecules), and
- lack of diversity required to block some covalent surfaces (surfaces that feature hydrophobic, ionic and covalent characteristics).

Despite its disadvantages, BSA is probably the most widely used blocking reagent for solid phase immunoassays.

The selection of an appropriate blocking system is essential to the development of a specific and sensitive assay. Most often the choice is based on convenience, literature and "what has traditionally worked".

2.5 Graphene

As a material with impressive mechanical, thermal, and electronic properties, graphene has attracted a lot of interest from researchers in materials science, condensed matter physics, and electronics. Theoreticians, experimentalists and engineers alike have been quick to investigate and publish intriguing characteristics of graphene since its demonstration in 2004 [83]. Graphene is essentially a monolayer of sp^2 bonded carbon atoms arranged in a honeycomb lattice. Its unit cell is comprised of two carbon atoms invariant under a rotation of 120° with an inter-atomic length of 1.42Å [84].

Many of the headline-grabbing numbers regarding graphene involve its electronic properties. These unusual electronic properties of graphene are caused by its unique band structure. Hybridization in the p orbitals of the carbon atoms forms the π^* (conduction) and π (valence) bands [85].

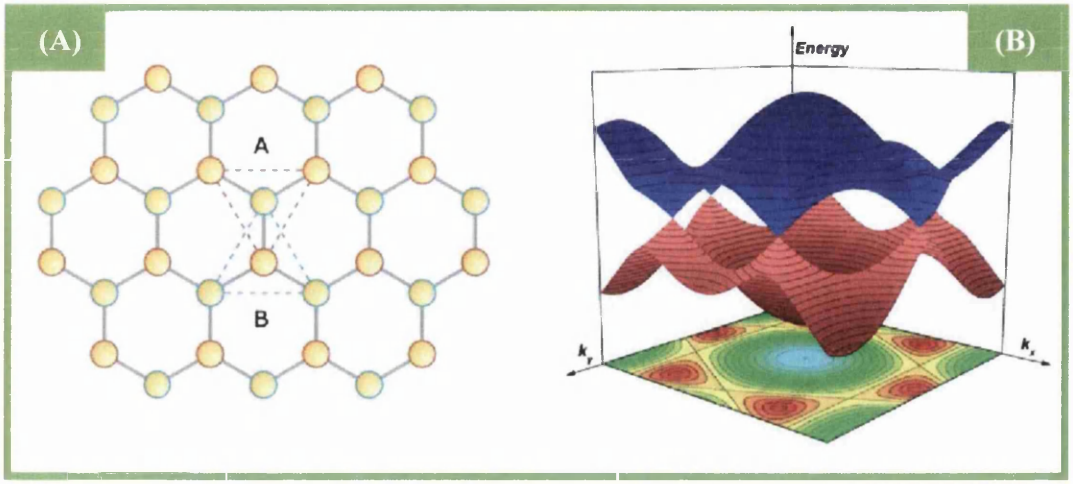

Figure 2.9 - Atomic and electronic structures of graphene. **(A)** Graphene lattice structure consisting of two triangular sub-lattices. **(B)** π (in blue) and π* (in red) band structure of graphene, represented in 3D in the first Brillouin zone. The six Dirac cones are positioned on a hexagonal lattice.

Graphene is the basic structural element of several carbon allotropes, including graphite, carbon nanotubes and fullerenes [86]. The fourth electron of each carbon in graphene, a p-orbital electron, forms a π bond that is oriented in the z-direction (orthogonal to the plane of the carbon atoms). This π orbital can be seen as a pair of symmetric lobes, oriented along the z-axis and centered on the carbon nuclei. Each carbon atom has one of these π bonds, which are then hybridized together to form what are referred to as the bonding π band and anti-bonding π* bands (Figure 2.9). These bands equate to the valence and conduction bands in graphene and are responsible for many of the unusual electronic properties of graphene. Separating the valence and conduction bands is a neutral point where there is a zero gap (the so-called Dirac point). Graphene is thus a zero-gap semiconductor because the conduction and valence bands meet at the Dirac points - locations in momentum space, on the edge of the Brillouin zone (the plane connecting the Dirac points).

The band structure of graphene relates to the energy and momentum of electrons within the material [86]. In graphene devices, the Fermi energy can be significantly different from the Dirac energy. Electrons within about 1eV of the Dirac energy (the energy of the Dirac point) have a linear dispersion relation [87]. This infers that charge carriers in graphene behave like relativistic particles with an effective speed of light given by the Fermi velocity. This behaviour is one of the most interesting aspects about graphene, and is responsible for much of the research attention that graphene has received [88].

2.5.1 Surface Functionalization of Graphene

The mechanical, electrical and chemical properties of chemically modified graphene are intrinsically linked to its structure [89]. Graphene has an intrinsic zero band-gap energy. In order to use graphene as a sensor, the band-gap has to be opened; then graphene can be used in electronic devices, single-molecule gas sensors, bio-sensors or as a transparent electrode [90].

Modification of the surface chemistry of graphene via chemical functionalization can be used to open the band gap in graphene. [91]. The modification of the surface chemistry of graphene via chemical functionalization can be useful for introducing new properties to the material – for example, functionalization can modify the carrier concentrations and other electronic properties of graphene [86].

By altering the electronic structure, structural "imperfections" can alter the chemical properties and reactions of graphene. If atoms or molecules can react selectively with a specific region of graphene, it becomes possible to build integrated circuits, as multifunctional sensors, and as devices by using selective functionalization [91].

In Figure 2.10 it is a schematic of a graphene biosensor. By chemically modifying (or functionalizing) the graphene surface, biological materials (such as antibodies) can be bound to graphene. These can give a specific electrochemical response, for example, to disease biomarkers. By using lithographic patterning techniques used in the processing of semiconductors, micron-sized channels of graphene can be fabricated. By functionalizing these channels, biosensor devices are developed which offer high sensitivity to disease biomarkers, which may be present in very low concentrations in clinical samples.

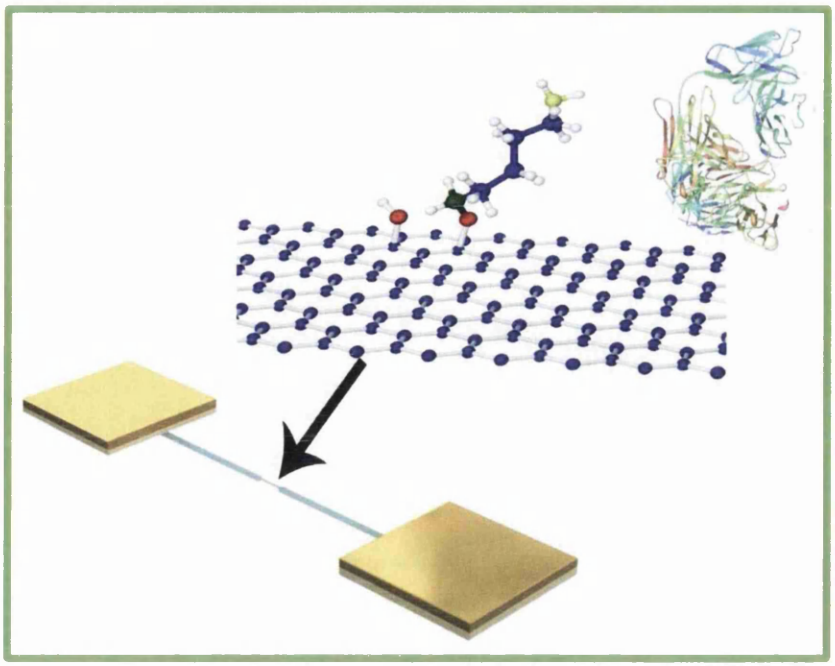

Figure 2.10 - Schematic of a graphene biosensor. By chemically modifying the graphene surface, biological materials (such as antibodies) can be bound to graphene. These can give a specific electrochemical response.

Composed of sp^2 carbon, graphene is chemically unsaturated. Intrinsically, it is possible to undergo covalent addition to change the carbons from sp^2 to sp^3 hydridization. However, carbon atoms in the graphene basal plane are protected by their π-conjugation system, whose motion is constrained by surrounding carbon atoms. Therefore, basal plane covalent addition usually encounters large energy barriers, and reactive chemical groups, such as atomic hydrogen, fluorine, and pre-cursors of other chemical radicals, are usually needed as the reactants. So far, the chemical modification of graphene cannot be fully controlled. Therefore, most of the reactions can also take place on graphene edges.

2.5.1.1 Hydrogenation and dehydrogenation

Hydrogenation of the free-standing graphene and of graphene located on top of oxidized Si substrates has been investigated both experimentally and theoretically [92-96]. The supported graphene displays different structures and electronic properties before and after hydrogenation. Hydrogenation changes the hybridization of carbon atoms from sp^2 to sp^3, resulting in elongated C–C bonds in the H-modified graphene. Hydrogen atoms tend to react with both surfaces of the plane of pristine graphene (Figure 2.11). If only one side is hydrogenated, it can then be rolled to form CNTs because of the unbalanced external stress [97].

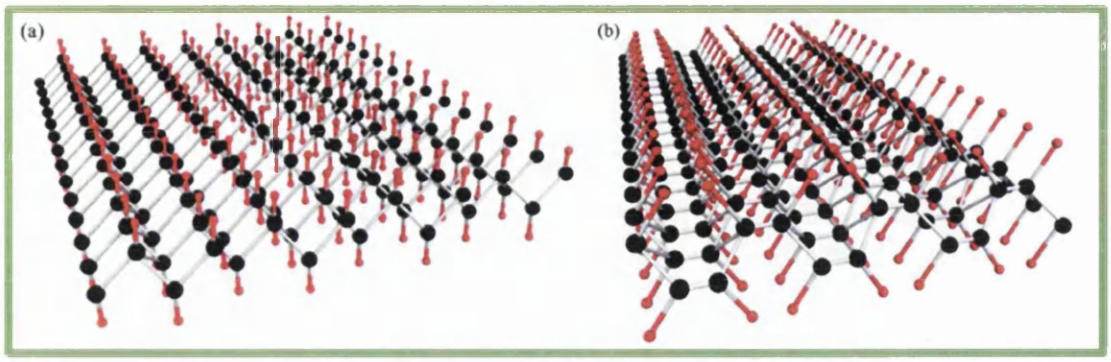

Figure 2.11 - The most favorable conformations of graphene after hydrogenation, the chair (a) and boat (b) conformations. Carbon is shown as black and hydrogen is shown as red. In functionalization, hydrogen tends to attach to both sides of the graphene plane.

2.5.1.2 Oxidation reactions

The oxidized graphene sheet is one of the most important forms of graphene, in which graphene is heavily oxygenated with a wide variety of oxygen species such as carbonyl, carboxyl, and hydroxyl groups [98]. Because of the existence of oxygen-containing functional groups, graphene oxides react easily with soluble moieties. This enables changing the hydrophilicity, hydrophobicity, or organophilicity of graphene, as required for many applications. For example, many modified graphene sheets are readily dispersed in organic solvents for further functionalization, or for mixing with organic matrices to form new nanocomposite materials. Oxidation can also generate a monotype of oxygen-containing functional group, such as graphene with only hydroxyls (graphenol), or only carboxyls (graphenic acid) on the basal plane.

2.5.1.3 Diazotization

Graphene has an electron-rich surface due to its π electrons. When electron-accepting moieties such as aryl diazonium salts react with graphene, electrons can transfer from the basal plane to the reactant. Because of the increase of pyramidalization of the deformed plane, diazonium salts easily react with graphene. Diazotization could be used to regulate electrical conductivity of the graphene since it can modulate the surface potential of graphene via regiofunctionalization [99-101]. Chemical converted graphene and epitaxial graphene (EG) have been successfully modified by diazotization at room temperature [102, 103]. Nitro groups on the surface of diazotized graphene can be reduced further to amine. The amine groups make sub-sequent

graphene functionalization possible because amine can react with many other groups, such as hydroxyl radicals, carboxyl groups, and acyl chlorides.

2.5.2 Graphene Sensors

Particularly important to this thesis are graphene sensors. Graphene has been actively studied as a chemical sensor since shortly after it was isolated in 2004. Increasingly sophisticated device processing has revealed that early measurements on graphene exhibited chemical sensing responses that were amplified by unintentional functionalization [104].

Several methods have been successfully established for graphene preparation, such as peeling-of graphite [105], liquid-phase exfoliation [106-108], chemical vapour deposition [109-112], graphitization of silicon carbide [113, 114], templating [115, 116], reduction of graphene oxide [117, 118], unzipping carbon nanotubes [119, 120], organic synthesis [121, 122], and anodic bonding.[123] These different methods produce graphene with different size, shape, chemical composition, and environment all of which have different requirements for functionalization.

The sensitivity of graphene to atoms and molecules adsorbed on the surface is indicative of its suitability for use in chemical sensors. Just a few extra electrons from atoms or molecules adsorbed on the surface of graphene can give rise to notable relative changes in carrier concentration. This impressive sensitivity is caused by the low-noise nature of graphene, which is a result of its high conductivity [124]. Graphene and graphene composites have been used to fabricate sensors for biologically relevant molecules such as glucose [125], hydrogen peroxide [126], or NADH [127] with impressive sensitivities such as μAmp.

The highly sensitive electronic response of graphene to its chemical environment allows for the detection of ultra-low concentrations of biologically relevant molecules and enzymes [128]. This level of sensitivity is necessary in a number of fields, from researching processes in cells to clinical diagnostics [129].

Despite the wide range of possible applications, there are still many challenges for graphene to reach its full potential. For example, graphene has an intrinsic zero band-gap energy. In addition, graphene is insoluble in organic solvents and susceptible to aggregation in aqueous solutions. Therefore, functionalization approaches that can modify the structural, electronic, and chemical properties of graphene are critical for applications. In principle, graphene can be functionalized at two classes of locations: the basal plane and the edges. On the basal plane, sp^2 hybridization of carbon leads to a strong covalent bonding, as well as to

delocalization of the π electrons. The interaction of the basal plane with guest atoms or molecules leads to modification of the π–π conjugation and thus the electron density distribution and the physical and chemical properties. The dangling bonds at edge sites of graphene are highly reactive to guest atoms or molecules. Typically, functionalization approaches used for fullerenes and carbon nanotubes (CNTs) can be applied to graphene. There are significant chemical differences due to the single atomic layer of graphene sheets. Much of this chemistry remains to be explored. The rehybridization from sp^2 to sp^3 via covalent reaction occurs both at the edges and on the basal plane.

2.5.2.1 Enzyme – based sensors

Glucose oxidase biosensors - The metabolic disorder of diabetes mellitus results in the deficiency of insulin and hyperglycemia and is reflected by blood glucose concentration higher or lower than the normal range of 80–120mg/dL (4.4–6.6mM). The disease is a major cause of death and disability [130]. Therefore, the diagnosis and management of diabetes requires close monitoring of blood glucose levels. The application of graphene in high sensitivity and cost-effective biosensors can aid the diagnoses. Various research groups have shown that graphene-based glucose biosensors exhibit good sensitivity, selectivity and reproducibility [131]. Kang *et al.* [132] fabricated chitosan – graphene/glucose oxidase modified electrodes for direct electrochemical glucose sensing. The excellent performance of the biosensors was attributed to the large surface area to volume ratio and high conductivity of [133]. Introduction of platinum nanoparticles increased the sensor's sensitivity, allowing a detection limit of 0.6μM glucose. The biosensor possessed good reproducibility and long-term stability with negligible interference signals from ascorbic acid and uric acid. Shan et al. [134] designed chitosan – graphene/gold nanoparticles nanocomposite films for glucose sensing, which exhibited good amperometric responses to glucose with a response of 2–10mM (R = 0.999) at −0.2V and 2–14mM (R = 0.999) at 0.5V. Chen *et al.* [135] prepared Nafion-graphene/graphene oxide film-modified electrodes for the detection of glucose. The sensor showed good stability, with a standard deviation of 4.21% (n = 5).

Nicotinamide Adenine Dinucleotide biosensor - NADH is an important coenzyme that takes part in more than 300 dehydrogenase enzymatic reactions. Electrocatalytic oxidation of NADH has been investigated as part of the development of dehydrogenase-based biodevices. However, its electrochemical oxidation at bare glass carbon electrodes in neutral solutions occurs at a high over potential (ca. 0.5V) because of slow electro transfer kinetics and electrode fouling [136]. Therefore, the effective oxidation of NADH at low potentials would aid the

development of NADH-based biodevices. Tang *et al.* [137] studied the electrochemical behavior of NADH on reduced graphene sheet film. It showed increased electro transfer kinetics and excellent electrocatalytic activity compared with bare glass carbon electrodes. The peak potential of NADH oxidation shifted from 0.75V on bare glass carbon to 0.42V on the reduced graphene sheet film/glass carbon electrode.

Hemoglobin (Hb) biosensor - Hb is the most important part of blood and is responsible for transporting O_2 throughout the circulatory system. Changes of Hb concentration in blood can cause several diseases and even death. Therefore, accurate determination of Hb content in blood is medically essential. Xu *et al.* [138] used a chitosan – graphene modified electrode for the electroanalysis of Hb. The cyclic voltammogram of Hb at the chitosan - graphene/glass carbon electrode showed a well-resolved redox peak compared with a chitosan/glass carbon electrode. The current response of Hb at the chitosan - graphene/glass carbon electrode increased linearly with scan rate from 30 to 150mV s^{-1} indicating a surface-controlled electrochemical process.

Cholesterol biosensor - Cholesterol and its ester are essential constituents of all animal cells. They are precursors of bioanalytes such as bile acid and steroid hormones. However, increases of cholesterol levels can cause life-threatening coronary heart diseases, cerebral thromboses, and artherosclerosis [139], therefore accurate detection of cholesterol level is medically useful. Dey and Raj [139] developed a highly sensitive amperometric biosensor based on a hybrid material derived from platinum nanoparticles and graphene for the detection of H_2O_2. The cholesterol biosensor was developed by immobilizing cholesterol oxidase and cholesterol esterase on the surface of the graphene/platinum nanoparticles hybrid material. The sensitivity and detection limit of the electrode towards cholesterol ester were 2.07 ± 0.1 μA μM^{-1} cm^{-2} and 0.2 μM, respectively.

Ascorbic acid (AA), uric acid (UA) and dopamine (DA) - Simultaneous determination of AA and DA is problematic in analytical neuro- and bio-chemistry [140]. The oxidation peaks of both the compounds appear almost at the same potential range. Therefore, their simultaneous detection is very difficult. Recently, graphene-based electrodes have been used for simultaneous detection of AA, DA, and UA. Shang *et al.* [141] used multilayer graphene nanoflakes for the selective determination of DA, AA and UA in 50mM PBS solution containing 1mM AA, 0.1mM DA, 0.1mM UA, and their ternary mixture at a scan rate of 100mV s^{-1}. The multilayer graphene nanoflakes demonstrated good electron transfer kinetics and allowed well-resolved simultaneous discrimination of AA, DA and UA at a detection limit of 0.17 μm. Zhou *et al.* [142] investigated the biosensing efficiency of chemical reduced – graphene oxide. The electroanalytical performances towards the detection of AA, DA and UA were much better

compared to bare glass carbon or graphite/glass carbon electrode. Wang *et al.* [143] employed a graphene-modified electrode for the selective detection of DA. The CV curve of 1mM DA on chitosan – graphene/glass carbon, chitosan/glass carbon, and glass carbon electrodes show well-defined and resolved voltammetric peaks for the direct oxidation of DA on chitosan – graphene/glass carbon as compared with chitosan/glass carbon or glass carbon.

DNA sensors - Sensitive, selective, rapid, and cost-effective analysis of biomolecules is important in clinical diagnosis and treatment. Carbon nanostructures, such as CNTs have been used for this purpose. Recently, Lu *et al.* [144] reported that graphene and ssDNA assemblies can be used for the homogeneous detection of biomolecules. Lu *et al.* [144] studied fluorescence quenching properties of GO in DNA biosensing. GO sheets were employed as a novel DNA biosensor by applying the GO in an array to recognize specific DNA–DNA hybridization.

Gas sensors - Graphene has potential use in gas sensors [145, 146] owing to its 2D structure with extremely high surface area. Gas sensing by graphene generally involves the adsorption and desorption of gaseous molecules (which act as electron donors or acceptors) on the graphene surface, leading to change in conductance in the graphene layer. The high sensitivity of graphene towards different gaseous molecules has led to its use in hydrogen, carbon monoxide, ammonia, chlorine, nitrogen dioxide and oxygen gas sensors. Schedin *et al.* [146] prepared a gas sensor using graphene. Gases such as NO_2, H_2O, iodine vapor, NH_3, CO and ethanol vapor were detected individually by Hall measurement. Moradian *et al.* [147] observed that armchair graphene can form p- or n-type semiconductors through adsorption of finite concentration adsorption of gas molecules.

2.5.2.1 Antibody – based sensors

Jung *et al.* [148] developed a novel GO-based immunobiosensor that could quickly detect viruses with high sensitivity and selectivity. The fluorescence quenching efficiency of GO arrays was affected by several factors, such as the concentration of immobilized Ab, their surface area and the number of AuNP quenchers.

Proof-of-concept graphene biosensors for the detection of glucose [149], hydrogen peroxide [150], and paracetamol [151] have been reported. These sensors were shown to demonstrate high sensitivity and reproducibility. More recently, biosensor devices based on the

attachment of a biomarker or enzyme to an appropriate linking/functional group to the graphene surface have been investigated [152].

Highly sensitive detection, in the range of the fmol, of specific species can be achieved by attaching biological molecules such as antibodies to the organic linking group. The development of a generic sensor technology for the detection of a variety of biomarkers could ultimately allow for fast, cheap, highly sensitive biosensors.

2.6 CNT

Carbon nanotubes (CNTs) have received great attention since they were discovered in 1991 by Iijima [153]. There are two classes of CNTs, single-wall carbon nanotubes (SWCNTs) and multiwall carbon nanotubes (MWCNTs) (Figure 2.12). The first consist of a single sheet of graphene rolled seamlessly, defining a cylinder of 1-2 nm diameter. MWCNTs can be visualized as several concentric tubes of graphene inside one another with diameters typically ranging from 2 to 100 nm with each tube, separated by a distance of 0.3-0.4 nm [154-157]. Because of their unique structure, mechanical strength, and electronic properties, CNTs are attractive materials for a wide range of applications [158-167].

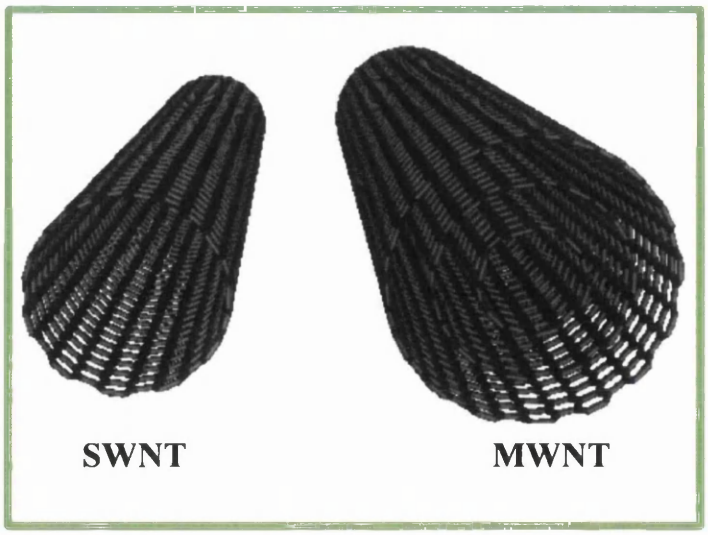

Figure 2.12 – Structure of SWNT and MWNT.

In electroanalytical chemistry, CNTs are used as electrode modifiers in order to decrease the potential and/or increase the rate of reaction of various electroactive substrates

[159]. CNT modified electrodes show better electrochemical performance than conventional carbon electrodes. There have been several reports which show that the electroactivity of CNTs is due to the presence of reactive groups on their surface and/or defect-areas of the nanotubes [154, 155]. A number of authors [158-160] have considered the advantages of using CNTs for electrode surface modification in the development of new designs of electrochemical sensors and biosensors.

2.6.1 CNT as sensor

In conventional single-walled carbon nanotube (SWCNT)-modified electrodes, such as SWCNT-modified glassy carbon electrodes [168], screen-printed carbon electrodes (SPCEs) [169], the electrochemical signals come from both the SWCNTs and the supporting electrodes (carbon or platinum, etc.) because the supporting electrodes are also exposed to the electrolyte solutions. In most of these cases, SWCNTs exhibit greatly enhanced electrochemical signals, so that the contribution of the supporting electrodes is negligible.

Several research groups are working on the functionalization of CNTs with different materials to enhance their sensing performance [170]. There are two main approaches for the surface functionalization of CNTs: covalent functionalization and non-covalent functionalization, depending on the types of linkages of the functional entities onto CNTs. Functionalized CNT sensors often offer a higher sensitivity and a better selectivity, compared with pristine (defect-free) CNT sensors. CNT/polymer nanocomposites as a non-covalent functionalization method without destruction of the physical properties of CNTs offer promising features as a sensing material. An et al. [171] fabricated SWNT and polypyrrole (PPy) nanocomposite based gas sensors. The sensor was formed by spin-coating nanocomposites onto prefabricated electrodes. The sensitivity of the nanocomposites was about ten times higher than that of polypyrrole alone. Abraham et al. developed a wireless gas sensor using a multi- walled carbon nanotube (MWNT) and PMMA composite film. The sensor was fabricated by dip-coating the composite film on a pair of electrodes with interdigital fingers. The sensor showed a fast response and a large change of resistivity of an order of magnitude for sensing dichloromethane, acetone, and chloroform [172].

Challenges for the realization of commercially viable devices are numerous. They include: the development of a detailed fundamental understanding of the sensing mechanisms of these novel sensors and the utilization of this information for the rational design of nanostructured sensing materials; the development of analyte-specific, fast and stable sensors and sensor arrays together with appropriate numerical methods to analyze sensor array data; and

the development of suitable high throughput nanomanufacturing techniques that enable mass production of high density sensor arrays.

References

[1]. Cole, L., et al., *Gestational trophoblastic diseases: 2. Hyperglycosylated hCG as a reliable marker of active neoplasia.* Gynecologic oncology, 2006. **102**(2): p. 151-159.

[2]. Chen, J., et al., *A gold nanoparticles/sol-gel composite architecture for encapsulation of immunoconjugate for reagentless electrochemical immunoassay.* Biomaterials, 2006. **27**(10): p. 2313-2321.

[3]. Zhang, B., et al., *A novel piezoelectric quartz micro-array immunosensor based on self-assembled monolayer for determination of human chorionic gonadotropin.* Biosensors & bioelectronics, 2004. **19**(7): p. 711-720.

[4]. Albert, F.C., K.Y.W. Danny, and C.S. Margaret, *An Indirect Perfluorosulfonated Ionomer-Coated Electrochemical Immunosensor for the Detection of the Protein Human Chorionic Gonadotrophin.* Analytical chemistry, 1999. **71**.

[5]. Kelly, L., S. Birken, and D. Puett, *Determination of hyperglycosylated human chorionic gonadotropin produced by malignant gestational trophoblastic neoplasias and male germ cell tumors using a lectin-based immunoassay and surface plasmon resonance.* Molecular and cellular endocrinology, 2007. **260-262**: p. 33-39.

[6]. Chen, J., et al., *Reagentless amperometric immunosensor for human chorionic gonadotrophin based on direct electrochemistry of horseradish peroxidase.* Biosensors & bioelectronics, 2005. **21**(2): p. 330-336.

[7]. Jin, C., et al., *Electrochemical Immunoassay of Human Chorionic Gonadotrophin Based on Its Immobilization in Gold Nanoparticles-Chitosan Membrane.* Electroanalysis, 2006. **18**.

[8]. Tan, F., F. Yan, and H. Ju, *Sensitive reagentless electrochemical immunosensor based on an ormosil sol-gel membrane for human chorionic gonadotrophin.* Biosensors & bioelectronics, 2007. **22**(12): p. 2945-2951.

[9]. Wu, L., F. Yan, and H. Ju, *An amperometric immunosensor for separation-free immunoassay of CA125 based on its covalent immobilization coupled with thionine on carbon nanofiber.* Journal of immunological methods, 2007. **322**(1-2): p. 12-19.

[10]. Dai, Z., et al., *Novel amperometric immunosensor for rapid separation-free immunoassay of carcinoembryonic antigen.* Journal of immunological methods, 2004. **287**(1-2): p. 13-20.

[11]. Mitala, J.J. and A.C. Michael, *Improving the performance of electrochemical microsensors based on enzymes entrapped in a redox hydrogel.* Analytica chimica acta, 2006. **556**.

[12] Kausaite-Minkstimiene, A., et al., *Comparative study of random and oriented antibody immobilization techniques on the binding capacity of immunosensor.* Analytical chemistry, 2010. **82**(15): p. 6401-6408.

[13] Wan, Ying; Su, Yan; Zhu, Xinhua; Liu, Gang; Fan, Chunhai (2013). Biosensors & bioelectronics 47C: 1-11.

[14] Rosales-Rivera, L.; Acero-Sánchez, J.; Lozano-Sánchez, P.; Katakis, I.; O'Sullivan, C. (2011). Biosensors & bioelectronics 26(11): 4471-4476.

[15]. J. Lu, S. Liu, S. Ge, M. Yan, J. Yu,, X. Hu, *Biosens. Bioelectron.*, 2012, **33**, 29-35.

[16]. Q. Wei, R. Li, B. Du, D. Wu, Y. Han, Y. Cai, Y. Zhao, X. Xin, H. Li, M. Yang, *Sens. Actuat B*, 2011, **153,** 256-260.

[17]. D. Wu, Y. Zhang, L. Shi, Y. Cai, H. Ma, B. Du, Q. Wei, *Electroanal.* 2013, **25**, 427 – 432.

[18]. R. Li, D. Wu, H. Li, C. Xu, H. Wang, Y. Zhao, Y. Cai, Q. Wei, B. Du, *Anal. Biochem.*, 2011, **414**, 196–201.

[19]. H. Yang, R. Yuan, Y. Chai, Z. Ying, *Colloids and surfaces. B: Biointerfaces*, 2011. **82**(2): p. 463-469.

[20]. C. Jin, Y. Feng, D. Zong, J. Huangxian, *Biosens. Bioelectron.*, 2005, **21**, 330-336.

[21]. J. Wang, R. Yuan, Y. Chai, S. Cao, S. Guan, P. Fu, L. Min, *BioChem. Eng. J.*, 2010, **51**, 95–101

[22]. H. Yang, R. Yuan, Y. Chai, Y. Zhuo and H. Su, *J. Chem. Technol. Biotech.*, 2010, **85**, 577–582.

[23]. S. Cao, J. Wang, R. Yuan, Y. Chai, *Sensor Lett.* 2011, **9**, 1636-1642

[24]. R. Chai, R. Yuan, Y. Chai, C. Ou, S. Cao and X. Li, *Talanta*, 2008, **74**, 1330–1336.

[25]. J. Y. Liao, *Appl. Microbiol. Biotech.*, 2007, **74**, 1385-1391.

[26]. J. Chen, J. H. Tang, F. Yan, H. X. Ju, *Biomaterials*, 2006, **27**, 2313- 2321.

[27]. L. T.N. Truong, M. Chikaea, Y. Ukitaa, Y. Takamura, *Talanta*, 2011. **85**(5): p. 2576-2580.

[28]. Lien, N. X. Viet, M. Chikae, Y. Ukita and Y. Takamura, *J. Biosens. Bioelectron.*, 2011, **2**, 107, pp. 6, Doi:10.4172/2155-6210.1000107.

[29]. K. Kerman, N. Nagatani, M. Chikae, T. Yuhi, Y. Takamura and E. Tamiya, *Anal. Chem.,* 2006, **78**, 5612-5616

[30]. F. Yu and W. Knoll, *Anal. Chem.,* 2004, **76**, 1971-1975

[31]. B. Zhanga, Q. Mao, X. Zhang, T. Jiang, M. Chen, F. Yu and W. Fu, *Biosens. Bioelectron.,* 2004, **19**, 711-720.

[32]. M. Lu, D. Fang, J. Zhang and K. Chen, *Acta Phys. Sin.*, 1992, **8**, 523-526.

[33] N. Li, R. Yuan, Y. Chai and S. Chen, *Bioproc. Biosyst. Eng.*, 2008, **31**, 551-558.

[34]. M. Tao, X. Li, Z. Wu, M. Wang, M. Hua and Y. Yang, *Clin. Chim. Acta-Int. J. Clin. Chem.*, 2011, **412**, 550-555.

[35]. C. Jin, Y. Feng, D. Dan, W.Jie and J. Huangxian, *Electroanal.*, 2006, **18**,7, 670-676.

[36]. H.Yang, R. Yuan, Y. Chai, H. Su, Y. Zhuo, W. Jiang and Z. Song, *Electrochim. Acta*, 2011, 56 1973–1980.

[37]. G. Yang, Y. Chang, H. Yang, L. Tan, Z. Wu, X. Lu and Y. Yang, *Anal. Chim. Acta*, 2009, **644**, 72-77.

[38] J. Chen, F. Yan, F. Tan and H. Ju, *Electroanal.*, 2006, **18**, 1696-1702.

[39]. M. Akram, M. C Stuart and D. K. Y. Wong, *Electroanal.*, 2006, **18**, 237-246.

[40]. A. F. Chetcuti, D. K. Y. Wong and M. C. Stuart, *Anal. Chem.*, 1999, **71**, 4088-4094.

[41]. Tan, F., F. Yan and H. Ju, *Biosens. Bioelectron.*, 2007, **22**, 2945-2951.

[42]. S. Sanchez, M. Roldan, S. Perez and E. Fabregas, *Anal. Chem.*, 2008, **80**, 6508-6514.

[47]. M. Chikae, K. Idegami, N. Nagatani, E. Tamiya and Y. Takamura, *Electrochem.*, 2010, **78**, 748-753.

[43]. K. Idegami, M. Chikae, K. Kerman, N. Nagatani, T. Yuhi, E. Endo and E. Tamiya, *Electroanal.,* 2008, **20**, 14-21.

[44]. M. Santandreu, S. Alegret and E. Fabregas, *Anal. Chim. Acta*, 1999, **396**, 181-188.

[45]. J. Wang, R. Yuan,Y. Chai, B. Yin, Y. Xu and S. Guan, *Electroanal.,* 2009, **21**, 707-714.

[46]. L. Mao, R. Yuan, Y. Chai, Y. Zhuo and X. Yang, *Sens. Actuat. B-Chem.,* 2010, **149**, 226-232.

[47]. J. M. Fowler, M. C. Stuart and D. K. Y. Wong, *Electrochem. Commun.*, 2008, **10**, 1020-1023.

[48]. J. A. Fowler, M. C. Stuart and D. K. Y. Wong, *Biosens. Bioelectron.,* 2007, **23**, 633-639.

[49]. M. S. Wilson, W. Nie and Weiyan, *Anal. Chem.*, 2006, **78**, 6476-6483

[50]. Y. Zhang, S. Ge, S. Wang, M. Yan, J. Yu, X. Song and W. Liu, *Biosens. Bioelectron.*, 2013, **42**, 592-597.

[51]. Y. Zhang, S. Ge, S. Wang, M. Yan, J. Yu, X. Song and W. Liu, *Analyst*, 2012, **137**, 2176-2182.

[52]. Leland C. Clark Jr., C.L., Electrode systems for continuos monitoring in cardivascular surgery. Clinical Chemistry, 1962. **Volume 102**: p. 29–45.

[53]. Rechnitz, G., et al., *A bio-selective membrane electrode prepared with living bacterial cells.* Analytica chimica acta, 1977. **94**(2): p. 357-365.

[54]. Thévenot, D., et al., *Electrochemical biosensors: recommended definitions and classification.* Biosensors & bioelectronics, 2001. **16**(1-2): p. 121-131.

[55]. Heller, A., *Amperometric biosensors.pdf.* Current Opinion in Biotechnology, 1996(7): p. 50-54.

[56].North, J.R., *Immunosensors - Antibody - based Biosensors.* Trends in biotechnology, 1985. **3**(7): p. 180-186.

[57]. Luppa, P., L. Sokoll, and D. Chan, *Immunosensors--principles and applications to clinical chemistry.* Clinica chimica acta; international journal of clinical chemistry, 2001. **314**(1-2): p. 1-26.

[58]. Bertold, H., *Antibodies for immunosensors a review.* Analytica chimica acta, 1997. **347**.

[59]. Morgan, C., D. Newman, and C. Price, *Immunosensors: technology and opportunities in laboratory medicine.* Clinical chemistry, 1996. **42**(2): p. 193-209.

[60]. M. Aizawa, A.M., S. Suzuki, Y. Nagamura, *Enzyme immunosensor. III. Amperometric determination of human chorionic gonadotropin by membrane-bound antibody.* Analytical biochemistry, 1979. **94**(1): p. 22-28.

[61]. Stephen G. Weber, W.C.P., *Homogeneous Voltammetric Immunoassay: A Preliminary Study.* Analytical Letters, 1979(1): p. 1-9.

[62]. A. E. Rachkov, M.I.R., T. A. Sergeyeva, S. A. Piletsky, *Method and apparatus for the detection of the binding reaction of immunoglobulins.* Sensors and Actuators B, 1994. **19**(1-3): p. 610-613.

[63]. Fred J. Hayes, H.B.H., William R., *Simultaneous Immunoassay Using Electrochemical Detection of Metal Ion Labels.* analytical chemistry, 1994. **66**(11): p. 1860-1865.

[64]. Soldano, C., A. Mahmood, and E. Dujardin, Production, properties and potential of graphene. Carbon, 2010. 48.

[65]. Wan, Ying; Su, Yan; Zhu, Xinhua; Liu, Gang; Fan, Chunhai (2013). Biosensors & bioelectronics 47C: 1-11.

[66]. Bo, Feng; Yueping, Luo; Fei, Ge; Lu, Wang; Liqun, Huang; Youzhi, Dai, (2011). Surface and Interface Analysis 43.

[67]. Rosales-Rivera, L.; Acero-Sánchez, J.; Lozano-Sánchez, P.; Katakis, I.; O'Sullivan, C. (2011). Biosensors & bioelectronics 26(11): 4471-4476.

[68]. Ferreira, N. and M. Sales (2014). Biosensors & bioelectronics 53: 193-199.

[69]. Chuan Liang Feng, Zhihong Zhang, Renate Förch, Wolfgang Knoll, G Julius Vancso, and Holger Schönherr. Reactive thin polymer films as platforms for the immobilization of biomolecules. Biomacromolecules, 6(6):3243–3251, 2005.

[70]. Christof M Niemeyer. Semisynthetic dna–protein conjugates for biosensing and nanofabrication. Angewandte Chemie International Edition, 49(7):1200–1216, 2010.

[71] M. Shen, T.A. Horbett, J. Biomed. Mater. Res. 57 (2001) 336–345.

[72] J.M. Nam, C.S. Thaxton, C.A. Mirkin, Science 301 (2003) 1884–1886.

[73] C. Sandu, R.K. Singh, Food Technol. 45 (1991) 84–91.

[74] J.W. Costerton, K.-J. Cheng, G.G. Geesey, T.I. Ladd, J.C. Nickel, M. Dasgupta, T. Marrie, J. Annu. Rev. Microbiol. 41 (1987) 435–464.

[75] G.A. Rechnitz, Chem. Eng. News 66 (1988) 24–36.

[76] M. Rankl, T. Ruckstuhl, M. Rabe, G.R.J. Artus, A. Walser, S. Seeger, Chem. Phys. Chem. 7 (2006) 837–846.

[77] K. Ishihara, H. Oshida, Y. Endo, T. Ueda, A. Watanabe, N. Nakabayashi, J. Biomed. Mater. Res. 26 (1992) 1543–1552.

[78] K. Reimhult, K. Pertersson, A. Krozer, Langmuir 24 (2008) 8695–8700.

[79] J.J. Ramsden, G.I. Bachmanova, A.I. Archakov, Biosens. Bioelectron. 11 (1996) 523–528.

[80] J.J. Ramsden, P. Schneider, Biochemistry 32 (1993) 523–529.

[81] R. Kurrat, J.J. Ramsden, J.E. Prenosil, J. Chem. Soc. Faraday Trans. 90 (1994) 587–590.

[82] R. Kurrat, J.E. Prenosil, J.J. Ramsden, J. Colloid Interface Sci. 185 (1997) 1–8.

[83] A. Fernandez, J.J. Ramsden, J. Biol. Phys. Chem. 1 (2001) 81–84.

[84]. Daniel, R.C., et al., Experimental Review of Graphene. ISRN Condensed Matter Physics, 2012. 2012.

[85]. Pirjo Pasanen, M.V., Meri Helle, Xuefeng Song and Pertti J Hakonen, Graphene for future electronics. The Royal Swedish Academy of Sciences, 2012.

[86]. Wilson, N.R., et al., On the structure and topography of free-standing chemically modified graphene. New Journal of Physics, 2010. 12.

[87]. Yan, L., et al., Chemistry and physics of a single atomic layer: strategies and challenges for functionalization of graphene and graphene-based materials. Chemical Society reviews, 2012. 41(1): p. 97-114.

[88]. Ye, L., et al., DNA-decorated graphene chemical sensors. Applied Physics Letters, 2010. 97.

[89]. Minghui, L. and Z. Linjie, Graphene-based electrode materials for rechargeable lithium batteries. Journal of Materials Chemistry, 2009. 19.

[90]. Pumera, M., et al., A mechanism of adsorption of beta-nicotinamide adenine dinucleotide on graphene sheets: experiment and theory. Chemistry (Weinheim an der Bergstrasse, Germany), 2009. 15(41): p. 10851-10856.

[91]. Berger, C., et al., Ultrathin Epitaxial Graphite: 2D Electron Gas Properties and a Route toward Graphene-based Nanoelectronics. The Journal of Physical Chemistry B, 2004. 108.

[92]. Ryu, S., et al., *Reversible basal plane hydrogenation of graphene.* Nano letters, 2008. 8(12): p. 4597-4602.

[93]. Savchenko, A., *Materials science. Transforming graphene.* Science (New York, N.Y.), 2009. 323(5914): p. 589-590.

[94]. Sofo, J., C. Ajay, and B. Greg, *Graphane: A two-dimensional hydrocarbon.* Physical Review B, 2007. 75.

[95]. Singh, A., E. Penev, and B. Yakobson, *Vacancy clusters in graphane as quantum dots.* ACS nano, 2010. 4(6): p. 3510-3514.

[96]. Elias, D., et al., *Control of graphene's properties by reversible hydrogenation: evidence for graphane.* Science (New York, N.Y.), 2009. 323(5914): p. 610-613.

[97]. Yu, D. and F. Liu, *Synthesis of carbon nanotubes by rolling up patterned graphene nanoribbons using selective atomic adsorption.* Nano letters, 2007. 7(10): p. 3046-3050.

[98]. Chattopadhyay, J., et al., *Graphite epoxide.* Journal of the American Chemical Society, 2008. 130(16): p. 5414-5415.

[99]. Sharma, R., et al., *Anomalously large reactivity of single graphene layers and edges toward electron transfer chemistries.* Nano letters, 2010. 10(2): p. 398-405.

[100]. Sinitskii, A., et al., *Kinetics of diazonium functionalization of chemically converted graphene nanoribbons.* ACS nano, 2010. 4(4): p. 1949-1954.

[101]. Huang, P., et al., *Graphene covalently binding aryl groups: conductivity increases rather than decreases.* ACS nano, 2011. 5(10): p. 7945-7949.

[102]. Lomeda, J., et al., *Diazonium functionalization of surfactant-wrapped chemically converted graphene sheets.* Journal of the American Chemical Society, 2008. 130(48): p. 16201-16206.

[103]. Bekyarova, E., et al., *Chemical modification of epitaxial graphene: spontaneous grafting of aryl groups.* Journal of the American Chemical Society, 2009. 131(4): p. 1336-1337.

[104]. Schedin, F., et al., Detection of individual gas molecules adsorbed on graphene. Nature materials, 2007. 6(9): p. 652-655.

[105] Novoselov, K., et al., *Electric field effect in atomically thin carbon films.* Science (New York, N.Y.), 2004. 306(5696): p. 666-669.

[106]. Hernandez, Y., et al., *High-yield production of graphene by liquid-phase exfoliation of graphite.* Nature nanotechnology, 2008. 3(9): p. 563-568.

[107]. Lotya, M., et al., *Liquid phase production of graphene by exfoliation of graphite in surfactant/water solutions.* Journal of the American Chemical Society, 2009. 131(10): p. 3611-3620.

[108]. Arnab, M., et al., *Water-Soluble Graphite Nanoplatelets Formed by Oleum Exfoliation of Graphite.* Chemistry of Materials, 2011. 23.

[109]. Zhu, Y., et al., *Carbon-based supercapacitors produced by activation of graphene.* Science (New York, N.Y.), 2011. 332(6037): p. 1537-1541.

[110]. Land, T.A., et al., *Direct observation of surface reactions by scanning tunneling microscopy: Ethylene→ethylidyne→carbon particles→graphite on Pt(111).* The Journal of Chemical Physics, 1992. 97.

[111]. Reina, A., et al., *Large area, few-layer graphene films on arbitrary substrates by chemical vapor deposition.* Nano letters, 2009. 9(1): p. 30-35.

[112]. Bae, S., et al., *Roll-to-roll production of 30-inch graphene films for transparent electrodes.* Nature nanotechnology, 2010. 5(8): p. 574-578.

[113]. Berger, C., et al., *Ultrathin Epitaxial Graphite: 2D Electron Gas Properties and a Route toward Graphene-based Nanoelectronics.* The Journal of Physical Chemistry B, 2004. 108.

[114]. Emtsev, K., et al., *Towards wafer-size graphene layers by atmospheric pressure graphitization of silicon carbide.* Nature materials, 2009. 8(3): p. 203-207.

[115]. Wei, D., et al., *Scalable synthesis of few-layer graphene ribbons with controlled morphologies by a template method and their applications in nanoelectromechanical switches.* Journal of the American Chemical Society, 2009. 131(31): p. 11147-11154.

[116]. Zhang, W., et al., *A strategy for producing pure single-layer graphene sheets based on a confined self-assembly approach.* Angewandte Chemie (International ed. in English), 2009. 48(32): p. 5864-5868.

[117]. Gómez-Navarro, C., et al., *Electronic transport properties of individual chemically reduced graphene oxide sheets.* Nano letters, 2007. 7(11): p. 3499-3503.

[118]. Gilje, S., et al., *A chemical route to graphene for device applications.* Nano letters, 2007. 7(11): p. 3394-3398.

[119]. Jiao, L., et al., *Narrow graphene nanoribbons from carbon nanotubes.* Nature, 2009. 458(7240): p. 877-880.

[120]. Kosynkin, D., et al., *Longitudinal unzipping of carbon nanotubes to form graphene nanoribbons.* Nature, 2009. 458(7240): p. 872-876.

[121]. Yang, X., et al., *Two-dimensional graphene nanoribbons.* Journal of the American Chemical Society, 2008. 130(13): p. 4216-4217.

[122]. Qian, H., et al., *Fully conjugated tri(perylene bisimides): an approach to the construction of n-type graphene nanoribbons.* Journal of the American Chemical Society, 2008. 130(52): p. 17970-17976.

[123]. Moldt, T., et al., *High-yield production and transfer of graphene flakes obtained by anodic bonding.* ACS nano, 2011. 5(10): p. 7700-7706.

[124]. Shao, Y., et al., Graphene Based Electrochemical Sensors and Biosensors: A Review. Electroanalysis, 2010. 22.

[125]. Zhou, M., Y. Zhai, and S. Dong, Electrochemical sensing and biosensing platform based on chemically reduced graphene oxide. Analytical chemistry, 2009. 81(14): p. 5603-5613.

[126]. Cracknell, J., K. Vincent, and F. Armstrong, Enzymes as working or inspirational electrocatalysts for fuel cells and electrolysis. Chemical reviews, 2008. 108(7): p. 2439-2461.

[127]. Martin, P., et al., Graphene for electrochemical sensing and biosensing. TrAC Trends in Analytical Chemistry, 2010. 29.

[128]. Yang, W., et al., Carbon nanomaterials in biosensors: should you use nanotubes or graphene? Angewandte Chemie (International ed. in English), 2010. 49(12): p. 2114-2138.

[129]. Kang, X., et al., Glucose oxidase-graphene-chitosan modified electrode for direct electrochemistry and glucose sensing. Biosensors & bioelectronics, 2009. 25(4): p. 901-905.

[130]. Wang, J., *Electrochemical glucose biosensors.* Chemical reviews, 2008. 108(2): p. 814-825.

[131]. Yang, M.H., et al., *Development of a Glucose Biosensor Using Advanced Electrode Modified by Nanohybrid Composing Chemically Modified Graphene and Ionic Liquid.* Electroanalysis, 2010. 22.

[132]. Kang, X., et al., *Glucose oxidase-graphene-chitosan modified electrode for direct electrochemistry and glucose sensing.* Biosensors & bioelectronics, 2009. 25(4): p. 901-905.

[133]. Wu, H., et al., *Glucose biosensor based on immobilization of glucose oxidase in platinum nanoparticles/graphene/chitosan nanocomposite film.* Talanta, 2009. 80(1): p. 403-406.

[134]. Shan, C., et al., *Graphene/AuNPs/chitosan nanocomposites film for glucose biosensing.* Biosensors & bioelectronics, 2010. 25(5): p. 1070-1074.

[135]. Chen, X., et al., *Electrochemiluminescence Biosensor for Glucose Based on Graphene/Nafion/GOD Film Modified Glassy Carbon Electrode.* Electroanalysis, 2010. 22.

[136]. Behera, S. and C.R. Raj, *Self-assembled monolayers of thio-substituted nucleobases on gold electrode for the electroanalysis of NADH, ethanol and uric acid.* Sensors and Actuators B: Chemical, 2007. 128.

[137]. Kim, Y.-R., et al., *Electrochemical detection of dopamine in the presence of ascorbic acid using graphene modified electrodes.* Biosensors & bioelectronics, 2010. 25(10): p. 2366-2369.

[138]. Xu, H., H. Dai, and G. Chen, *Direct electrochemistry and electrocatalysis of hemoglobin protein entrapped in graphene and chitosan composite film.* Talanta, 2010. 81(1-2): p. 334-338.

[139]. Dey, R.S. and C.R. Raj, *Development of an Amperometric Cholesterol Biosensor Based on Graphene−Pt Nanoparticle Hybrid Material.* The Journal of Physical Chemistry C, 2010. 114.

[140]. Zhou, M., Y. Zhai, and S. Dong, *Electrochemical sensing and biosensing platform based on chemically reduced graphene oxide.* Analytical chemistry, 2009. 81(14): p. 5603-5613.

[141] Shang, N.G., et al., *Catalyst-Free Efficient Growth, Orientation and Biosensing Properties of Multilayer Graphene Nanoflake Films with Sharp Edge Planes.* Advanced Functional Materials, 2008. 18.

[142]. Ming, Z., Z. Yueming, and D. Shaojun, *Electrochemical Sensing and Biosensing Platform Based on Chemically Reduced Graphene Oxide.* Analytical chemistry, 2009. 81.

[143]. Wang, Y., et al., *Application of graphene-modified electrode for selective detection of dopamine.* Electrochemistry Communications, 2009. 11.

[144]. Lu, C.-H., et al., *A graphene platform for sensing biomolecules.* Angewandte Chemie (International ed. in English), 2009. 48(26): p. 4785-4787.

[145]. Arsat, R., et al., *Graphene-like nano-sheets for surface acoustic wave gas sensor applications.* Chemical Physics Letters, 2009. 467.

[146]. F. Schedin, A.K.G., S. V. Morozov, E. W. Hill, P. Blake, M. I. Katsnelson and K. S. Novoselov, *Detection of individual gas molecules adsorbed on graphene.* Nature Materials 2007. 6: p. 652 - 655.

[147]. Moradian, R., Yawar Mohammadi and Nader Ghobadi, *Investigation of gas sensing properties of armchair graphene nanoribbons.pdf.* J. Phys.: Condens. Matter 2008. 20(425211 (12pp)).

[148]. Jung, J., et al., *A graphene oxide based immuno-biosensor for pathogen detection.* Angewandte Chemie (International ed. in English), 2010. 49(33): p. 5708-5711.

[149]. Zhao, G.-C., et al., Direct electrochemistry of cytochrome c on a multi-walled carbon nanotubes modified electrode and its electrocatalytic activity for the reduction of H2O2. Electrochemistry Communications, 2005. 7.

[150]. Kang, X., et al., A graphene-based electrochemical sensor for sensitive detection of paracetamol. Talanta, 2010. 81(3): p. 754-759.

[151]. Fedorov, A., The all-organic route to doping graphene. Physics, 2010. 3.

[152]. Sumio, I., Helical microtubules of graphitic carbon. Nature, 1991. 354.

[153]. Arben, M., et al., New materials for electrochemical sensing VI: Carbon nanotubes. TrAC Trends in Analytical Chemistry, 2005. 24.

[154]. Rivas, G., et al., Carbon nanotubes for electrochemical biosensing. Talanta, 2007. 74(3): p. 291-307.

[155]. Agüí, L., P. Yáñez-Sedeño, and J. Pingarrón, Role of carbon nanotubes in electroanalytical chemistry: a review. Analytica chimica acta, 2008. 622(1-2): p. 11-47.

[156]. Gregory, G.W., et al., Chemically Modified Carbon Nanotubes for Use in Electroanalysis. Microchimica Acta, 2005. 152.

[157]. Banks, C. and R. Compton, Exploring the electrocatalytic sites of carbon nanotubes for NADH detection: an edge plane pyrolytic graphite electrode study. The Analyst, 2005. 130(9): p. 1232-1239.

[158]. Carla, G.-C., P. Rasa, and M.A.B. Christopher, Development of electrochemical oxidase biosensors based on carbon nanotube-modified carbon film electrodes for glucose and ethanol. Electrochimica Acta, 2008. 53.

[159]. Guang-Chao, Z., et al., Direct electrochemistry of cytochrome c on a multi-walled carbon nanotubes modified electrode and its electrocatalytic activity for the reduction of H2O2. Electrochemistry Communications, 2005. 7.

[160]. Yajing, Y., et al., Immobilization and direct electrochemistry of cytochrome c at a single-walled carbon nanotube-modified electrode. Journal of Solid State Electrochemistry, 2006. 11.

[161]. Qiang, Z., G. Zhenhai, and Z. Qiankun, Electrochemical Sensors Based on Carbon Nanotubes. Electroanalysis, 2002. 14.

[162]. Saito, R., et al., Electronic structure of chiral graphene tubules. Applied Physics Letters, 1992. 60.

[163]. Dresselhaus, M.S., et al., Nanowires and nanotubes. Materials Science and Engineering: C, 2003. 23.

[164]. Wei, B.Q., R. Vajtai, and P.M. Ajayan, Reliability and current carrying capacity of carbon nanotubes. Applied Physics Letters, 2001. 79.

[165]. Wang, J., et al., Electrocatalytic oxidation of 3,4-dihydroxyphenylacetic acid at a glassy carbon electrode modified with single-wall carbon nanotubes. Electrochimica Acta, 2001. 47.

[166]. Sha, Y., et al., Multilayer films of carbon nanotubes and redox polymer on screen-printed carbon electrodes for electrocatalysis of ascorbic acid. Talanta, 2006. 70(3): p. 556-560.

[167]. Okuno, J., et al., Label-free immunosensor for prostate-specific antigen based on single-walled carbon nanotube array-modified microelectrodes. Biosensors & bioelectronics, 2007. 22(9-10): p. 2377-2381.

[168]. Tsujita, Y., et al., Microfluidic and label-free multi-immunosensors based on carbon nanotube microelectrodes. Jpn J Appl Phys, 2009. 48(6).

[169]. Zhang, T., et al., Recent progress in carbon nanotube-based gas sensors. Nanotechnology, 2008. 19(33): p. 332001.

[170]. An, K.H., et al., Enhanced Sensitivity of a Gas Sensor Incorporating Single-Walled Carbon Nanotube–Polypyrrole Nanocomposites. Advanced Materials, 2004. 16.

[171]. Abraham, J., K., et al., A compact wireless gas sensor using a carbon nanotube/PMMA thin film chemiresistor. Smart Materials and Structures, 2004. 13.

CHAPTER 3

"A theory is something nobody believes, except the person who made it. An experiment is something everybody believes, except the person who made it"

Albert Einstein (1879-1955), German Theoretical Physicist

Fabrication process

Thorough attention to detail, and a keen regard to cleanliness, is critical in any cleanroom process. Contamination during a fabrication process, such as dust, will render the fabrication of multiple channel devices inreproducible, or with a very low yield. Surface treatment and cleanliness will make all the difference between a metal contact sticking or peeling off. The fabrication of a channel device requires several steps and several techniques, which are presented in this chapter, and each of those has to be understood properly in order to optimise the device.

3.1 Cleaning

✓ **Solvent clean**

Photoresist on the top of the SiC wafer (from the laser cutting of the wafer) is removed using acetone. SiC is cleaned by submersing the samples clean in an ultrasonic bath for 15 minutes in solutions of trichloroethylene, acetone, isopropyl alcohol and methanol respectively.

✓ **Piranha clean**

The sample is then immersed in concentrated sulphuric acid (H_2SO_4), and hydrogen peroxide (H_2O_2) is added every 5 minutes 3 times in order to provide a self-heating effect, this solution is meant for remove organic residues off substrates. This yields a thin oxide layer on the surface, which is subsequently removed with HF.

✓ **RCA clean**

The sample is immersed in a solution of $5H_2O$ (deionised water):$1H_2O_2$ (hydrogen peroxide):$1NH_4OH$ (ammonium hydroxide) maintained at 75°C for 5 min, this solution is meant for the removal of insoluble organic contaminants. The sample is then dipped in HF for 3 minutes to remove the thin silicon dioxide layer resulting from the RCA clean. The sample is then ready for graphene growth in the Rapid Thermal Annealing (RTA) furnace.

3.2 Graphene Growth

3.2.1 Graphene preparation on SiC by sublimation

Graphene samples have been grown on 4H-SiC in a Jipelec SiC rapid thermal annealing furnace. This furnace, primarily meant to activate dopants in SiC, can also be used to grow graphene on SiC if the vacuum is low enough to prevent effects such as step bunching [1,2]. To prevent step bunching, the system was fitted with an extra turbo molecular pump, allowing the base pressure in the chamber to decrease from 10^{-2} mbar to 10^{-5}mbar.

The furnace is an induction furnace for heat treatment of samples, up to 2 inches in diameter, at temperatures up to 2000°C. Samples are placed on a graphite susceptor that is installed at the top of a glassy carbon tube and inside a quartz chamber. The furnace temperature is measured using an optical pyrometer. In order to get a controlled RTA growth, the growth temperature has to be obtained rapidly, which is permitted by this system, since it has a temperature ramp rate of 500°C/min.

The growth of graphitic layers on SiC substrates by the sublimation of Si, has been known since 1975 [3]. After the famous discovery of graphene in 2004, the electronic properties of

these graphitic layers were found to be comparable to that of isolated graphene sheets [4] [5]. This technique seems to be most compatible with current standard semiconductor device fabrication technology, opening up prospects of achieving practical graphene technology with more complex functionality and performance [5].

In the sublimation technique, silicon atoms in the top layer(s) of a semi-insulation SiC substrate are removed through annealing at elevated temperatures (>1200°C), leaving behind an electronically decoupled epitaxial graphene layer (illustrated in Figure 3.1). However, the realization of an atomically flat surface covered by a graphene monolayer requires advances in SiC substrate preparation and comprehensive understanding of the graphene nucleation and growth process. SiC substrates are grown, cut, and polished with an intension to get an impeccably flat surface but these are never perfectly on-axis.

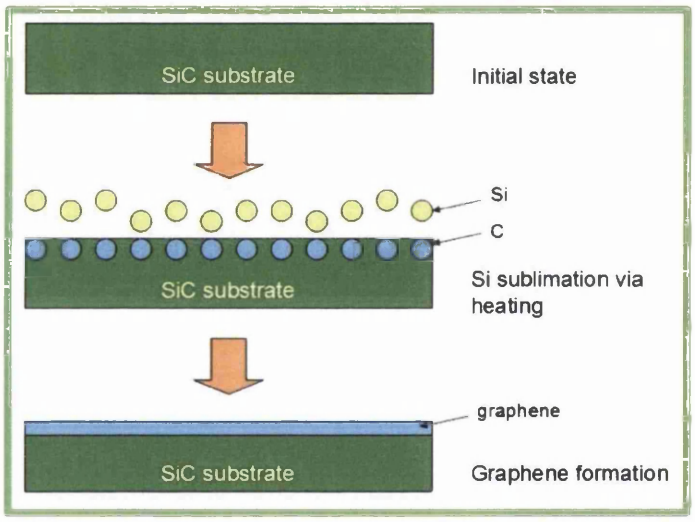

Figure 3.1 - Schematic illustration of the graphene formation on SiC by sublimation.

3.3 Standard fabrication techniques

3.3.1 Photolithography

Photolithography is the process by which a pattern from a template, or mask, is transferred into a stack of thin films on the surface of a silicon wafer in order to create integrated circuits. These patterns may be transistor gates, metal interconnect lines to connect devices, contacts or vias to connect between layers, or a variety of other features.

The photolithography process is accomplished by illuminating the mask from behind and forming a demagnified image of it on the surface of the wafer. The wafer is coated with a material called photoresist that undergoes a chemical reaction when exposed to light [6] .

Photoresists are photoactive polymers which are used as a protective or mask material in electronic device fabrication processes. Photoresists undergo a photochemical reaction and subsequent change in their solubility on exposure to light. Photoresists can be categorized as positive or negative resists. Positive are degraded when exposed to light and exposed areas become soluble to solvents in which the resist isn't soluble, whereas negative resists are based on using the energy provided by the incident beam to cross-link the polymer chain, and thus become less soluble [6].

A chemical known as a developer is then used to remove the less soluble areas of the photoresist, leaving the desired pattern behind. This pattern may then be etched into the underlying film stack. After etching, the remaining photoresist may be removed, leaving the desired pattern in the film stack [6].

Photoresists have enabled the modern electronic revolution. The patterns of conductive tracks on circuit boards and the tiny transistors on microchips are "patterened" using photoresists. The technology of photoresists has been refined to the point where many millions of micron-sized devices can be fabricated simultaneously and reliably on silicon or other semiconductor substrates. Research on yet smaller (and therefore more dense and efficient) circuitry continues apace today. Photolithography is still the predominant technology, but polymers for extreme ultraviolet and electron beam lithography are becoming increasingly important as the evolution of electronic devices. Nano-lithography techniques such as electron beam lithography and Nano Imprint Lithography also utilise photochemistry to achieve nanoscale patterns [6].

3.3.2 Electron beam lithography (EBL)

Electron beam lithography (EBL) is one of the most common techniques used for patterning features at the nanoscale. The usual resists are polymers dissolved in a liquid solvent. Liquid resist is dropped onto the substrate, which is then spun at 1000 to 6000rpm to form a coating – as in photolithography. After baking out the casting solvent, exposure to the electron beam modifies the resist. As in optical lithography, there are two types of e-beam resists: positive tone and negative tone, with the usual behaviour, i.e., positive resists develop away at exposed regions, whereas in the case of negative resist the developed region remains after development.

Polymethyl methacrylate (PMMA) is the standard positive e-beam resist, usually purchased in two high molecular weight forms (495K or 950K) in a casting solvent such as chlorobenzene or anisole. Electron beam exposure breaks the polymer into fragments that can be dissolved in a 1:2 MIBK:IPA developer (MIBK is Methyl Isobutyl Ketone and IPA in Isopropyl Alcohol).

The main issue encountered when using standard lithography is the wavelength of the photon source used, since the minimum feature size is directly related to the wavelengths, which are, with an Hg light source, 436nm ("g-line"), 405nm ("h-line") and 365nm ("i-line").

The wavelength for electron beam lithography is usually in the pm range. A combination of various effects increase the beam size, such as the interaction between electrons (coulomb repulsion) within the beam, the interaction between the incident electrons and the returning secondary electrons, the cyclonic movement introduced by the magnetic lenses (in the plane perpendicular to the electron beam), and, more significantly, the electron source. The smaller the electron emitting source is, the sharper the energy dispersion will be. State-of-the-art systems can reach a spot size of less than 1nm. Practically, it is difficult to achieve feature size of less than 10nm due, mostly, to the electron/matter interactions. These contributions can be attributed to two main types of scattering each of which can be treated separately and modelled by Gaussian distributions [7].

- Inelastic scattering generates the secondary electrons that will expose the resist, or that can be used to image the surface. However, high energy electrons are only slightly deviated from the incident direction, thus increases in the electron energy reduces the lateral dispersion of secondary electrons.
- Elastic collisions (backscattered electrons), though, consist of a large modification of the incident electron direction without any loss of energy and can be generated deep within the substrate. The back scattered electron can therefore be directed back to the surface in a location far from the incident beam, thus exposing the resist where it wasn't intended to. Successive exposures around the same area can therefore fully expose the resist outside the designed writing area. This is called the proximity effect.

3.3.3 Reactive Ion etching (RIE)

After a photoresist image has been formed on the surface of a wafer, the next process often involves transferring that image into a layer under the resist by etching.

It is useful to begin this discussion of etching by identifying the appropriate figures of merit. The primary one is the etch rate, which has dimensions of thickness per unit time. A high etch rate is generally desirable in a manufacturing environment. Too high an etch rate, however, may

render a process difficult to control. Common desired etch rates are tens or hundreds of nanometers per minute. Etch rate uniformity is measured in terms of percentage variation of the etch rate. It is quoted across a wafer and from wafer to wafer. Selectivity is the ratio of the etch rates of various materials, such as the photoresist or the underlying layer, referenced to the etch rate of the film being patterned. Undercut is the lateral extent of etch under the photoresist mask [8].

Etching in a plasma environment has several significant advantages when compared with wet etching. Plasmas are much easier to start and stop than simple immersion wet etching. Furthermore, plasma etching processes are much less sensitive to small changes in the temperature of the wafer. These two factors make plasma etching more repeatable than wet etching. Most important for small features, plasma etches may have high anisotropies. Plasma environments may also have far fewer particles than liquid media.

For a plasma etching process to proceed, six steps must occur. A feed gas introduced into the chamber must be cracked into chemically reactive species by the plasma. These species must diffuse to the surface of the wafer and be adsorbed. Once on the surface, they may move about (surface diffusion) until they react with the exposed film [8]. The reaction product must be desorbed, diffused away from the wafer, and transported by the gas stream out of the etch chamber. As with wet etching, the etch rate is determined by the slowest of these steps.

In a typical plasma etch processes, the surface of the film to be etched is subjected to an incident flux of ions, radicals, electrons, and neutrals. Although the neutral flux is by far the largest, physical damage is related to the ion flux. Chemical attack depends on both ion flux and radical flux. Often this bombardment sets up a modified surface layer that is many atomic layers thick [8].

Reactive ion etching involves both physical and chemical processes. The physical process includes ionization of reactive gas molecules and ion sputtering of sample surface, both of which take place in a plasma. Plasma can be loosely defined as partially ionized gases. In a confined space such as a vacuum chamber, the ionized particles collectively set up a long-range electrostatic field which has an important influence on the behaviours of these charged particles. The electric field is created because electrons in the plasma tend to move faster than ions. The fast moving electrons hit the chamber wall before ions do, causing the wall to be charged up negatively. The negatively charged wall surface pushes other electrons away from the wall, creating a layer of positively charged region where an electrical field is created to accelerate the ions toward the wall surface [9].

3.3.4 Sputtering (magnetron)

Sputtering and sputter deposition are widely used techniques for the erosion of surfaces and the deposition of films. Sputtering, also known as sputter etching, is used for patterning semiconductor wafers, for cleaning surfaces, for micromachining, depth profiling, and a number of applications which require careful, microscopic erosion of a surface. Sputter deposition is used for film deposition on semiconductor wafers, on magnetic media and head surfaces, for coating tools and cutting surfaces for wear resistance, for reflective coatings on window glass, for coating the insides of plastic bags and the surfaces of automobile parts, and a number of other wide ranging applications.

Sputtering is usually practiced by means of plasmas which generate charged particles which can be accelerated towards a surface electrically.

Sputtering is simply the process of erosion of that surface by the energetic particles, a sort of atomistic sandblasting. Sputter deposition is nothing more than the accumulation of these atoms which are blasted off the surface onto a nearby sample.

Magnetron sputtered films now outperform films deposited by other physical vapour deposition (PVD) processes, and can offer the same functionality as much thicker films produced by other surface coating techniques such as evaporation. Consequently, magnetron sputtering now makes a significant impact in application areas including hard, wear-resistant coatings, low friction coatings, corrosion-resistant coatings, decorative coatings and coatings with specific optical, or electrical properties [10].

The term "magnetron" was originally used to describe tubes used to generate microwave power for radar applications. It is still used for this purpose, and the builder or owner of a microwave plasma system will use a "magnetron" power source to run their plasma. The same general magnetron effect found in these tubes can be altered somewhat to make an extremely efficient sputtering cathode.

These cathodes operate in a diode mode, either in rf or dc, but are rarely, if ever, called diodes. Magnetron sputtering sources are the current workhorse of the sputter deposition field, used in perhaps 95% of all sputtering applications [11].

3.5 Device analytical performance

3.5.1 Electrochemical

Electrochemical biosensors are affinity-based biosensors, using an immobilized recognition element that binds selectively to the target molecule. When the target binds to the recognition

element at the surface of the biosensor, it generates current and/or voltage changes at that surface.

Based on their operating principle, electrochemical biosensors can employ potentiometric, amperometric and impedimetric transducers, converting the chemical information into a measurable electrical output signal. Due to their low cost and capacity for miniaturization, electrochemical biosensors hold great promise for POC applications, where minimizing size and cost are crucial. Potentiometric-based methods are amongst the oldest class of electrochemical sensors, usually correlated to the conventional pH glass electrode.

3.5.1.1 Cyclic voltammetry

Cyclic Voltammetry (CV) is the most common, simple, fast and perhaps most straightforward electroanalytical technique for acquiring both qualitative and quantitative information about any electroactive species (i.e. a species that can be oxidized and/or reduced) involved in electrochemical reactions.

This reversible technique has proven to be very useful in obtaining information about fairly complicated electrode reactions [14].

It consists of applying a linear potential (*E*) sweep at a steady scan-rate to a working electrode (*WE*), leading to sequential linear potential increases or decreases between minimum and maximum potential limits. The CV plot measures the resulting electrical current at the electrode surface (*I*) against the applied potential. The application of this potential sweep is controlled by a reference electrode and has a triangular waveform when plotted against time [15], with minimum and maximum potential limits established within the procedure (Figure 3.2).

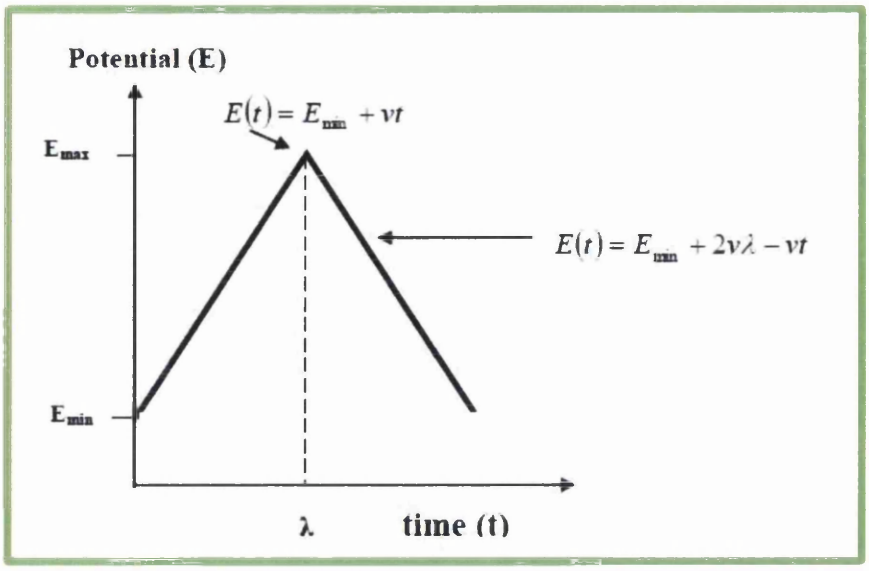

Figure 3.2 - Variation of the applied potential to the WE with the time in CV: E_i- Initial potential; E_f- final potential; E_{min}– minimum potential; E_{max} - maximum potential, t_x- time for the reverse scan.

The electrical current response of the electrode *versus* the applied potential constitutes the cyclic voltammogram and has different characteristics according to the type of redox system involved. The shape of the observed voltammogram depends on the reversibility of the redox couple (O/R), and/or the electrostatic repulsive or attractive forces. Regarding the redox couples, these can be subdivided in to reversible, quasi-reversible and irreversible categories.

3.5.1.1.1 Reversible systems

In the CV of reversible systems, where the kinetics of the couple O/R is fast enough to keep the electron transfer process in equilibrium, the product of the initial oxidation or reduction is oxidized or reduced, on reversing the scan direction. The typical response of such reversible redox process may be seen in Figure 3.3.

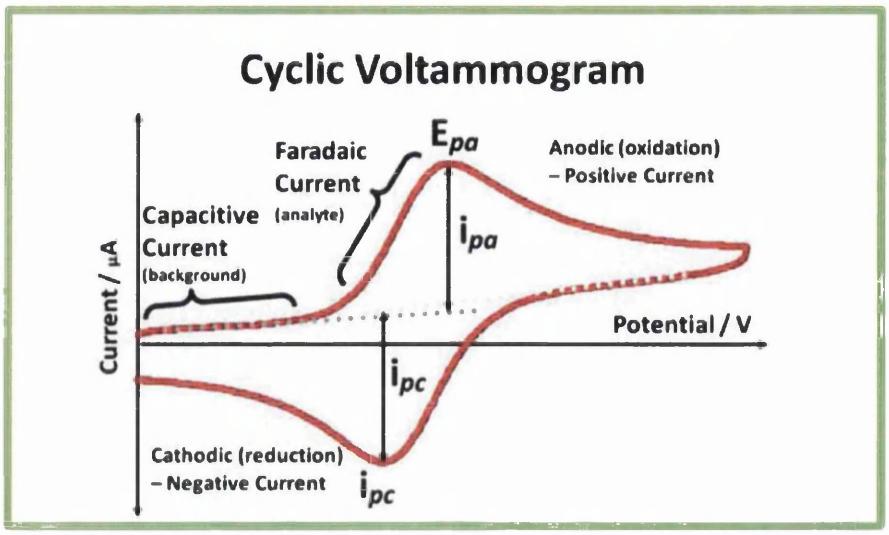

Figure 3.3 - Typical voltammogram for a reversible system.

Assuming that the scan starts at a positive potential, when the electrode potential reaches the potential of the redox couple (E^0), reduction begins and current starts to flow. As the potential shifts to more negative values, the surface concentration of oxidized species decreases and the current increases. As the potential moves past E° towards more negative values, the concentration of the oxidized species at the surface drops to nearly zero, mass transfer of species to the surface reaches a maximum rate, and then declines as the depletion of the reducing species from the diffusion layer effect sets in, thus generating a peak. A similar but opposite peak may be observed in the reverse scan, provided that a reversible redox system is present. The reduced species generated in the forward half-cycle are re-oxidized and the anodic peak appears.

The first theoretical analysis of the wave shape for a reversible system was achieved by Randles and Sevcik [16]. The Randles-Sevcik equation allows determination of the peak current (I_p):

$$I_p = (2.69 \times 10^5) n^{3/2} A D^{1/2} v^{1/2} C \qquad (3.1)$$

In this equation, n is the number of electrons involved in the reaction, A is the electrode surface area (cm^2), D is the diffusion coefficient ($cm^2\ s^{-1}$), C is the bulk concentration of the species ($mol\ dm^{-3}$), v is the scan-rate ($V\ s^{-1}$), and I_p is the peak current. Overall, the information

provided by the Randles-Sevcik equation can be presented in the form of an analysis tool for cyclic voltammograms of reversible systems [13] using the following conditions:

$$I_p \sim \nu^{1/2} \quad \textbf{(3.2)}$$

$$E_p \text{ independent of the } \nu \quad \textbf{(3.3)}$$

$$\left| E_p - E_{p/2} \right| = (RT/nF) \quad \textbf{(3.4)}$$

$$\Delta E_p = \left| E_{Pa} - E_{Pc} \right| \neq 0 = (2.3RT / nF) = 59 / n \quad \textbf{(3.5)}$$

$$\left| I_{pa} / I_{pc} \right| = 1 \quad \textbf{(3.6)}$$

where E_p the peak potential, E_{pa} is the peak potential anode, E_{pc} is the peak potential cathode, R is the gas constant or resistance, T is temperature and F faraday, n is the number of electrons involved in overall electrode reaction.

When all these conditions are verified simultaneously, the peak separation can be used to determine the number of electrons involved in the electron transfer process of reversible systems.

3.5.1.4 Irreversible and quasi-reversible systems

In irreversible processes the electron transfer kinetics is very slow-moving compared to the time-scale of the sweep. In such a condition, concentrations of the oxidized and reduced species do not follow the Nernst equation (relates the numerical values of the concentration gradient to the electric gradient that balances it) and the individual O/R peaks are reduced in size and widely separated. This means that totally (O/R) irreversibility is characterized by a shift of the

peak potential with sweep rate and peak intensity [17]. In irreversible systems the linear potential sweep and CV lead to the same voltammetry profile, since no reverse peaks appear on changing the sweep direction, which means that re-reduction or re-oxidation cannot occur (Figure 3.4).

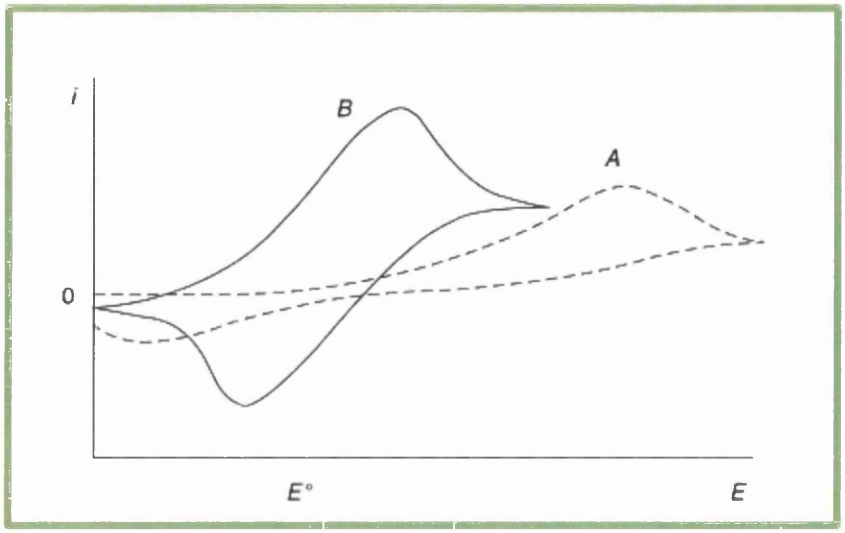

Figure 3.4 - Electrochemically-irreversible voltammogram (curve A) and quasi-reversible (curve B).

In order to observe the net current, the forward process must be so strongly activated, by application of overpotential, that the reverse reaction is virtually completely inhibited [13].

In a completely irreversible processes the peak current (I_p) is given by:

$$I_p = (2.99\times10^5)\alpha^{1/2} n^{3/2} A D^{1/2} \nu^{1/2} C \qquad (3.7)$$

From Equation 3.7 it is clear that the peak current (I_p) for the oxidized or reduced species is still directly proportional to the concentration of the species (C) and to the square root of the scan rate ($\nu^{1/2}$), but is lower when compared with reversible systems because of the shape of the peak.

From the information provided by equation 3.7 the following diagnostic criteria for cyclic voltammograms of totally irreversible systems may be deduced:

$$I_p \sim \nu^{1/2} \tag{3.8}$$

E_p independent of the ν **(3.9)**

$$\left| E_p - E_{p/2} \right| = \frac{47.7}{\alpha n} \tag{3.10}$$

$$\Delta E_p = \left| E_{Pa} - E_{Pc} \right| \geq 59/n \tag{3.11}$$

$$\left| I_{pa} / I_{pc} \right| = 1 \tag{3.12}$$

Electrode processes are not always easy and fast (reversible systems) or very slow (irreversible systems), and sometimes we must consider the whole voltammogram characteristics. In such *quasi-reversible* or *quasi-nerstian* systems, the net current, which is controlled by both the charge transfer and mass transport, involves activated components from the forward and reverse charge transfers. In these systems the reverse peak appears but is smaller than the forward peak. For electrochemically quasi reversible reactions, the surface concentration is controlled both by kinetics and diffusion processes.

The peak shape and associated parameters can be expressed by a parameter, Λ, which is a quantitative measure of the reversibility, being effectively defined as the ratio of kinetics/transport:

$$\Lambda = \frac{k_0}{(D_o^{\alpha_a} D_R^{\alpha_c} \alpha)^{1/2}} = \frac{k_0}{(D_o^{1-\alpha^c} D_R^{\alpha_c} \alpha)^{1/2}} \tag{3.13}$$

$$\sigma = v(nF / RT). \qquad (3.14)$$

Where K_0 is the rate constant, D the diffusion coefficient, α transfer coefficient and σ surface excess charge density.

When the diffusion coefficients of the oxidized and reduced species are equal $D_o = D_R = D$ the equation can be rewritten:

$$\Lambda = k_o D^{-1/2} \sigma^{-1/2} \qquad (3.15)$$

Showing that when the scan rate (v) increases, and σ is high, the reversibility degree is low and Λ is small.

The parameter Λ can be estimated by using the parameter ψ, a numerical approach, which expresses the relation between the separation of the anodic and cathodic peaks with the degree of reversibility (Equation 3.16):

$$\psi = \Lambda \pi^{1/2} = \frac{k_0}{(D\pi v \frac{nF}{RT})^{1/2}} \qquad (3.16)$$

where π is surface pressure.

As a general conclusion, when ψ increases, at very slow sweep rate (v), the system approaches reversibility. For small values of ψ, at very fast sweep rate, the system exhibits an irreversible behaviour in which there is a decrease in the peak current relative to the reversible case and increasing separation between the anodic and cathodic peaks.

3.5.1.5 Electrochemical impedance spectroscopy

Electrochemical Impedance Spectroscopy (EIS) is a widely used technique for the characterization of electrochemical systems. The electrical resistance is a very well-known

concept, corresponding to the ability of a circuit element to resist the flow of electrical current. Ohm`s law (Equation 3.17) defines resistance (R) in terms of ratio between voltage (E) and current (I), as follow:

$$R = \frac{E}{I} \tag{3.17}$$

This equation is applied to only one circuit element, the ideal resistor. The ideal resistor displays several simplifying proprieties including: i) it follows Ohm´s law at all current and voltage levels; ii) its resistance value is independent of frequency; iii) AC (alternating current) and voltage signals through a resistor are in phase with each other.

Impedance is a measure of the ability of a circuit to resist the flow of electrical current, but it is not limited by the simplifying proprieties listed above. The impedimetic approach consists in the application of a small sinusoidal excitation signal to the WE of the electrochemical system under investigation and measurement of the subsequent response of the system.

In EIS, the current signal can be analyzed as a sum of sinusoidal functions. The potential and the current changes with the time are represented by a sinusoidal function. Figure 3.5 shows a typical graph that illustrates the relationship between two related sinusoidal signals, such as AC and E signals rotating at the same angular frequency (ω).

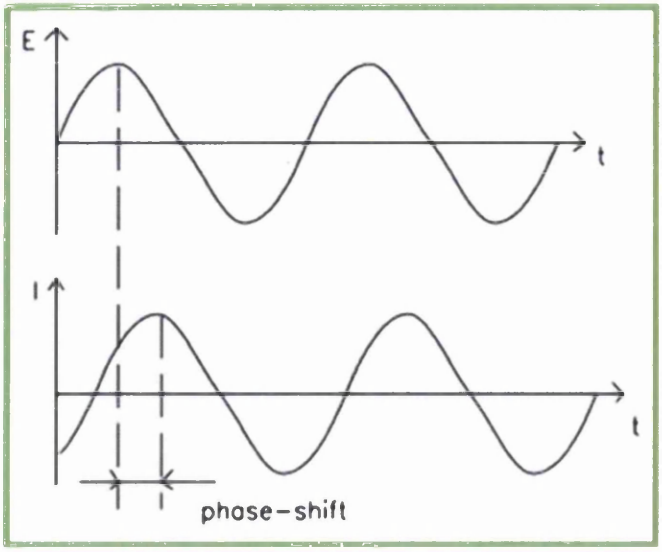

Figure 3.5 - Sinusoidal current response in a linear system after applying an alternating current.

Normally, in a linear system, as shown in Figure 3.5, the current response to an applied sinusoidal potential perturbation is sinusoidal at the same frequency but differs in phase and amplitude from the applied signal. Consequently, their phases will be separated by a certain phase angle (ϕ).

EIS measurements can take from some minutes to hours, depending on the selected frequency range. The time required to measure the EIS should be adapted to each system, otherwise EIS analysis tools may give inaccurate results due the growth of an oxide layer, adsorption of solution impurities, coating degradation, temperature changes, and so on [17].

The application of a purely sinusoidal voltage to the electrode/electrolyte solution interface, expressed as a function of time, has the form:

$$E(t) = E_0 \sin(\omega t) \qquad \textbf{(3.18)}$$

Where E(t) is the applied voltage at a time t, E_0 is the oscillation amplitude of the excitation signal, and ω is the angular frequency of the sinusoidal excitation (rad s^{-1}). ω is 2π times higher than the conventional frequency (Hz) in agreement with the equation 3.19:

$$\omega = 2\pi f \tag{3.19}$$

In linear systems, the current response (I), which has different oscillation amplitude (I_0) and is shifted in phase (ϕ) relatively to the excitation signal, is expressed by:

$$I(t) = I_0 \sin(\omega t + \phi) \tag{3.20}$$

The electrical impedance of the system (Z) is defined as the proportionality factor between the applied potential perturbation and the current response. Using an expression analogous to Ohm's law, one calculates the impedance of sinusoidal system as follows:

$$Z = \frac{E(t)}{I(t)} = \frac{E_0 \sin(\omega t)}{I_0 \sin(\omega t + \phi)} = Z_0 \frac{\sin(\omega t)}{\sin(\omega t + \phi)} \tag{3.21}$$

Where the impedance (Z) is characterized by the magnitude (Z_0) and phase angle (ϕ). Using Euler's equation:

$$\exp(j\phi) = \cos(\phi) + j\sin(\phi) \tag{3.22}$$

It is possible to express the impedance as a complex function. In this way, the potential is described as:

$$E(t) = E_0 \exp(i\omega t) \tag{3.23}$$

Where i is the imaginary number defined as $i = (-1)^{1/2}$.

Thus, the impedance can be represented as a complex number:

$$Z = Z_0 \frac{\exp(j\omega t)}{\exp[j(\omega t - \phi)]} = |Z|\exp(j\phi) = |Z|(\cos\phi + j\sin\phi) \quad \textbf{(3.24)}$$

Equation 3.25 states that in the complex plane, the impedance is composed of real $(Z' = Z_0 \cos\phi)$ and imaginary $(Z'' = Z_0 \sin\phi)$ parts, at any value of ω, as follows:

$$Z = Z' + j\,Z'' \quad \textbf{(3.25)}$$

$$Z_{\equiv} = \frac{1}{\frac{1}{R_2} + jwc} = \frac{\frac{1}{R_2} - jwc}{\left(\frac{1}{R_2}\right)^2 + w^2 c^2} = \frac{R_2 - jR_2^2 wc}{1 + R_2^2 w^2 c^2} \quad \textbf{(3.26)}$$

$$Z'_{eq} = R_1 + \frac{R_2}{1+(R_2 wc)^2}\,;\; Z'(0) = R_1 + R_2\,;\; Z'(\infty) = R_1 \quad \textbf{(3.27)}$$

$$Z''_{eq} = -\frac{R_2^2 wc}{1+(R_2 wc)^2}\,;\; Z''(0) = 0;\; Z''(\infty) = 0 \quad \textbf{(3.28)}$$

A Nyquist plot is obtained by plotting the real part (Z`) on the X-axis and the imaginary part (Z``) on the Y-axis of a chart (Figure 3.6). In this plot the Y-axis is negative and each point is the impedance at a specific angular frequency (ω).

As it is indicated in the Figure 3.6, low frequency data are on the right side of the plot and higher frequencies are on the left. However, this criterion is only valid for electric circuits in EIS data where the impedance usually decreases as frequency increases. Furthermore, on the

Nyquist plot, the impedance can be represented as a vector of length $|Z|$. The angle between this vector and the X-axis, generally called as a phase angle, is defined as $\phi = \arg Z$.

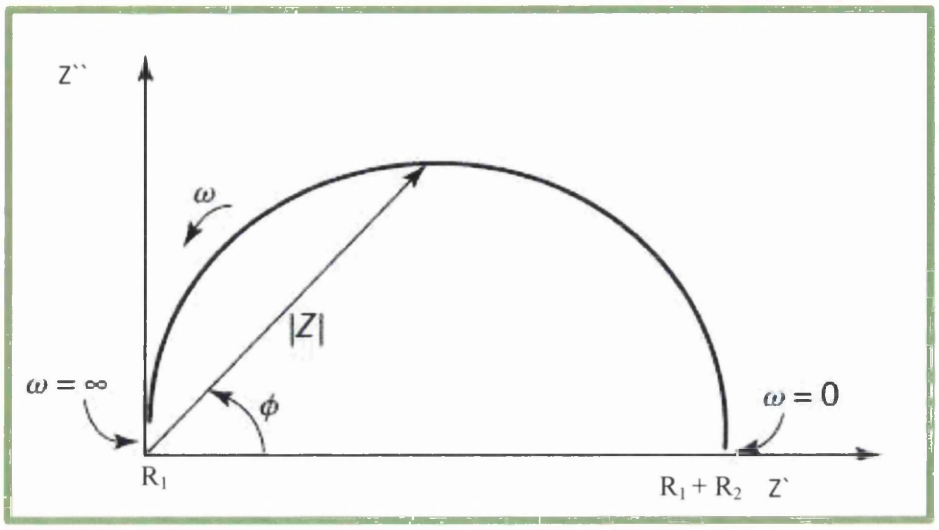

Figure 3.6 - Nyquist plot that illustrates both real (Z′) and imaginary (Z″) components of impedance at each ω.

The Nyquist plot gives a quick overview of the EIS data, allowing some qualitative interpretations. The semicircle presented in Figure 3.6 is characteristic of a simple equivalent electrical circuit.

3.5.1.6 Commom Equivalent Electrical Circuit Models

The characterization of the electrochemical systems with impedance spectroscopy requires the interpretation of the data with the help of suitable equivalent circuit models. These models can be divided into two broad categories: equivalent electrical circuit models and process models (consists in developing mathematical methods based on the kinetics of heterogeneous reactions involved). The models are regressed to experimental data in order to estimate the parameters that can be used to describe, interpret and fit the impedance data adequately. The models can also be used to predict the behaviour of the system under different conditions [18].

3.5.1.6.1 Randles Equivalent Circuit: The R(RC) Equivalent Circuit

The Randles equivalent circuit, *R(RC)*, is one of the simplest and most commom equivalent circuit models. It includes a solution resistance (R_Ω), a double layer capacitance (C_{dl}) or a constant phase element (*CPE*), and a charge transfer (R_{CT}) or a polarization resistance (R_p). This model assumes that the double layer capacitance is in parallel with the charge transfer resistance. In addition, to being a useful model in its own right, the simplified Randles equivalent circuit is often the starting point for other more complex models. The simplified Randles equivalent circuit, *R(RC)*, is shown in Figure 3.7. An example of a Nyquist plot for this model is shown in Figure 3.8 [19].

The Nyquist plot for a simplified Randles equivalent circuit is always a semicircle. The solution resistance (R_Ω) can be found by reading the real axis value at the high frequency intercept. This is the intercept near the origin of the plot. The real axis value at the other intercept is the sum of the solution resistance and the charge transfer resistance ($R_\Omega + R_{CT}$). The diameter of the semicircle is therefore equal to the charge transfer resistance.

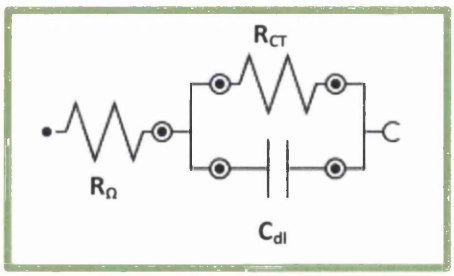

Figure 3.7 - Typical simplified Randles equivalent circuit (R(RC)).

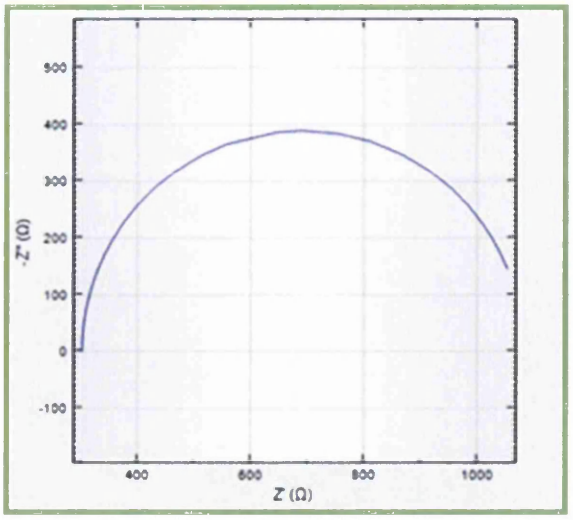

Figure 3.8 - Typical Nyquist plot for a simplified R(RC) Randles equivalent circuit.

3.6 Experimental characterisation methods

3.6.1 Scanning Electron Microscopy (SEM)

The scanning electron microscope (SEM) uses a focused beam of high-energy electrons to generate a variety of signals at the surface of solid specimens. The signals that derive from electron-sample interactions reveal information about the sample including morphology (texture), chemical composition, crystalline structure and orientation of the materials making up the sample. In most applications, data are collected over a selected area of the sample surface, and a 2-dimensional image is generated that displays variations in these properties, spatially [20].

The Hitachi S-4800 field emission scanning electron microscope features a maximum resolution of 1.0 nm and a variable acceleration voltage of 0.5 - 30 kV (0.7nm at 30kV; 1.0nm at 15kV; 1.4nm at 1kV). Both secondary electron and backscattering electron detectors are available for imaging. It features an image capture system for digital storage of images and image files can be transferred through network or USB drive. It can handle samples from piece-parts to 6" wafers. The stage can rotate 360° and tilt -5° to 70°. It provides scanning transmission electron microscope (STEM) imaging capability from 100V to 30kV, which may be useful for STEM imaging in biological samples that cannot withstand 200kV accelerating voltage in standard transmission electron microscope (TEM).

SEM provides optimum resolution and high beam current for fast and accurate analytical X-ray mapping and quantitative analysis. It gives the elemental composition of sample and a lateral resolution depends on beam energy and the sample properties.

The Hitachi S-4800 is equipped with both a lower and upper secondary electron detector system. The lower detector is utilised for enhanced surface topography imaging while the "through the lens" upper detector is utilized for high resolution imaging.

3.6.2 X-ray Photoelectron Spectroscopy (XPS)

X-ray photoelectron spectroscopy (XPS) detects the quantity of elements on a sample surface. It operates on the photoelectric effect, by exciting core electrons on a sample surface and recording both the number and energy of the resulting ejected electrons. Since the energy of the ejected electrons is specific to an element, the identity of the element can therefore be determined. This technique detects all elements except hydrogen and helium.

When a sample is irradiated with an energetic electromagnetic wave with a certain frequency, υ, some core electrons capture the energy and escape from the material. The kinetic energy of these ejected electrons, K.E., is given by:

$$K.E. = h\upsilon - B.E. - \Phi \qquad \textbf{(3.29)}$$

where h is the Planck's constant, B.E. the binding energy of the electrons, and ϕ the work function of the spectrometer. The binding energy of core electrons in a specific element is known and it is usually in the range of 0 to 1100eV depending on the electronic structure of the atom. Each element has a unique set of core electrons and their energy states are characteristic of that element [21]. As a result, the number of ejected electrons is recorded as a function of their binding energy in order to identify the element and its abundance. This technique is sensitive to the outermost few nanometers of the sample surface, since only the electrons near the surface can overcome inelastic collisions with neighboring atoms to reach the detector.

XPS can also be used for detecting elements at different depths in a sample (Figure 3.9). This is particularly relevant to this study since the samples were surface-modified and did not have uniform chemical compositions at all depths. This function is achieved by varying the take-off angle between the sample surface and the detector. When the take-off angle is increased, a larger number of electrons are able to escape from the bulk by traveling a shortener

distance within the sample, and thus the sample is examined to a greater depth [22]. The number of detected electrons, N, is related to the depth via

$$\frac{N}{N_0} = e^{\frac{-t}{\lambda \sin\theta}} \qquad \textbf{(3.30)}$$

where N_0 is the number of electrons produced at depth, t the time, λ is the mean free path of the electron, and θ is the take-off angle.

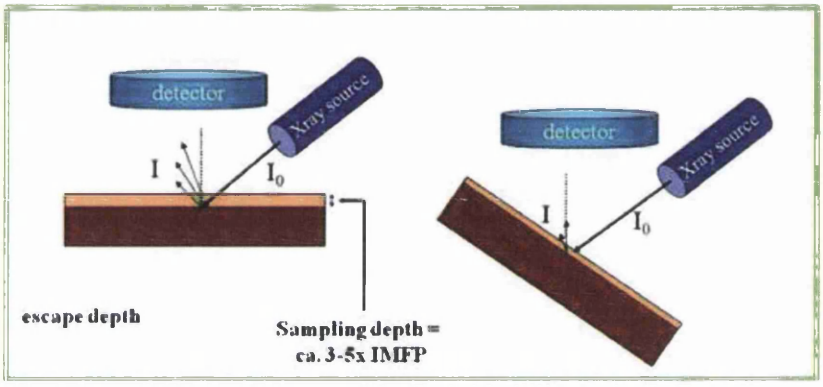

Figure 3.9 - X-ray photoelectron spectroscopy at different depths in a sample.

The value of λ for electrons in a solid is greatly dependent on the kinetic energy of the electron and the relationship between the two is shown in Figure 3.10 [21].

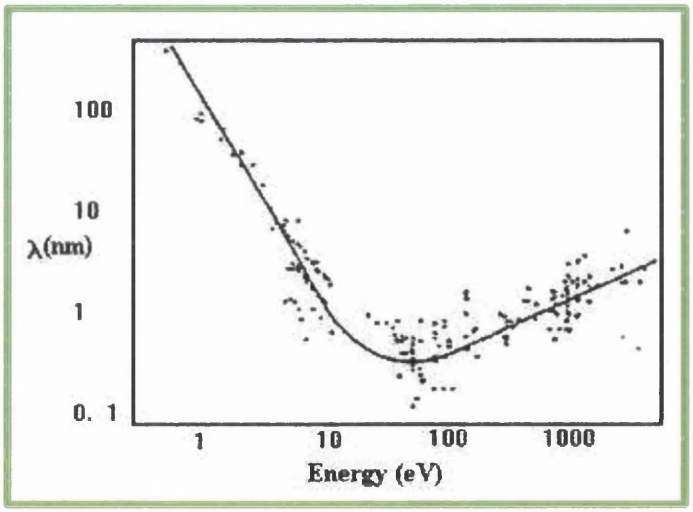

Figure 3.10 - The dependence of the mean free path λ on the emitted electron energy [21].

3.6.3 Atomic Force Microscopy (AFM)

Atomic force microscopy (AFM) investigates surface features at micro to nanoscopic resolution.

AFM images are acquired by measuring the deflections of the cantilever due to the interactions between the tip and the surface. The tip-surface interaction encompasses a variety of forces that can be van der Waal's, electrostatic, magnetic, etc.. As a result, this technique can be applied to both conducting and insulating materials.

The deflection of the cantilever is governed by Hooke's law,

$$F = -Kx \tag{3.31}$$

where F is the restoring force exerted by the cantilever that corresponds to the tip-surface force, K is the spring constant, that depends on the elasticity of the cantilever material, and x is the displacement of the cantilever from its position of equilibrium. In theory, there are two major modes of operation: contact mode and tapping mode. In the contact mode, the tip is maintained at a fixed height above the surface and the tip-surface forces are measured continuously as the tip scans across the surface. The output signals are converted to height information of the surface and plotted against their spatial positions on the sample. This operation mode may cause undesired damage to the sample when the tip touches the surface. In the tapping mode, the height of the tip is varied to maintain a constant force between the tip and the surface. Again, the output signals are converted to height information of the surface and plotted against their positions. This mode helps to preserve the surface features of a sample.

Attractive, as well as repulsive forces, exist between tip and sample atoms. The variation of the force as a function of distance is shown in Figure 3.11.

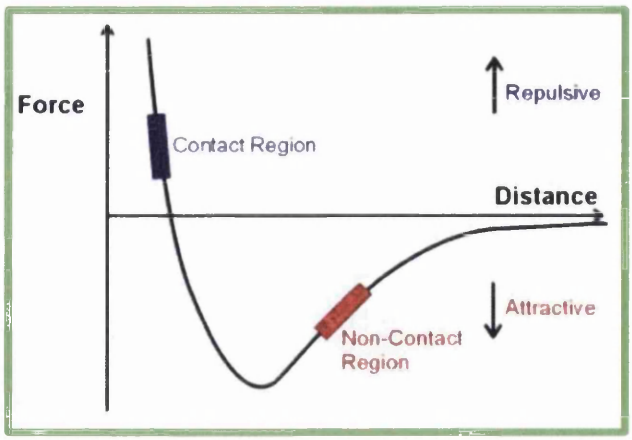

Figure 3.11 - Plot of the forces between tip and sample.

In practice, the constant-height mode is realized using contact mode AFM. The tip maintains contact with the surface usually through an adsorbed fluid layer on the sample surface. The tip-surface interaction is usually dominated by short-range interatomic forces, which are measured by measuring static cantilever deflections [23].

Tapping mode AFM operates by scanning a tip across a sample surface (Figure 3.12).

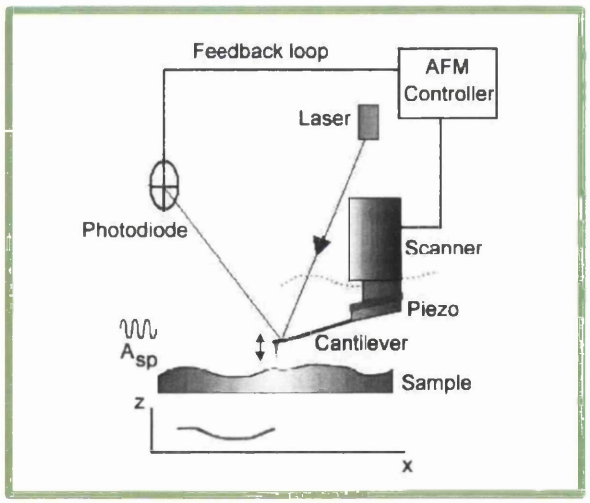

Figure 3.12 - Atomic force microscope components and operation schematic [24].

3.6.4 Contact angle (CA)

The contact angle can be defined in several ways. Qualitatively, a contact angle is the macroscopic representation of microscopic phenomena. Microscopic characteristics such as surface roughness, surface energies and surface chemistry of the materials involved, and surface coatings play a role in the wettability of a material for a given fluid, usually water. Quantitatively, a contact angle is the interior angle formed by the substrate being studied and the tangent to the drop interface at the apparent intersection of all two interfaces. This intersection is called the contact line. Figure 3.13 illustrates the tangent line and contact angle of a liquid drop on a surface. Historically a static contact angle on a flat surface is defined by the Young Equation (Equation 3.29) [25] using interfacial surface tensions between solid and liquid. Young's equation is essentially a force balance in the horizontal direction. The contact angle may also be directly measured to calculate the ratio of interfacial surface tensions if the interfacial surface tensions are unknown.

Young's Equation provides the basis for a quantitative description of wetting phenomena. If a drop of liquid is placed on a solid surface, two possibilities exist:

1) Liquid spreads on the surface completely (contact angle $\Theta = 0$)

2) Liquid establishes a finite contact angle

$$Y^{SV} = Y^{Sl} + Y^{lV} \cos\theta \qquad \textbf{(3.32)}$$

where θ is the contact angle, Υ^{Sl} is the solid/liquid interfacial free energy, Υ^{SV} is the solid surface free energy and Υ^{lV} is the liquid surface free energy.

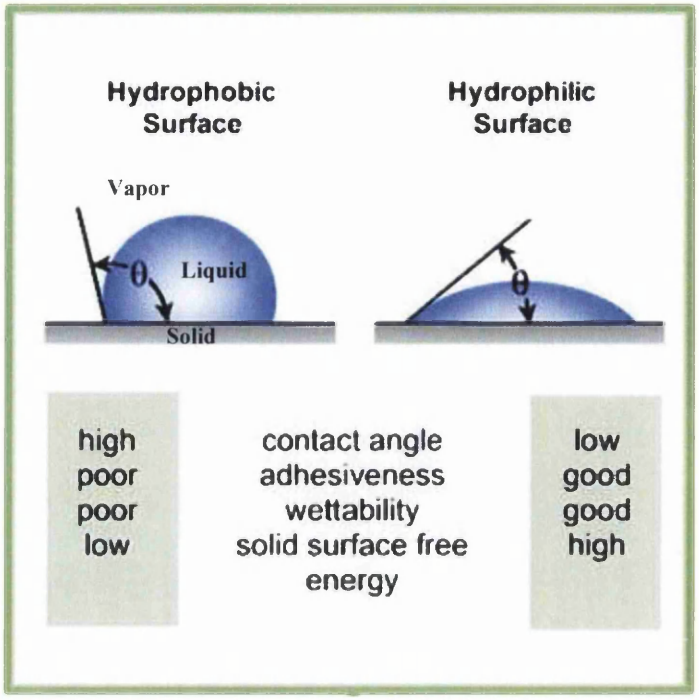

Figure 3.13 – Conditions for hydrophobic and hydrophilic surface in contact angle.

Young's equation is used to describe the interactions between the forces of cohesion and adhesion between sample and fluid and measure what is referred to as surface energy.

A drop with a contact angle over 90° indicates a hydrophobic surface. This condition is exemplified by poor wetting, poor adhesiveness and the solid surface free energy is low. A drop with a small contact angle indicates a hydrophilic surface. This condition reflects better wetting, better adhesiveness, and higher surface energy.

Contact angle measurements are used to study the hydrophobicity/hidrophilicity of samples surfaces before and after surface modification.

3.6.5 Raman Spectroscopy

Raman spectroscopy is a technique employed for studying vibrational, rotational, and other low-energy modes in a material. It is based on inelastic scattering of monochromatic light (e.g., laser light). When, the light beam is directed towards the sample, the energy of the light photons changes after interacting with the atoms of the sample. Light photons are absorbed by the sample and then reemitted. The energy of the reemitted photons is higher or lower relative to the incident energy, a phenomenon known as the Raman Effect. This change in energy yields

information about vibrational, rotational and other low frequency modes of the material under analysis. Raman spectroscopy is an extremely important spectroscopic technique for analyzing graphene, as graphene's vibrational and electronic structure is distinctively captured in its Raman spectrum. Raman fingerprints for single layer, bilayer, and multi-layer graphene allow for a reliable nondestructive characterization of graphene. Vibrational modes of graphene are important to comprehend the Raman spectra [26].

The most prominent features in the Raman spectra of graphene are the G band (~1582cm-1), the 2D band (~2700cm-1) and the disorder-induced D band (~1350cm-1), at about half of the frequency of the 2D band, under 2.41 eV laser excitation [26]. The G band is related with the in-plane TO (transverse optical) and LO (longitudinal optical) vibrations. The G band is the only band in graphene originator from a standard first order Raman scattering process. The 2D and D bands come from a second-order process, involving two TO phonons near the K point for the 2D band and one TO phonon and one defect in the case of the D band [27,28].

In contrast to infrared spectroscopy, where the transition from the ground vibrational state to the first excited vibrational state is monitored, access to vibrational transitions is achieved quite differently for Raman measurements. In Raman spectroscopy the sample is excited with a laser. The Raman effect is a scattering phenomenon, such that the laser light is 'scattered' by the molecules. Most of the scattered radiation will have the same energy as the original light and this type of scattering is called Rayleigh scattering. This elastically scattered light is eliminated using an efficient blocking filter. A very small part of the laser light (around 1 photon out of 1,000,000 or less) undergoes a slight energy change, i.e., the light is shifted from its original frequency, and this is called the Raman shift.

Raman can yield information about: crystallite size; clustering of the sp^2 phase (the presence of multiple layers of graphene); the presence of sp^2-sp^3 hybridization and the introduction of chemical impurities; substrate influence on graphene; the influence of functionalisation of graphene on the Fermi level in graphene; the magnitude of the mass density; the optical energy gap; elastic constants; doping; defects and other crystal disorder; edge structure; strain, number of graphene layers which make graphene unique [29].

3.7 Graphene device fabrication process

3.7.1 Diagram

Graphene that has been grown epitaxially or transferred onto an appropriate substrate can be processed using standard semiconductor techniques.

The objective was to fabricate a device whose channel can be used as a graphene sensor resistance. This graphene channel can be chemically or biologically functionalized, and the change in electrical properties of the device used to detect the presence of certain analytes. Specifically, changes in the resistivity of graphene channel devices have been used to detect the hCG biomarker. The fabrication process for the sensor device, prior to any functionalization, is illustrated in Figure 3.14.

First generation devices consisted of a channel between two metal contact pads. However, the contact resistance of the pads seemed to vary greatly and to have a significant contribution relative to the channel resistance. Therefore, in order to measure accurately the channel changes in resistance, 4-point measurement devices were also fabricated.

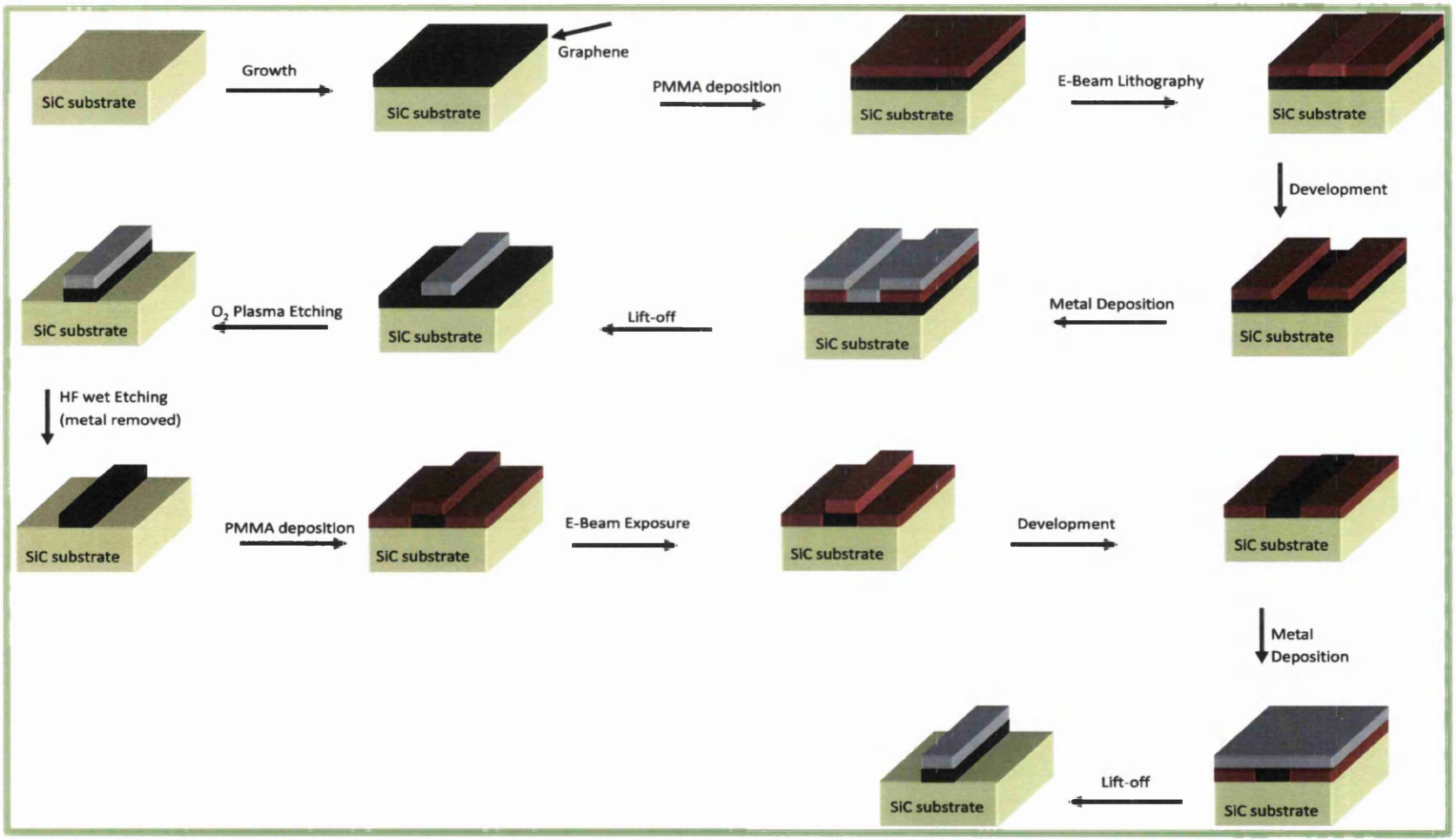

Figure 3.14 - Schematic of the fabrication process of the device.

Electron beam lithography (EBL) was used to fabricate the devices. It is a more flexible technique than standard UV lithography, since the patterns can be adjusted easily where in UV lithography as a new photomask would have to be made each time the device design was modified. Also, patterned graphene proved very difficult to observe optically and therefore difficult to overlay 2nd mask layers on, whereas the contrast between graphene and SiC was much greater if observed with electron microscopy due to the very different conduction properties between both materials. Thus, alignment of devices features was easier to achieve using EBL.

3.7.2 Materials

Silicon carbide (SiC) was purchased from Cree Research Inc. N-type 4H-SiC carbon face (000-1) and silicon face (0001), on axis, semi insulating with a Chemical Mechanical Polishing (CMP) polished silicon face was used.

3.7.3 Graphene growth

Graphene was grown epitaxially on 4H-SiC by annealing at temperatures above 1500°C. At these temperatures, Si atoms sublime from the SiC surface, leaving carbon atoms to reconstruct into graphene. The number of graphene layers produced can be controlled by optimization of the growth conditions such as the growth temperature and the pressure.

Details of specific growth conditions can be found in each subsequent device chapter.

3.7.4 The fabrication process

The fabrication process involves a three-layer electron beam lithography process.

Firstly the graphene layer is patterned, then the metal layer, and lastly the channels, so that the graphene modification reactions can be performed without interference with the metal contacts. This third layer is referred to as the "Fenton window", which is required as the Fenton reaction seemed to react with the metal contact, thus requiring this extra layer to prevent any reaction. The device design is presented in Figure 3.15. The active areas exposed through the Fenton window are 25μm and 50 μm in width, and 1mm long.

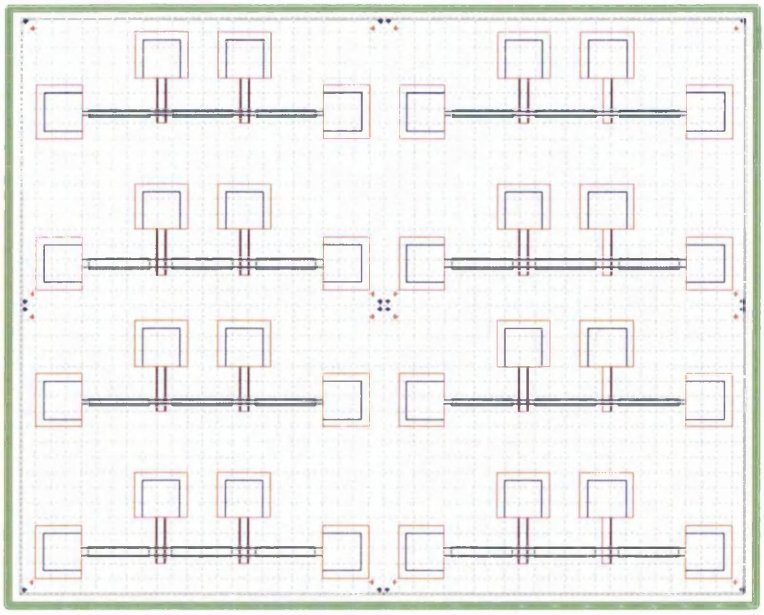

Figure 3.15 - Three layer pattern used to create the graphene device. In red is the metal layer, in blue the graphene and in green the Fenton window. The grid lines represent the 100 μm write field used for this pattern.

The first part of the fabrication involves the creation of a graphene channel. The design pattern for the channel consists of both the active area of the device and the contact areas, along with alignment marks for the next layer, as illustrated in Figure 3.16. The graphene sample used for device fabrication was grown using the epitaxial growth method. The sample was firstly coated with PMMA (950K, 2% in chlorobenzene). The PMMA was spun on the surface at 4000RPM for 40s, and then baked at 180°C for 3 min. The sample was then loaded into the electron beam lithography tool, and the first layer was exposed (Figure 3.16 and 3.17).

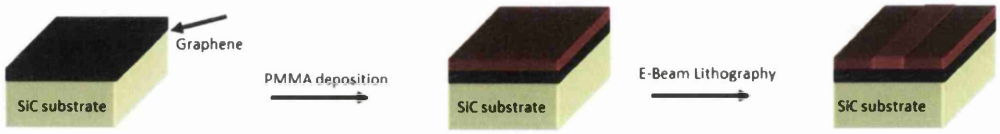

Figure 3.16 – PMMA deposition and E-Beam lithography.

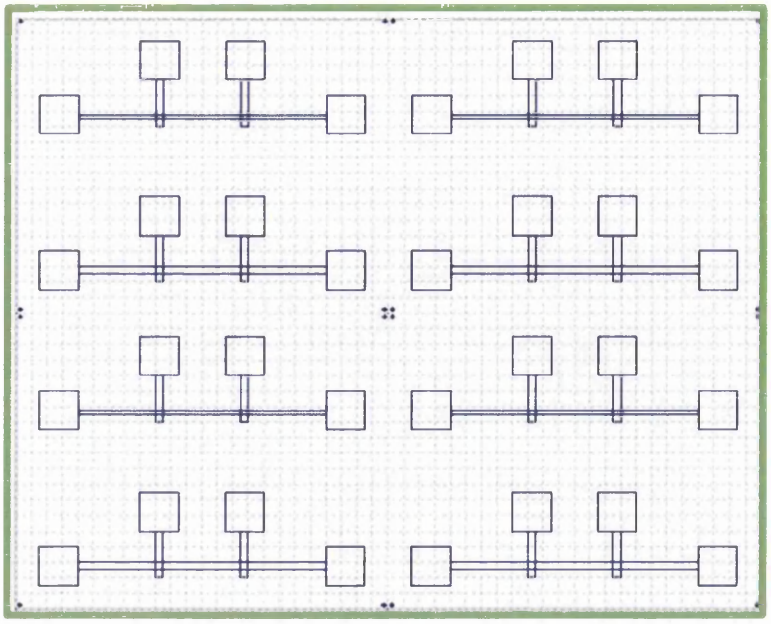

Figure 3.17 - Graphene layer pattern. The outline areas are all graphene. The rest of the areas expose the SiC substrate.

The exposure settings were as follows:

- ✓ an aperture of 60μm, yielding a beam current of 0.957641nA
- ✓ an acceleration voltage of 10kV
- ✓ a write field size of $100\mu m^2$
- ✓ an area dose of 160μC/cm2
- ✓ a step size of 0.05μm, yielding a dwell time of 4.177μs, and a beam speed of 15mm/s

The sample was developed using Methyl isobutyl ketone (MIBK) in isopropanol (1:3) for 1 min and stopped using isopropanol (IPA) for 30 sec. A 50nm layer of aluminium was then sputtered onto the patterned graphene sample (Figure 3.18). Metal sputtering was performed in a Lesker 75 PVD system, using the following conditions:

- ✓ a residual system pressure under 10^{-5}Torr
- ✓ an argon flow of 30sccm, providing a pressure of 1.5mTorr
- ✓ a power setpoint of 100W
- ✓ a rotation speed of the sample holder of 1rpm – in order to obtain a uniform deposition

Those conditions yielded a deposition rate of 0.09nm/s

Figure 3.18 – Developing and metal deposition on the sample.

The sample was immersed in acetone, lifting off the areas of resist that were not exposed during the electron beam lithography process, and also the metal on top of them. At this stage in the fabrication process, the result is patterned aluminium on a complete sheet of graphene, corresponding to the pattern written by EBL. The purpose of the aluminium is to act as a mask for the patterning of the graphene layer using an oxygen plasma etching (Figure 3.19).

To selectively remove graphene and pattern the graphene channel, the sample was etched by Reactive Ion Etching (RIE) in an Oxford Instruments Plasmalab 80 Plus. The etch conditions were as follow:

- ✓ a flow of 50sccm of oxygen
- ✓ a pressure of 75mTorr
- ✓ a RF power setpoint of 50W
- ✓ an etch duration of 60seconds

The aluminium layer was removed using hydrofluoric acid (HF), prior to O_2 plasma etching of graphene.

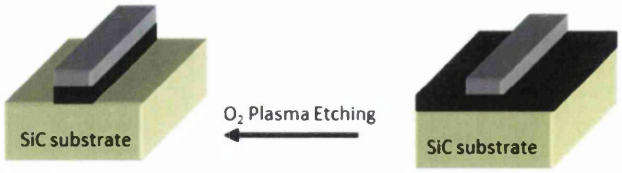

Figure 3.19 – Lift-off and O_2 plasma etching.

The second part of the fabrication of the graphene channel device is the fabrication of metal contacts on the graphene surface, at either end of the graphene channel, in order to be able to apply a bias to the active channel area. An applied bias is required for the electrochemical (characterization of the device) functionalization process and also in order to perform electrical measurements on the device. The sample was firstly coated with PMMA (950K, 2% in chlorobenzene). The PMMA was spun on the surface at 4000RPM for 40s, and then baked at 180°C for 3 min (Figure 3.20).

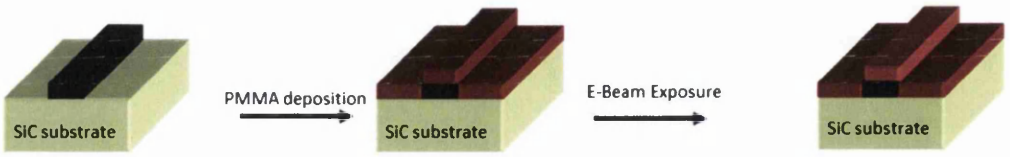

Figure 3. 20 – PMMA deposition and E-Beam exposure.

The sample was then loaded into the electron beam lithography tool, and the second layer was exposed (Figure 3.21). The first set of alignment marks (made out of graphene) permitted this overlay with the first graphene layer, and a second set of alignment marks was added in order to subsequently align with the 3rd mask layer.

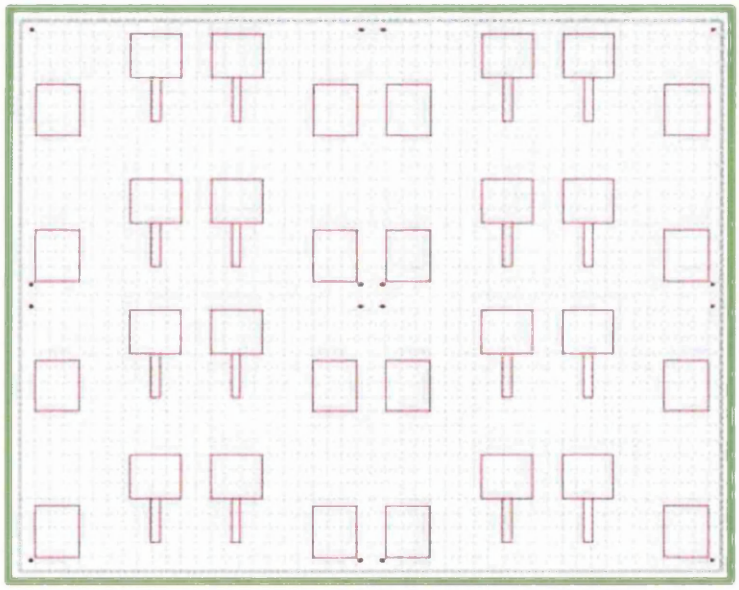

Figure 3.21 - Metal mask layer pattern (2nd layer).

The exposure settings were as follows:

- ✓ an aperture of 60μm
- ✓ e-beam current measured on the faraday cup was 0.969148nA
- ✓ an acceleration voltage of 10kV
- ✓ a write field size of $100\mu m^2$
- ✓ an area dose of $160\mu As/cm^2$

The sample was then developed using Methyl isobutyl ketone (MIBK) in isopropanol (1:3) for 1 min and IPA for 30 sec. A 100nm layer of titanium (interface layer between graphene and gold, to enhance adhesion) and 50nm of gold was then sputtered onto the graphene sample. The chamber pressure is identical to the aluminium deposition, and the deposition rate was 0.06nm/s for the titanium deposition at 100W, and 0.13nm at 45W for the gold deposition. The layers were deposited subsequently without venting the chamber, therefore limiting the oxidation of the Ti layer.

The sample was immersed in acetone, lifting off the areas of resist that were not exposed during the electron beam lithography process, and the metal on top of them. At this stage in the fabrication process, the result is gold/titanium contacts on a graphene channel, corresponding to the pattern written by EBL (Figure 3.22).

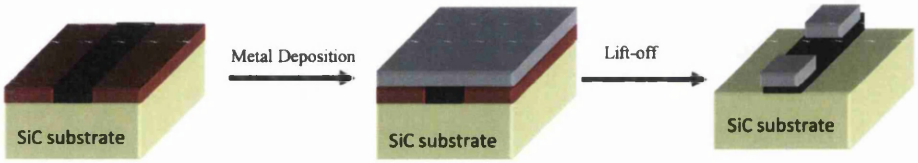

Figure 3.22 – Metal deposition and Lift-off.

The third part of the fabrication of the graphene channel device is the fabrication of a Fenton window on the graphene channel in order to be able to OH-terminate the surface of the active channel area, but avoid the Fenton reagents reacting with the metal contact pads. Again, the sample was firstly coated with PMMA (950K, 2% in chlorobenzene). The PMMA was spun on the surface at 4000RPM for 40s, then baked at 180°C for 3 minutes.

The sample was then loaded into the electron beam lithography tool, and the third layer was exposed (Figure 3.23), using the second set of alignment marks (made of Ti/Au), and developed using Methyl isobutyl ketone (MIBK) in isopropanol (1:3) for 1 min and IPA for 30 sec.

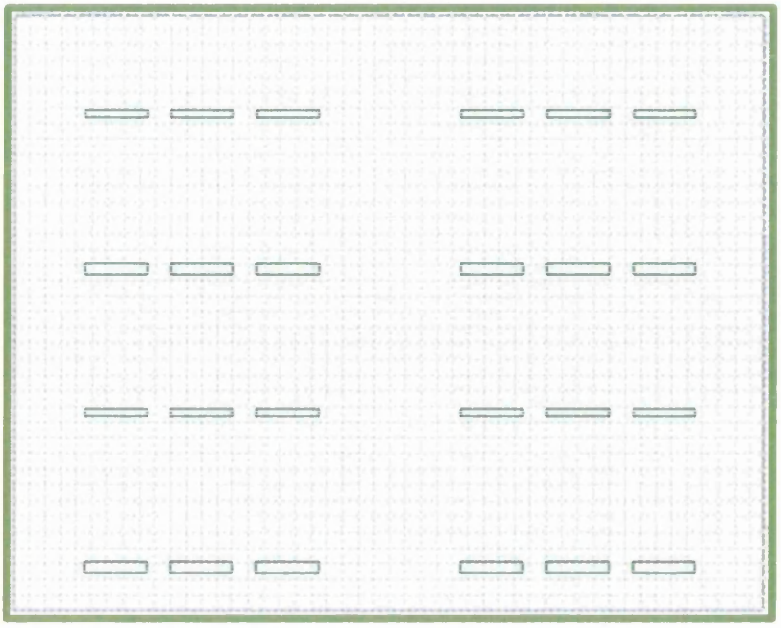

Figure 3.23 - Fenton window layer pattern.

The final device structure is 4 metal contacts pads with a channel between (Figure 3.15). This device structure was used for subsequent development of graphene biosensors.

References

[1] Guy, O.D., D. et al, Diamond and Related Materials, 2006. **15**: p. 1472.

[2] al., G.O.J.e., Applied Surface Science, 2008. **254**: p. 8098.

[3] A. J. Van Bommel; J. E. Crombeen, a.A.V.T., *LEED and Auger electron observations of the SiC (0001) surface.* Surface Science, 1975. **48**: p. 463-472.

[4] C. Berger; Z. Song; X. Li; X. Wu, N.B.C.c.N.D.M., T. Li; J. Hass; A. N. Marchenkov; E. H. Conrad; P. N. First and W. A. de Heer, *Electronic Confinement and Coherence in Patterned Epitacial Graphene.* Science 2006. **132**: p. 1191-1196.

[5] J. Robinson; X. Weng; K. Trumbull; R. Cavalero; M. Wetherington; E. Frantz; M. LaBella; Z. Hughes, M.F.a.D.S., *Nucleation of epitaxial Graphene on SiC(0001).* ACS Nano 2012. **4**: p. 153-158.

[6] Nguyen Xuan, V., et al., *Gold-linked electrochemical immunoassay on single-walled carbon nanotube for highly sensitive detection of human chorionic gonadotropin hormone.* Biosensors & bioelectronics, 2013. **42**: p. 592-597.

[7] Zhang, Y., et al., *Magnetic beads-based electrochemiluminescence immunosensor for determination of cancer markers using quantum dot functionalized PtRu alloys as labels.* Analyst, 2012. **137**(9): p. 2176-2182.

[8] Wani, T.A. and I.A. Darwish, *An automated flow immunosensor based on kinetic exclusion analysis for measurement of a free beta-subunit of human chorionic gonadotropin in serum.* New Journal of Chemistry, 2012. **36**(4): p. 1114-1120.

[9] Truong, L.T.N., et al., *Labelless impedance immunosensor based on polypyrrole-pyrolecarboxylic acid copolymer for hCG detection.* Talanta, 2011. **85**(5): p. 2576-2580.

[10] Lu, J., et al., *Ultrasensitive electrochemical immunosensor based on Au nanoparticles dotted carbon nanotube-graphene composite and functionalized mesoporous materials.* Biosensors & bioelectronics, 2012. **33**(1): p. 29-35.

[11] Wu, D., et al., *Electrochemical Immunosensor for Ultrasensitive Detection of Human Chorionic Gonadotropin Based on Pd@SBA-15.* Electroanalysis, 2013. **25**(2): p. 427-432.

[12] Jiang, Z., et al., *Resonance Scattering Assay for Trace Human Chorionic Gonadotrophin Using Gold-platinum Nanoalloy Immunoprobe as Catalyst.* Acta Chimica Sinica, 2012. **70**(16): p. 1748-1754.

[13] Buck, R.P. and E. Lindner, *Recommendations for nomenclature of ion-selective electrodes - (IUPAC Recommendations 1994).* Pure and Applied Chemistry, 1994. **66**(12): p. 2527-2536.

[14]Randles, J.E.B., *A Cathode Ray Polarograph 2. The Current-Voltage Curves.* Transactions of the Faraday Society, 1948. **44**(5): p. 327-&.

[15] Borges, J., *Adsorption of Proteins on Au Surfaces modified with SAMs and Biopolymeric Materials*, in *Department of Chemistry and Biochemistry*. 2013, Faculty of Sciences of Porto University.

[16] Christopher M. A. Brett, A.M.O.B., *Electrochemistry: Principles, Methods, and Applications*. 1993, Oxford University Press, Incorporated. p. 427.

[17] Billah, M., H.C.W. Hays, and P.A. Millner, *Development of a myoglobin impedimetric immunosensor based on mixed self-assembled monolayer onto gold.* Microchimica Acta, 2008. **160**(4).

[18] Fàbregas, S.S.M.R.S.P.E., *Toward a Fast, Easy, and Versatile Immobilization of Biomolecules into Carbon Nanotube/Polysulfone-Based Biosensors for the Detection of hCG Hormone.* Anal. Chem., 2008(80): p. 6508.

[19] Tsai, T.-W.W.H., Gustavo; Neves, Luís F; Tan, Yongqiang; Kao, Der-You Y; Harrison, Roger G; Resasco, Daniel E; Schmidtke, David W, *Adsorption of glucose oxidase onto single-walled carbon nanotubes and its application in layer-by-layer biosensors.* Anal. Chem., 2009(81): p. 7917.

[20] Hiroki Hibino, Hiroyuki Kageshima, and Masao Nagase. Epitaxial few-layer graphene: towards single crystal growth. Journal of Physics D: Applied Physics, 43(37):374005, 2010.

[21] Wen, Z.C., Suqin; Li, Jinghong, *Pt nanoparticles inserting in carbon nanotube arrays: Nanocomposites for glucose biosensors.* J. Phys. Chem. C, 2009(113): p. 13482.

[22] Pampalakis, G.K., Shana O, *An electrochemical immunosensor based on antibody-nanowire conjugates.* Analyst, 2009(134): p. 447.

[23] Wang, H., et al., *A nanostructured graphene/polyaniline hybrid material for supercapacitors.* Nanoscale, 2010. **2**(10): p. 2164-2170.

[24] Ohno, Y., K. Maehashi, and K. Matsumoto, *Label-free biosensors based on aptamer-modified graphene field-effect transistors.* Journal of the American Chemical Society, 2010. **132**(51): p. 18012-18013.

[25] Henry, D.T., L. Dan, and B.K. Richard, *One-Dimensional Conducting Polymer Nanostructures: Bulk Synthesis and Applications.* Advanced Materials, 2009. **21**.

[26] Sambhu Bhadra, N.K.S.a.D.K., *Polyaniline based anticorrosive and anti-molding.pdf.* Journal of Chemical Engineering and Materials Science, 2011. **2**(1): p. 1-11.

CHAPTER 4[2]

"Where there is love there is no question."

Albert Einstein (1879-1955), German Theoretical Physicist

Epitaxial graphene immunosensor for human chorionic gonadotropin

In this work, standard lithographic techniques have been used to pattern epitaxial graphene devices, whose dimensions are scalable and suitable for wafer scale production. Epitaxial graphene devices have been functionalized using APTES, the first reported use of APTES on epitaxial graphene devices, to achieve an amine-terminated graphene surface. Antibodies targeted against hCG have been bound to the amine-terminated graphene in the first reported amperometric immunosensor based on epitaxial graphene. Device fabrication and surface functionalisation methods are readily adaptable to other antibody/antigen systems, and are thus suitable as a generic immunosensor platform.

4.1 Introduction

Electrochemical immunosensors offer a number of significant advantages, including high sensitivity, fast response, simplicity, and relatively low cost [1,2] when compared with other types of immunosensor. These advantages make them attractive for high performance analytical detection of biomolecules [3]. Immunosensors capable of detecting nucleic acids [4], viruses [5], antigens [6], and hormone [7] biomarkers, based on silicon nanowire [5], carbon nanotube (CNT) [8] and graphite [9] have been widely reported. Since the pioneering work on SiNW sensors by Lieber *et al* [10], SiNW sensors have been developed that are capable of detection limits down to fg/ml concentrations – such as reported for prostate specific antigen (PSA) detection by Kim *et al* [11]. CNT sensors have also been used to achieve detection of antigens

[2] Sofia Teixeira, et al, Epitaxial graphene immunosensor for human chorionic gonadotropin, Sensors and Actuators B, 2014, 190, 723–729.

e.g. PSA at ng/ml [8, 12]. More recently, graphene has been utilized in a number of forms for sensor and biosensor applications [13-17].

Graphene's electronic structure and high surface to volume ratio contribute to the high sensitivity of graphene sensor devices [18]. Various forms of graphene and related materials (such as exfoliated graphene [19], graphene oxide and epitaxial graphene [20]), have been reported for use in graphene-modified electrodes and graphene-composite electrodes. An electrochemical sensor, using chemically modified exfoliated graphene to detect dopamine (DA), was reported to have a detection limit of 0.01μM. [21]. Li *et al.* reported a novel electrochemical immunosensor for the breast cancer marker protein CA 15-3 using a highly conductive graphene-modified electrode. This sensor was capable of sensitive and label-free detection with a detection limit of 0.012IU/mL [19]. Yasuhide *et al.* reported a label-free immunosensor based on an aptamer-modified graphene field-effect transistor (G-FET). The aptamer-modified G-FET showed selective electrical detection of IgE protein with a dissociation constant of 47nM, indicating good affinity and the potential for G-FETs to be used in biological sensors [15]. Srivastave *et al.* reported an easy method for producing functionalized multilayer graphene from multiwalled carbon nanotubes (MWCNTs) an a mass scale using only concentrated H_2SO_4/HNO_3, the biosensor showed linearity between 10-100 mg/dL, sensitivity of 5.43μA mg^{-1} dL cm^{-2}, and a lower detection limit of 3.9mg/dL, [22]. Lu *et al.* reported an hydrogen peroxide biosensor formed from single-layer graphene with a detection limit of $1.05x10^{-7}$M [23]. Schedin *et al.* reported a sensor for detection of individual gas molecules adsorbed on graphene with a detection limit of 1 ppb [24].

Epitaxial growth on silicon carbide (SiC) is a widely used method of producing high quality graphene. Using insulating or semi-insulating SiC substrates enables the lithographic fabrication of graphene devices for electronic applications, without the need for transfer to other substrates [25, 26]. Graphene can be grown on both the silicon and carbon faces of 4H-SiC, but growth is substantially different on each face, in terms of the morphology and electronic structure of the resulting graphene layers (Figure 4.1) [27]. Silicon face growth yields an interfacial layer between the SiC substrate and graphene, and typically grows layer-by-layer [28]. In contrast, carbon face growth yields layers which are decoupled from the SiC substrate, without a noticeable interface effect [29]. Larger growth domains are produced on the carbon face, which contributes to higher carrier mobilities in a microchannel device [30].

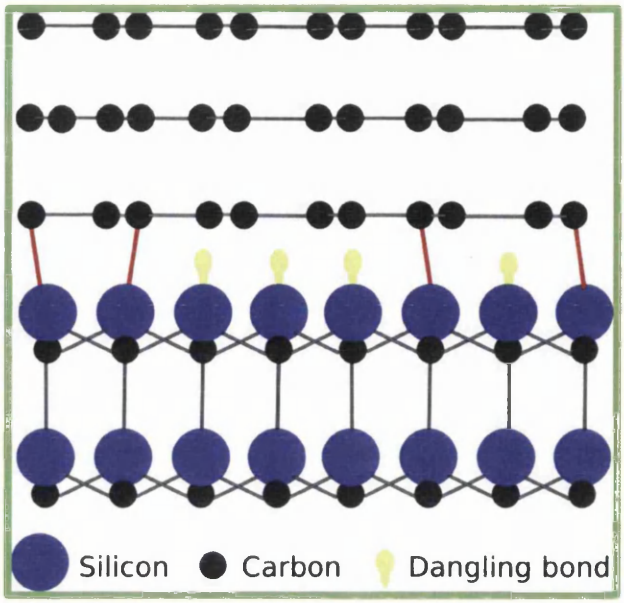

Figure 4.1 - Structure of graphene on SiC(0001) (Si face). The first carbon layer formed during high temperature annealing of the Si face is not a graphene layer, but an interface layer with 1/3 of the C atoms bonded to the SiC substrate. The interface layer between graphene and SiC influences its electronic properties.

Graphene biosensors can be fabricated by covalent immobilization, of proteins to graphene surfaces [31, 32]. Covalent immobilization of antibody molecules onto graphene requires a chemical reaction of the COOH functional groups of the antibody, with amine groups bound to the graphene surface, producing a peptide bond. Methods for amine functionalization of graphene include diazotization [33], and surface silanization using (3-Aminopropyl)triethoxysilane (APTES). APTES attachment can be performed on various substrates provided they contain surface hydroxyl groups, which can react with alkoxysilanes to form covalent Si-O-C bonds to the underlying substrate.

An epitaxial graphene immunosensor, capable of selectively detecting hCG, has been developed for human chorionic gonadotropin (hCG)

4.1.1 Fenton Oxidation Reaction

Advanced oxidation processes (AOPs) employ reactive oxidizing agents such as hydrogen peroxide or ozone, with or without the addition of catalysts or photolysis [34]. Many AOP technologies generate hydroxyl radicals [a strong oxidant, E^{o}= -2.8 V], addition of which to aromatic rings initiates ring opening and ultimate mineralization to CO_2 and H_2O. In homogenous photolysis, Ultra violet (290–200nm) radiation breaks down H_2O_2 or O_3, producing OH radicals. In heterogeneous photolysis, OH radicals are generated at the surface of a

semiconductor (usually TiO_2) in the presence of UVA light (400–320nm). Homogenous dark oxidation employs an oxidant and includes methods such as Fenton's reagent (H_2O_2+Fe^{2+}), ''peroxone'' (H_2O_2+ O_3), and hydrothermal (high temperature) water oxidation.

Li et al. (1998) [35] used Fenton's reagent (H_2O_2+Fe^{2+}), alone or in combination with UV light (254nm), for remediating aqueous wastes that contained nitro aromatic explosives.

The Fenton oxidation reaction, using a ferrous salt and hydrogen peroxide mixture is recognized as one of the most powerful advanced oxidation technologies available and can be used to degrade various organic compounds because of existence of hydroxyl radicals (HO•), which is known as one of the most active oxidants and has the highest oxidation potential than other oxidants among all known oxidants [36-38]. Generally, it is believed that HO• is generated by reaction of hydrogen peroxide (H_2O_2) and ferrous ion (Fe^{2+}), which acts as a catalyst. Its mechanism is as follows [39,40]:

$$Fe^{2+} + H_2O_2 \rightarrow Fe^{3+} + HO^{\bullet} + OH^{-} \quad \textbf{(4.1)}$$

$$Fe^{3+} + H_2O_2 \rightarrow Fe^{2+} + HOO^{\bullet} + H^{+} \quad \textbf{(4.2)}$$

$$Fe^{2+} + HO^{\bullet} \rightarrow Fe^{3+} + OH^{-} \quad \textbf{(4.3)}$$

$$HOO\bullet + Fe^{3+} \rightarrow Fe^{2+} + O_2 + H^{+} \quad \textbf{(4.4)}$$

$$HO^{\bullet} + H_2O_2 \rightarrow HOO^{\bullet} + H_2O \quad \textbf{(4.5)}$$

$$Fe^{2+} + HOO^{\bullet} \rightarrow Fe^{3+} + O_2H^{-} \quad \textbf{(4.6)}$$

In addition, $HO^{\bullet}$ can attack high electron density sites as an electrophilic reagent and easily carry out electrophilic addition reactions with the unsaturated bonds abundant in π-bonded molecules, such as alkenes, alkynes, aromatic compounds and fullerenes as well as graphene [41]. The chemical reactivity of these species is mainly due to their C=C double bonds. MWNTs are assemblies of concentric sp^2 bonded carbon tubes made of rolled-up graphite sheets, with π-bonding electrons in a carbon framework of nanotubes. MWNTs have been previously functionalized with the Fenton reaction and consequently, Fenton reagents for modified epitaxial graphene were employed successfully.

There are several operating parameters such as pH, dosage of H_2O_2 and Fe^{2+}, temperature and time, which can affect production of HO• and Fenton oxidation treatment of graphene. When dosage of H_2O_2 and Fe^{2+} are low, the amount of HO• is low, too. Also, an excess of H_2O_2 or Fe^{2+} may be unfavorable to Fenton oxidation treatment for reduction of highly active HO•. The detrimental effect of excess H_2O_2 can be explained with reaction (4.5), which shows that H_2O_2 can react with HO• like a scavenging agent, thus reducing the quantity of HO• present in the system. In other words, H_2O_2 competes with graphene for the hydroxyl radical, reducing the efficiency of HO• in modifying graphene [42].

Similarly, when Fe^{2+} is in excess, large quantities of HO• are produced quickly in the initial phase and bring about accumulation of HO•. Subsequently, their interactions produce water and HOO•, resulting in large loss of HO•. Therefore, the ratio of H_2O_2 and Fe^{2+} is an important factor for Fenton oxidation treatment of graphene.

4.2 Experimental Section

4.2.1 Materials and Reagents

Semi-insulating 4H-SiC substrates (nominally on-axis) were purchased from CREE. Synthetic urine was prepared with urea, sodium chloride, potassium chloride and sodium phosphate purchased from Sigma-Aldrich. N-Hydroxysuccinimide (NHS) and N-(3-Dimethylaminopropyl)-N-ethylcarbodiimide hydrochloride (EDAC), Di-tert-butyl dicarbonate (t-BOC), sodium bicarbonate, bovine serum albumin (BSA), phosphate buffered saline (PBS), Potassium hexacyanoferrate III ($K_3[Fe(CN)_6]$), potassium hexacyanoferrate II ($K_4[Fe(CN)_6]$) trihydrate, and trifluoroacetic acid were all purchased from Sigma-Aldrich. Electrochemical measurements of the surface modification were performed using an aqueous reference electrode (Ag/AgCl) purchased from IJ Cambria Scientific Ltd and platinum (Pt) auxiliary electrode from BASi. hCG protein was purchased from Abcam (UK). Anti-hCG antibody was supplied by Ig Innovations.

4.2.2 Apparatus

Graphene growth was performed in a Jipelec Rapid Thermal Processing SiC furnace fitted with a turbo molecular pump. The unit is designed for dopant annealing of silicon carbide wafers, and can reach temperatures of up to 2000°C with a rapid ramp rate. Samples were

loaded on a purified graphite susceptor. The furnace was fitted with a turbo molecular pump to reach pressures down to 2×10^{-5}mbar, as measured with an ion gauge. An e-Line (Raith GmBH) electron beam lithography system was used to define the graphene channels and contacts of the sensor device. Plasma etching of the graphene device was performed in an Oxford Instruments PlasmaLab 80 Plus. Cyclic voltammetry measurements were performed using an EmStat^2 Palm Sens potentiostat with the graphene channel device as the working electrode, a Pt auxillary electrode and Ag/AgCl reference electrode. Electrical measurements were performed using a Semi Probe LA-150 probe station with a Keithley 2602A Source Meter. Micro-Raman measurements were performed using a Renishaw InVia system with a 100mW 532nm excitation laser with approximately 10mW of power on the sample. X-ray photoelectron spectroscopy (XPS) measurements were performed in a VG ESCAlab MKII with an Al X-ray excitation source (Kα of 1486eV).

4.2.3 Graphene growth and device fabrication

4H-SiC wafers were cut into 10x10mm samples and cleaned using a standard RCA procedure. Samples were etched in HF immediately prior to furnace growth to remove the native oxide. Multilayer graphene (MLG) was grown on the C-face of 4H-SiC at 1650°C and a vacuum of 10^{-4}mbar.

Electron beam lithography (EBL) followed by oxygen plasma etching (50sccm O_2, 75mTorr and 50W RF power, 60 seconds) was used to pattern graphene channel devices. A second EBL exposure was used to define the sputtered Ti/Au metal contacts to the graphene device. A third EBL exposure was used to define a window in PMMA, thus exposing only the graphene channel and protecting the metal contacts and the SiC surface from any chemical exposure during surface modification steps (see Chapter 3 section 3.7.4).

4.2.4 Hydroxylation of surface

The surface of the graphene channel devices was modified using the Fenton reaction, yielding an –OH terminated graphene layer. Epitaxial graphene samples were immersed in a solution of hydrogen peroxide and iron (II) sulfate, maintained at pH 3 for 30 minutes. Since the reaction is strongly exothermic, iron sulfate powder was added to the solution incrementally and allowed to settle before introducing the graphene sample (Figure 4.2).

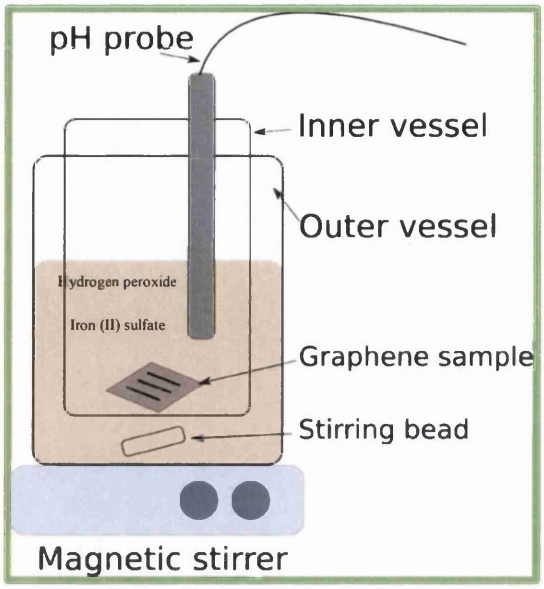

Figure 4.2 – Schematic of Fenton reaction.

Contact angle measurements taken before and after the –OH termination reaction showed that the graphene surface changed from hydrophobic (90°) to hydrophilic (26°) following –OH termination (Figure 4.3).

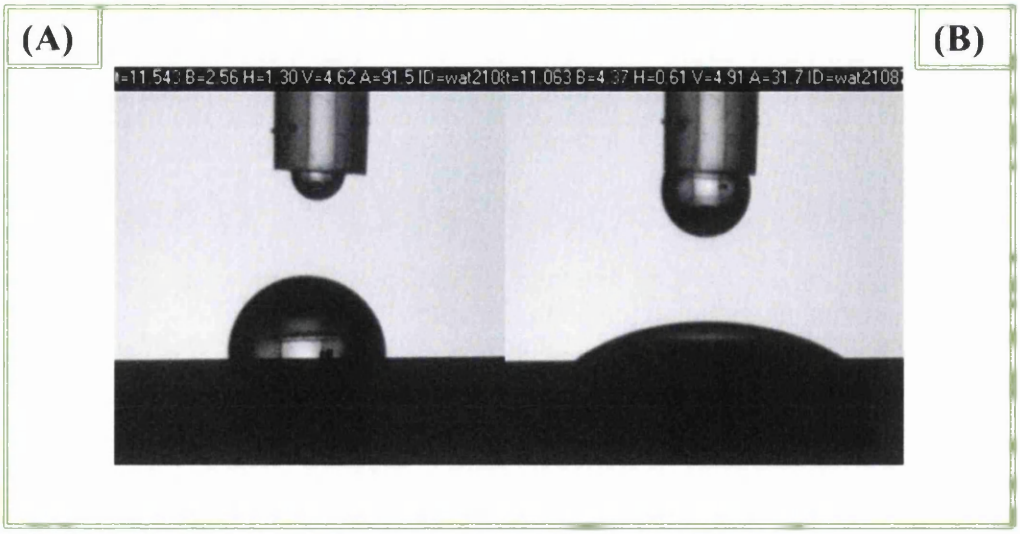

Figure 4.3 - Contact angle measurements before (A) and after (B) –OH termination.

4.2.5 Electrochemical assays

Cyclic Voltammetry (CV) measurements were conducted in 5.0mmol/L of $[Fe(CN)6]^{3-}$ and 5.0mmol/L of $[Fe(CN)6]^{4-}$, prepared in PBS buffer, pH 7.4. For CV assays, the potential was scanned from -0.7 V to +0.7 V, at 50mV/s. All assays were conducted in triplicate.

4.2.6 Antibody immobilization with APTES

The –OH terminated graphene surfaces were reacted in a solution of 40% (3-Aminopropyl) triethoxysilane (APTES) in ethanol for 1.5 hours, to obtain an amine-terminated surface (Figure 4.4). Amine groups of the anti-hCG antibody were protected using Di-tert-butyl dicarbonate (t-BOC) to prevent cross-linking and aggregation of antibodies. This also ensures that only the amine-terminated surface of the graphene channel binds to the carboxylic group of the antibody (Figure 4.5 and 4.6).

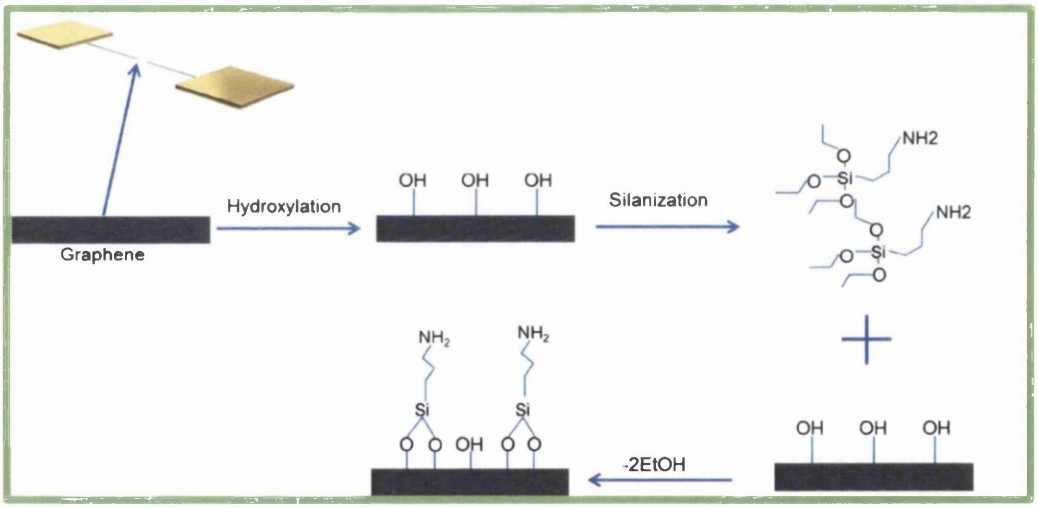

Figure 4.4 – Schematic of covalent attachment of 3-aminopropyltriethoxysilane (APTES) to the hydroxyl-terminated graphene surface.

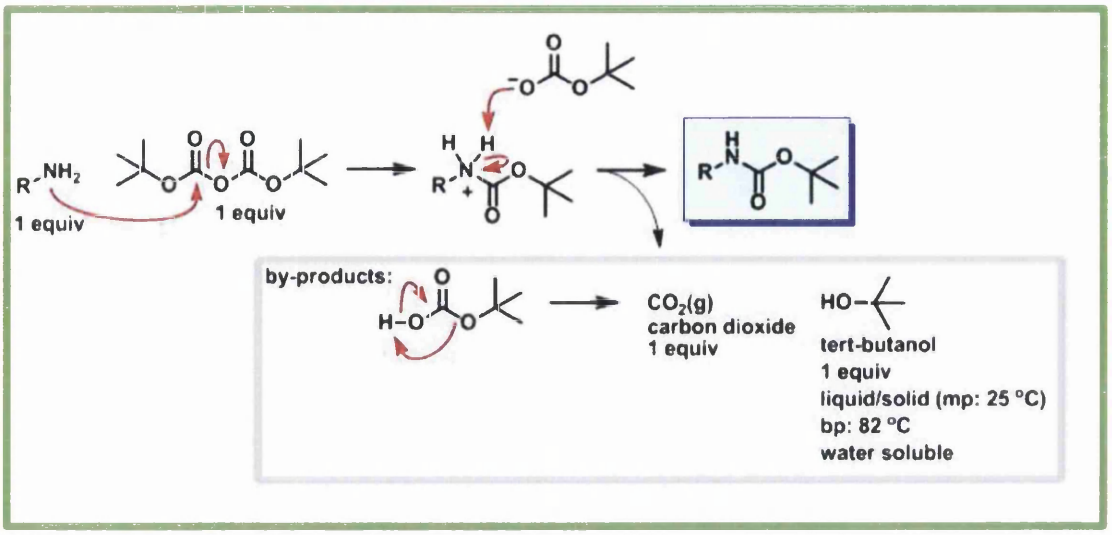

Figure 4.5 - BOC protection in chemical synthesis of peptides.

Steps:

- The amine attacks a carbonyl site on di-tert-butyl dicarbonate (Boc2O) resulting in tert-butyl carbonate leaving as a leaving group.
- Tert-butyl carbonate picks up the proton from the protonated amine.
- Tert-butyl bicarbonate breaks down into CO_2 (gas) and tert-butanol.

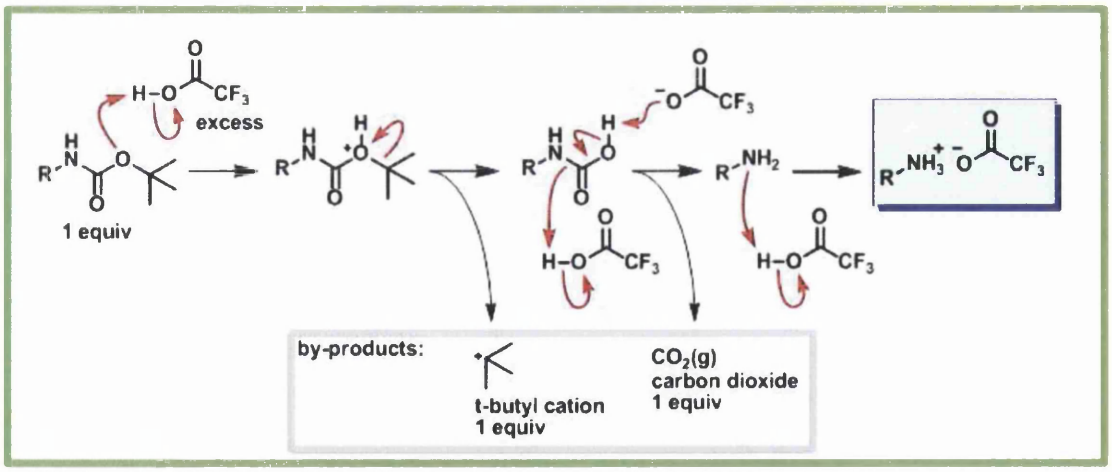

Figure 4.6 – BOC de-protection in chemical synthesis of peptides.

Steps:

- The tert-butyl carbamate becomes protonated.
- Loss of the tert-butyl cation results in a carbamic acid.

- Decarboxylation of the carbamic acid results in the free amine.

The carboxylic groups of the antibody were activated using 50mmol/L of N-(3-Dimethylaminopropyl)-N-ethylcarbodiimide hydrochloride (EDAC), and 25mmol/L of N-hydrosucchimide (NHS) (see Chapter 2 section 2.4.1.1). The EDAC generates an ester derivative of the antibody, which is subsequently stabilized by NHS in order to prevent it from undergoing hydrolysis and reverting back to the carboxylic acid. The ester derivative of anti-hCG subsequently reacts with the amine-terminated graphene surface, forming a peptide bond. The amine terminated graphene surface was exposed to a solution containing the activated antibodies for 2 hours at room temperature.

Removal of the t-BOC protecting groups, restoring the NH_2 groups on the antibody was achieved via cleavage of the amide bond between the t-BOC and the antibody using trifluoroacetic acid (TFA) for 1 hour. This also hydrolyses the ester, generated by the activation of the carboxylic groups by EDAC and NHS, back into carboxylic groups. Bovine serum albumin (5% BSA in PBS) solution was subsequently applied for 10 minutes to the surface to block non-specific binding of the target hCG molecule to any free surface-amine groups.

4.2.7 hCG binding

hCG suspended in synthetic urine was applied at increasing concentrations, ranging from 3.1mIU/mL to 28mIU/mL (0.62ng/mL to 5.62ng/mL) to the graphene channel. Each concentration was applied to the surface for 15 minutes, followed by washing in PBS and drying in nitrogen.

4.3 Results and discussion

4.3.1 Characterization of graphene devices

The thickness of the graphene overlayer was estimated by curve fitting the C_{1s} core level peak from the XPS spectra of graphene grown on SiC, and differentiating the components of this peak related to the SiC substrate and the graphene layer respectively (Figure 4.7 C). Assuming the graphene growth follows a Franck van der Merwe growth or layer-by-layer mode [45], the intensity of the SiC buried layer would decay exponentially with the increase in thickness of the graphene overlayer. This follows the propagation probability of the electrons

through the solid [46], with the mean free path calculated as being 1.39nm [47]; thus the graphene overlayer was estimated as being 3 layers thick.

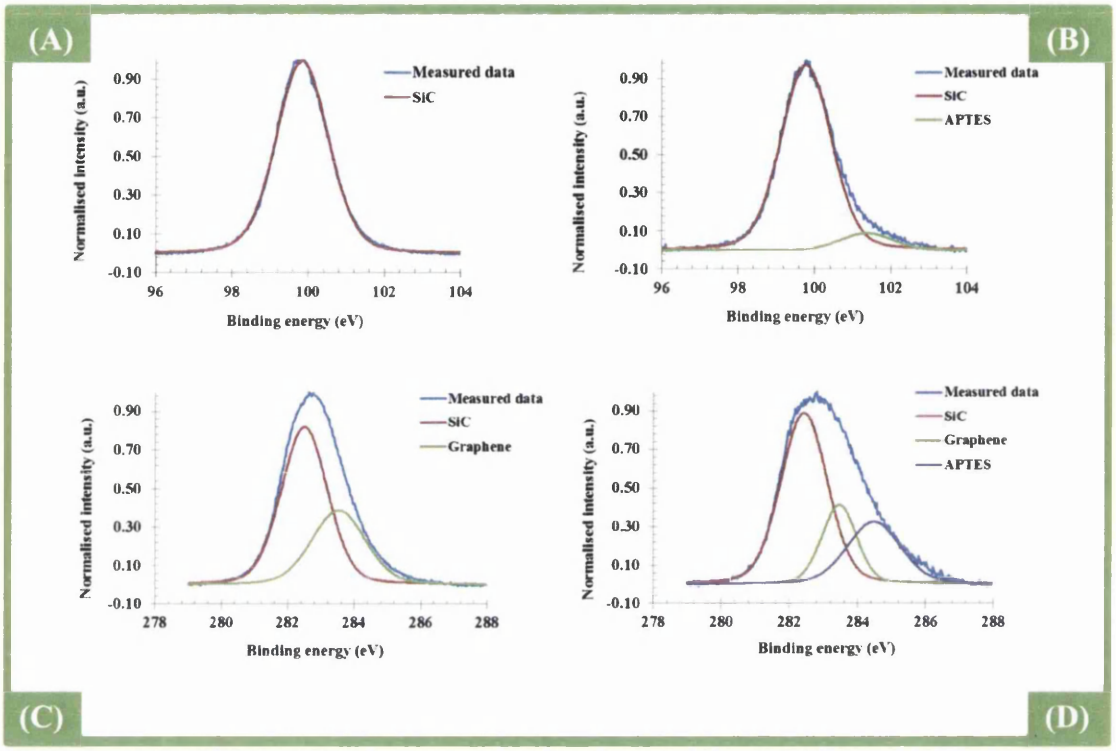

Figure 4.7 - (**A**) XPS core level spectrum of the Si_{2p} peak of an epitaxial graphene sample (grown on SiC) before functionalization, in black measured data and in red fitted peak attributed to SiC (**B**) XPS core level spectrum of the Si_{2p} peak of an epitaxial graphene sample after functionalization, in black measured data, in red fitted peak attributed to SiC and in blue fitted peak attributed to the silicon atom of the APTES molecule (**C**) XPS core level spectrum of the C_{1s} peak of a graphene sample before functionalization, in black measured data, in red fitted SiC peak and in blue fitted epitaxial graphene peak (**D**) XPS core level spectrum of the C_{1s} peak of a graphene sample after functionalization, in black measured data, in blue fitted graphene peak, in red fitted SiC peak and in green fitted APTES peak.

Raman measurements on graphene channels, performed after lithographic fabrication steps, did not demonstrate any shifts due to contamination or damage to the graphene substrate. The position of the G peak in the Raman spectrum ($1583cm^{-1}$), as well as the attenuation of the SiC substrate, as outlined in [48] were both used to determine the number of graphene layers, which was found to be in agreement with XPS results. The SiC background was subtracted from all Raman spectra to provide a clear comparison of the graphene peaks (Figure 4.9).

4.3.2 Characterization of surface modification

XPS was used to confirm the attachment of the aminosilane on the surface via the analysis of Si_{2p}, C_{1s} and N_{1s} peaks. Scans were performed with a pass energy of 10eV. Curve fitting of the C_{1s} and Si_{2p} peaks was performed with a G/L ratio of 30%. The energy separation between the C_{1s} peak attributed to the SiC and the C_{1s} peak attributed to the graphene was kept constant between the two experiments (before and after exposure to APTES), along with the FWHM of each peak.

Following APTES functionalization, the appearance of a nitrogen peak at 398.9eV, consistent with an amine group, and a secondary Si_{2p} peak at 101.4eV (Figure 4.7A and B), not present before functionalization, were observed. Taking into account the sensitivity factor of the different core levels, the contribution of both the nitrogen peak and the secondary silicon peak was found to be similar (Table 4.1), which is consistent with the 1:1 stoichiometric composition of the aminosilane. In addition, all the peaks shift by -0.1eV, illustrating a Fermi shift, ergo a modification of the surface properties.

Curve fitting of the C_{1s} peak after exposure to APTES showed the appearance of a third C_{1s} peak (in addition to the bulk SiC and graphene C_{1s} peaks) which was attributed to the aliphatic carbon atoms of the APTES molecule (Figure 4.7D). The contribution of these aliphatic carbon atoms to the XPS spectrum is just over 7 times that from the nitrogen or the silicon atoms of the APTES molecule. This is consistent with the stoichiometry expected when the APTES molecule (which should contain 9 carbon atoms) is bound to the graphene surface, after having lost an ethanol group, during the reaction with the hydroxyl-terminated surface. It was also observed that the intensity of the graphene peak decreased slightly, suggesting a modification of some of the sp^2 carbon atoms in the top most graphene layer to sp^3 hybridized carbon, due to the functionalization with hydroxyl groups.

Table 4.1 - Description of bonds and atomic abundances calculated from the fitted components of the C_{1s}, Si_{2p} and N_{1s} core peaks from XPS measurement before and after functionalization with APTES.

		GRAPHENE		APTES	
Peak	**Sensitivity factor**	**Measured area**	**Actual contribution %**	**Measured area**	**Actual contribution %**
C_{1s} SiC	0.25	2884	28.9	1235	23.8
C_{1s} graphene	0.25	3231	32.4	1202	23.1
C_{1s} APTES	0.25	0	0	892	17.2
Si_{2p} SiC	0.27	4172	38.7	1725	30.7
Si_{2p} APTES	0.27	0	0	156	2.8
N APTES	0.43	0	0	212	2.4

Chemical modification of graphene channels (the working electrode) can be measured by monitoring the changes in the electron transfer properties of the redox system $[Fe(CN)6]^{3-/4-}$ using cyclic voltammetry (CV). These studies are based on the assumption that the $[Fe(CN)6]^{3-/4-}$ redox reaction is a simple, reversible electron transfer reaction. The ferri/ferrocyanide couple provides an ideal electrochemical probe for the study of chemically modified surfaces, since its reduction and oxidation both proceed via simple one electron transfer redox processes [49].

$$Fe_3(CN)_6^{3-} \leftrightarrow Fe_2(CN)_6^{4-} \qquad \textbf{(4.9)}$$

The obtained CV results from the hydroxyl-terminated graphene electrode before (control) and after modification with APTES are presented in Figure 4.8. The redox peak current of the control sample, corresponding to the oxidation potential of Fe(II), was at 464mA. The peak current reduced to 110mA for the APTES modified sample. This 354mA shift of the redox peak indicates successful chemical modification of the surface with APTES as the formation of the C-O-Si bond, between the graphene electrode and the APTES molecule, impedes the transfer of electrons between the electrode surface and the $[Fe(CN)6]^{3-/4-}$ electrolyte.

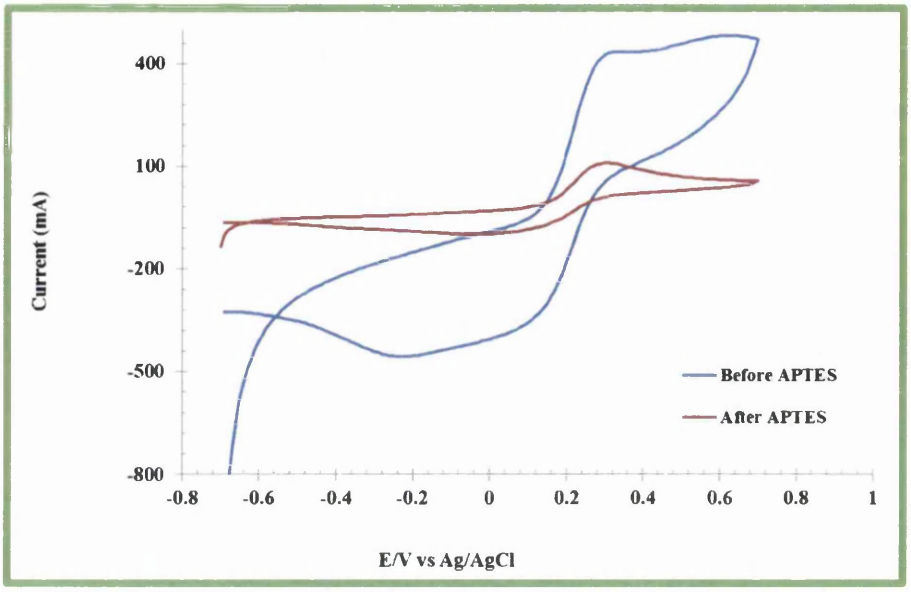

Figure 4.8 - Cyclic Voltammograms measurements before (▬) and after (▬) APTES attachment.

Raman measurements were performed to monitor the effect of hydroxylation and APTES functionalization on the Raman spectrum of graphene (Figure 4.9). A notable increase in the D band intensity at ~1350cm^{-1} was measured after APTES attachment, with the ratio of the D (sp^3 bonded C) to G (sp^2 bonded C) Raman peaks, I(D)/I(G), increasing from ~0.08 to ~0.8 after –OH and APTES modification. This can be understood as an increase in sp^3 hybridized carbon in the graphene layer, resulting from the functionalization reaction. This has been previously reported by Lee at al. [50], for the modification of exfoliated graphene with diazonium salts.

Raman mapping measurements were performed to assess any inhomogeneities in the APTES attachment. These mapping measurements of I(D)/I(G) indicated that APTES attached preferentially at the edges of the graphene channel, which may be caused by preferential hydroxylation of edge and defect sites during the Fenton reaction (Figure 4.10).

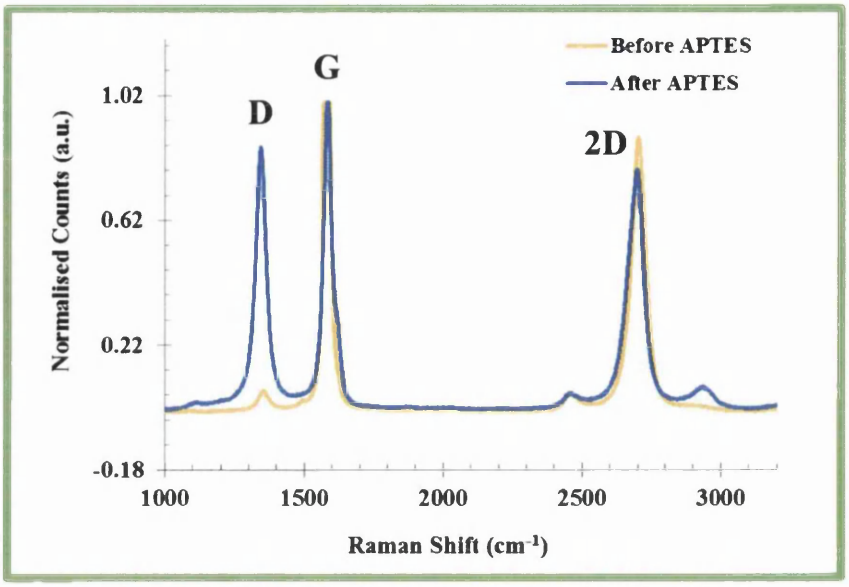

Figure 4.9 - Raman spectrum of graphene before (—) and after (—) APTES functionalization.

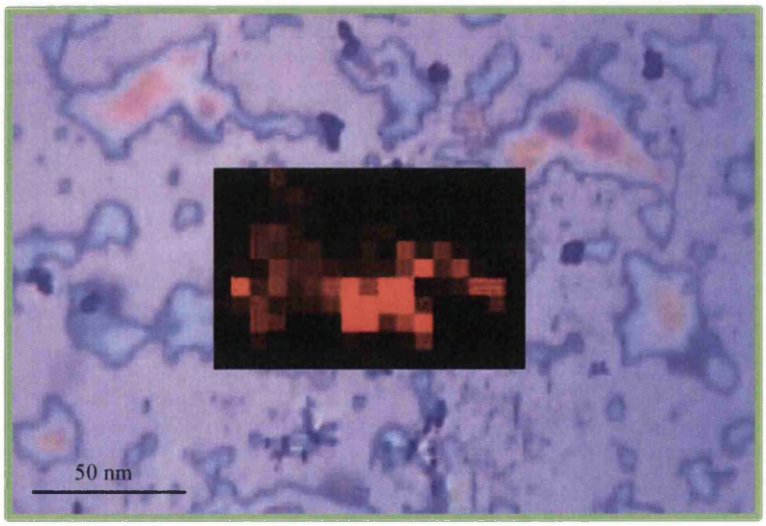

Figure 4.10 - Raman map of APTES modified epitaxial graphene channel. The intensity of the D band (~1350 cm^{-1}) is shown in red. After modification, the variation in D peak intensity increased, with the average D peak intensity also increasing. Presence of the APTES peaks correlated strongly with regions with higher D band intensity. It follows that APTES attachment occurs preferentially in areas with a higher concentration of –OH groups.

SEM and AFM were used to image the graphene surface before and after modification. Morphology of the graphene surface before modification is consistent with reports in the literature [51] for graphite capped C-face EG growth. The number of graphene layers on the surface varies considerably, with bare SiC visible in some regions between long terraces with graphene coverage in the centre of the sample. At the extremes of the sample, growth is considerably thicker, with some regions graphitic in nature. Representative areas from the centre of the sample before modification are shown in Figure 4.11 (AFM) and Figure 4.12 (SEM).

APTES is clearly visible after surface modification of MEG. Representative areas from the centre of the sample are shown in Figure 4.13 (AFM) and Figure 4.14 (SEM). Larger accumulations of APTES are visible; their location does not appear to be completely random, but instead preferential towards the edges of the graphene ribbons and other features on the surface.

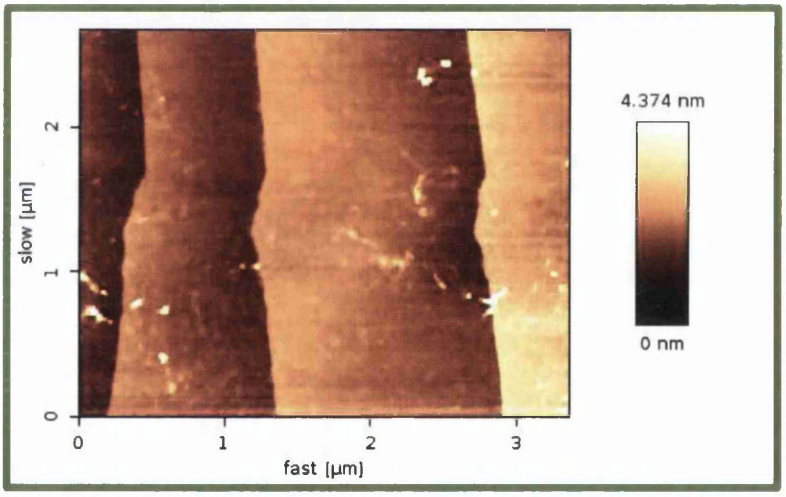

Figure 4.11 - AFM scan before modification.

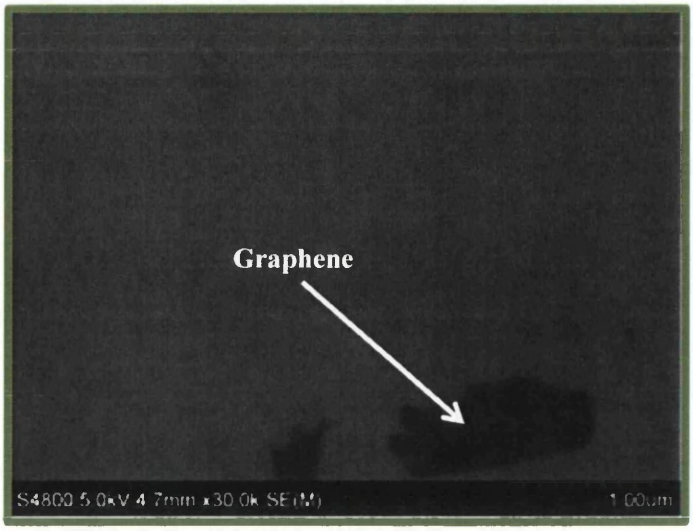

Figure 4.12 - SEM scan before modification.

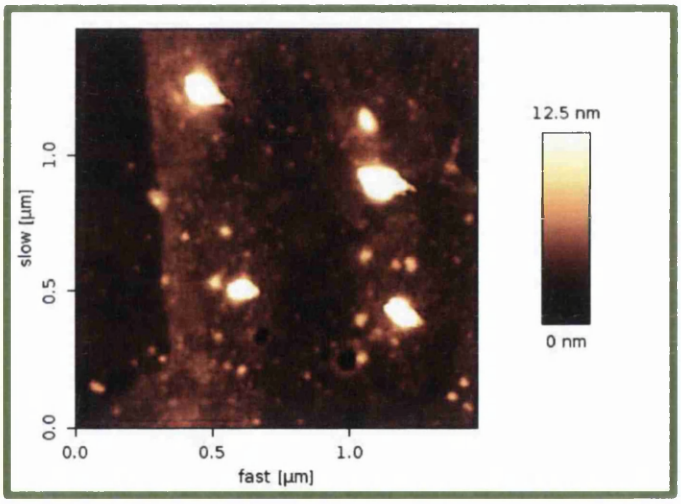

Figure 4.13 - AFM scan after APTES modification.

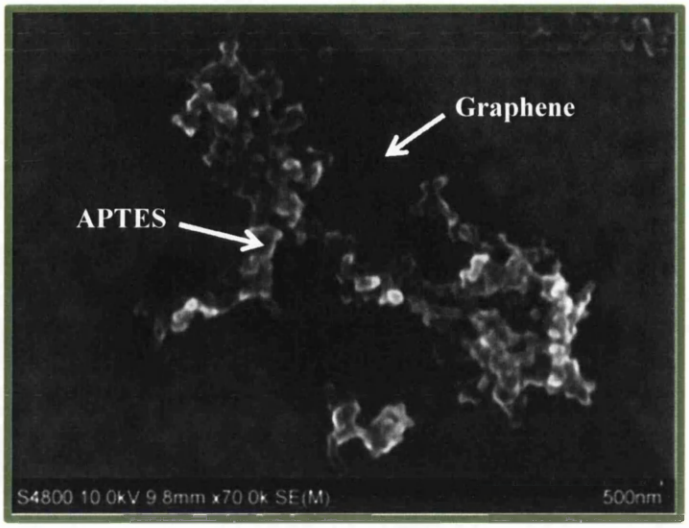

Figure 4.14 - SEM scan after APTES modification.

4.3.3 Analytical performance of the sensor

Current-voltage characterisation of the graphene channel device was performed after each step of the surface modification process; from pristine graphene to anti-hCG attachment, to application of hCG. The initial APTES attachment showed an increase by a factor of 4 in the channel resistivity, which is to be expected considering that covalent attachment to the surface induces a large amount of lattice defects (sp^3 sites) into the graphene lattice, as evidenced by the Raman spectra in (Figure 4.9). These defect sites enhance the scattering of charge carriers, thus reducing carrier mobility [52].

Epitaxial graphene samples have been characterized as both n-type or p-type (doped by the contact metal, depending on the work function of the metal) by different groups – depending on the growth conditions used [53]. In addition, the chemical functionalization of graphene may also influence the carrier type in graphene. The attachment of the negatively charged antibody is equivalent to a negative potential gating of the graphene channel, which if the graphene is n-type, would reduce the carrier density and thus the conductivity in the device.

Analogous sensing mechanisms have been outlined in [54] for the detection of negatively charged bacterial attachment to a p-type graphene-amine surface, whereby the hole current was increased by the negative gating potential. This mechanism is therefore similar to that of a graphene chemFET. Defective graphene and graphene influenced by extrinsic defects from the substrate, is reported to be particularly sensitive to this potential gating effect [55], whereas pristine (defect-free) graphene is not strongly sensitive to this sensing mechanism. The presence of defects in graphene causes the current modulation from chemical gating to be enhanced,

translating into superior sensitivity in chemFETS. Graphene grown on the C face of SiC is not a flat, uniform layer, but instead commonly grows into step-bunched terraces [56]. It is likely that structural defects from the epitaxial graphene growth, and chemical defects from the hydroxylation (Fenton) step, both contribute to the sensitivity of the current modulation from binding of the antibody.

Exposure of the antibody functionalized graphene sensor to the hCG antigen acts to increase the resistance across the channel. Indeed, increasing the concentration of hCG results in further increases in the graphene channel resistance, indicating that hCG was bound to the sensor. After exposure to concentrations above 5.62ng/mL, the sensor response saturated, indicating that the active receptor sites had been occupied by the bound antigens (Figure 4.15).

4.3.4 Sensitivity, selectivity and linearity of the sensor

Analysis of the biosensor response to hCG was carried out using varying concentrations of hCG in synthetic urine at pH 6.8. The sensor device showed detectable changes in channel resistance (increasing resistance) (Figure 4.15), upon exposure to hCG. The sensor had a linear response of 142Ω/ng/mL over the concentration range (0.62 to 5.62ng/mL) with a limit of detection (LOD) of 0.62ng/mL (3.1mIU/mL). This range was chosen because the normal urinary concentration range of hCG in pregnant women is 5mIU/mL to 117000mIU/mL in clinical samples [57]). The graphene biosensor is thus more than sufficiently sensitive to detect the lower limit of hCG in clinical samples. For comparison, Manlan Tao *et al.* reported an hCG immunosensor with a LOD of 12mIU/mL, which is linear in the range 25 to 400mIU/mL [58].

Optimization of the sensor or use of multiple sensors would be required in order to span the relevant clinical concentration range. Synthetic urine with no hCG analyte induced a small amperometric change in the device, probably due to the electrolytic gating effect.

The unmodified graphene device had a two-terminal resistance of 62Ω. This has no measurable response to hCG. After antibody attachment, the channel resistance increased by 16% on exposure to synthetic urine media (Figure 4.15, inset bottom right). Exposure to the first concentration of hCG (3.1mIU/mL) further increased the channel resistance by 43%. The final concentration of hCG (5.62mIU/mL) increased the channel resistance by 68% relative to the value in media. After antibody attachment, urea and cortisol were exposed to the antibody-modified graphene channels to measure the sensor selectivity to hCG. A negligible response was measured (Figure 4.15, inset top left) to both urea and cortisol. The sensor response (measured resistance) to urea and cortisol both vary by less than 20 Ohms, which is within the experimental error margin of the sensor. This is well below the response measured for hCG,

where the measured resistance increases by 620 Ohms over the same concentration range. This indicates that there is little if any non-specific binding from urea or cortisol and that hCG produces a clearly detectable and specific response in the sensor.

Figure 4.15 illustrates that the sensor response to hCG is linear and is repeatable in identical graphene sensors.

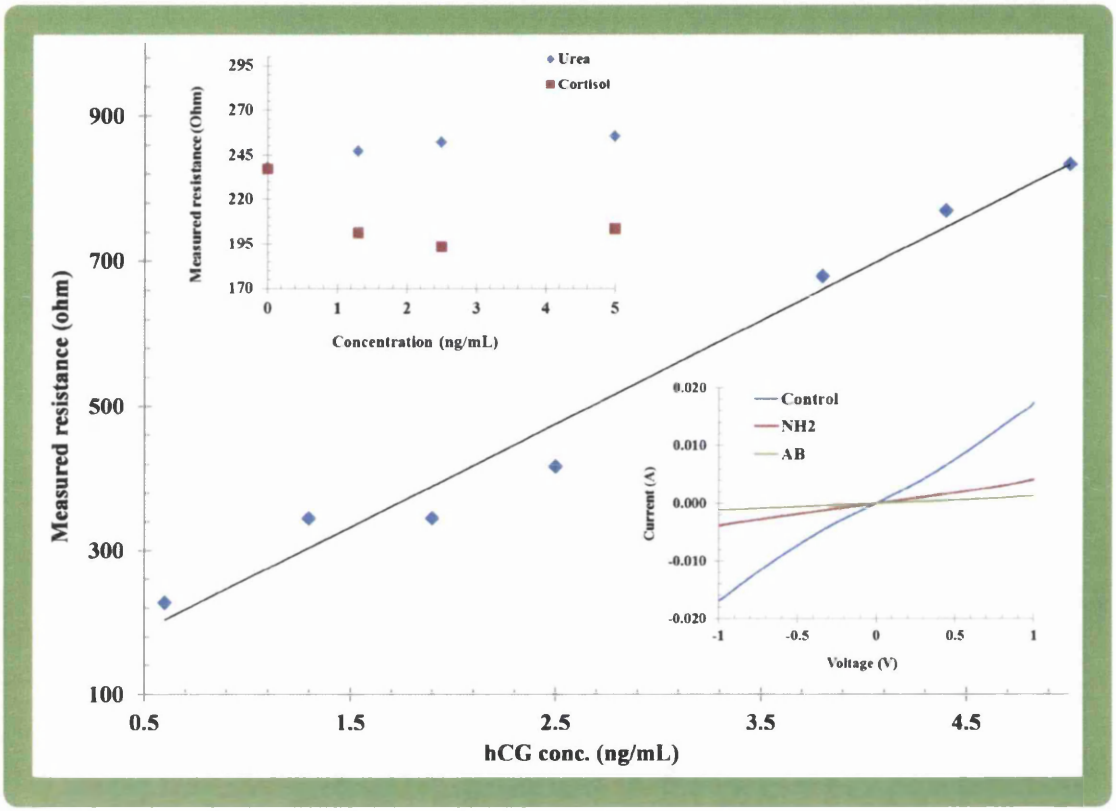

Figure 4.15 - hCG concentration as a function of the resistance across a 100μmx4mm graphene channel. Urea and cortisol concentration as a function of the resistance across the channel (inset, top left). The I-V characteristics are plotted (inset, bottom right) for the unmodified device ( ), amine terminated graphene surface ( ), and AB attachment ( ).

4.3.5 Comparison with ELISA

ELISA tests are a standard technique for detecting the presence of an antigen within a sample (see Chapter 2 section 2.2.1). The sandwich ELISA provides high specificity by capturing an antigen with a specific antibody immobilized on a solid surface. The antigen becomes immobilized and it can be detected by a second antigen specific antibody termed the detection antibody. Detection is accomplished by assessing the activity of a conjugated enzyme antibody, specific to the detection antibody, via incubation with a substrate to produce data

detectable change, usually through a color change. The most crucial element of the detection strategy is a highly specific antibody-antigen interaction.

A sandwich ELISA was developed using the sheep anti-hCG antibody as detection antibody to compare the sensitivity of an ELISA to that of the amperometric biosensor. The ELISA test was performed under the same conditions (temperature, primary antibody concentration) as used for the amperometric sensor. A detection limit of 78mIU/mL (15.6ng/mL) was obtained using the ELISA method – this is 30 times less sensitive than the amperometric graphene sensor.

4.4 Conclusions

APTES functionalization, for amine termination of epitaxial graphene in order to attach antibody bioreceptors, has been used in the fabrication of an amperometric immunosensor. The sensor is capable of selectively detecting the hormone hCG. This epitaxial graphene biosensor device has been demonstrated to be capable of detecting hCG concentrations as low as 0.62ng/mL, 30 times more sensitive than an ELISA test performed under the same conditions. Since the attachment mechanism uses non-specific sites of the antibody (i.e. carboxylic groups) to bond to the NH_2 terminated surface, this method could potentially be adapted to attach other antibodies for the detection of other biomarkers. Thus, the APTES-modified graphene channel devices offer an easily adaptable, generic sensing platform for detection of a range of target biomarkers.

References

[1] P. Erden, and E. Kılıç, *A review of enzymatic uric acid biosensors based on amperometric detection.* Talanta, 107 (2013) 312-323.

[2] P. Bobby and R.D. Marco, *Impedance spectroscopy: Over 35 years of electrochemical sensor optimization,* Electrochimica Acta, 51 (2006) 6217-6229.

[3] Y. Wan, et al., *Development of electrochemical immunosensors towards point of care diagnostics.* Biosensors & bioelectronics 47C (2013) 1-11.

[4] G. J. Zhang et al., *Highly sensitive and reversible silicon nanowire biosensor to study nuclear hormone receptor protein and response element DNA interactions.* Biosensors & bioelectronics 26(2) (2010) 365-370.

[5] D. Shirale, et al., *Effect of (L:D) Aspect Ratio on Single Polypyrrole Nanowire FET Device.* The journal of physical chemistry. C, Nanomaterials and interfaces 114(31) (2010) 13375-13380.

[6] Tian, L. and T. Heyduk, *Antigen peptide-based immunosensors for rapid detection of antibodies and antigens.* Analytical chemistry 81(13) (2009) 5218-5225.

[7] M. G. María et al., *Ultrasensitive detection of adrenocorticotropin hormone (ACTH) using disposable phenylboronic-modified electrochemical immunosensors.* Biosensors and Bioelectronics 35 (2012) 82-86.

[8] H.T.L. John, H. Sabahudin, and W. Dashan, *Multiwall Carbon Nanotube (MWCNT) Based Electrochemical Biosensors for Mediatorless Detection of Putrescine.* Electroanalysis 17 (2005) 47-53.

[9] S.S Ordóñez and E. Fàbregas, *New antibodies immobilization system into a graphite–polysulfone membrane for amperometric immunosensors.* Biosensors and Bioelectronics 22(6) (2007) 965-972.

[10] Y. Cui et al., *Nanowire nanosensors for highly sensitive and selective detection of biological and chemical species.* Science 293(5533) (2001) 1289-1292.

[11] A. Kim, et al., *Ultrasensitive, label-free, and real-time immunodetection using silicon field-effect transistors.* Applied Physics Letters, 91(10) (2007) 103901.

[12] J. Okuno et al., *Label-free immunosensor for prostate-specific antigen based on single-walled carbon nanotube array-modified microelectrodes.* Biosensors & bioelectronics 22(9-10) (2007) 2377-2381.

[13] E. Zor, et al., *An electrochemical biosensor based on human serum albumin/graphene oxide/3-aminopropyltriethoxysilane modified ITO electrode for the enantioselective discrimination of D- and L-tryptophan.* Biosensors & bioelectronics, 42 (2013) 321-325.

[14] K. Yu, Z. Bo, G. Lu, S. Mao, S. Cui, Y. Zhu, X. Chen, R.S. Ruoff and J. Chen, *Growth of carbon nanowalls at atmospheric pressure for one-step gas sensor fabrication.* Nanoscale research letters 6(202) (2011) 1-9.

[15] Y. Ohno, K. Maehashi, and K. Matsumoto, *Label-free biosensors based on aptamer-modified graphene field-effect transistors.* Journal of the American Chemical Society, 132(51) (2010) 18012-18013.

[16] M. Pumera, et al., *Graphene for electrochemical sensing and biosensing.* Trends in Analytical Chemistry, 29 (2010) 954-965.

[17] S Mao et al., *Highly sensitive protein sensor based on thermally-reduced graphene oxide field-effect transistor.* Nano Research 4 (10) (2011) 921-930.

[18] S. Yuyan et al., *Graphene Based Electrochemical Sensors and Biosensors: A Review.* Electroanalysis 22(10) (2010) 1027-1036.

[19] Li, H., et al., *Electrochemical immunosensor with N-doped graphene-modified electrode for label-free detection of the breast cancer biomarker CA 15-3.* Biosensors & bioelectronics 43 (2013) 25-29.

[20] O.J. Guy, G. Burwell, Z. Tehrani, A. Castaing, K.A. Walker, S.H. Doak, Materials Science Forum, 711 (2012) 246-249.

[21] T. Kuila et al., *Recent advances in graphene-based biosensors.* Biosensors & bioelectronics 26(12) (2011) 4637-4648.

[22] R. Srivastava et al., *Functionalized multilayered graphene platform for urea sensor.* ACS nano 6(1) (2012) 168-175.

[23] Q. Lu et al., *Direct electrochemistry-based hydrogen peroxide biosensor formed from single-layer graphene nanoplatelet-enzyme composite film.* Talanta 82(4) (2010) 1344-1348.

[24] F. Schedin, A.K. Geim, S.V. Morozov, E.W. Hill, P. Blake, M.I. Katsnelson, K. S. Novoselov, *Detection of individual gas molecules adsorbed on graphene.* Nature Materials 6(9) (2007) 652-655.

[25] A.E. Moutaouakil et al., *Room Temperature Logic Inverter on Epitaxial Graphene-on-Silicon Device.* Japanese Journal of Applied Physics 50(7) (2011) 113.

[26] Kang, H.C., Karasawa, H., Miyamoto, Y., Handa, H., Suemitsu, T., Suemitsu, M., & Otsuji, T., *Epitaxial graphene field-effect transistors on silicon substrates.* Solid-State Electronics (2010). 54: p. 1010-1014.

[27] J. Kedzierski, P.L. Hsu, P. Healey, P.W. Wyatt, C.L. Keast, M. Sprinkle, C. Berger, & W.A. de Heer, *Epitaxial graphene transistors on SiC substrates.* Electron Devices, IEEE Transactions 55(8), (2008) 2078-2085.

[28] N. Srivastava, G. He, R.M. Feenstra, & P. Fisher, *Comparison of graphene formation on C-face and Si-face SiC surfaces.* Physical Review B 82(23) (2010) 235406.

[29] N. Srivastava, G. He, P.C. Mende, R.M. Feenstra, Y. Sun, *Graphene formed on SiC under various environments: Comparison of Si-face and C-face.* Journal of Physics D: Applied Physics, 45 (2012) 154001.

[30] J.A. Robinson, M. Wetherington, J.L. Tedesco, P.M. Campbell, X. Weng, J. Stitt, M.A. Fanton, E. Frantz, D. Snyder, B.L.VanMil, *Correlating Raman spectral signatures with carrier mobility in epitaxial graphene: A guide to achieving high mobility on the wafer scale.* Nano letters 9(8) (2009) 2873-2876.

[31] C. Halliwell and A. Cass, *A factorial analysis of silanization conditions for the immobilization of oligonucleotides on glass surfaces.* Analytical chemistry 73(11) (2001) 2476-2483.

[32] S. Steingrimur, H.K. Hena, and A.S Nate, *Targeting Antibodies to Carbon Nanotube Field Effect Transistors by Pyrene Hydrazide Modification of Heavy Chain Carbohydrates.* Journal of Nanotechnology, (2012). 2012.

[33] E. Bekyarova et al., *Chemical modification of epitaxial graphene: spontaneous grafting of aryl groups.* Journal of the American Chemical Society 131(4) (2009) 1336-1337.

[34] Wei, Q., et al., *Multifunctional mesoporous silica nanoparticles as sensitive labels for immunoassay of human chorionic gonadotropin.* Sensors and Actuators B-Chemical, 2011. **153**(1): p. 256-260.

[35] Tao, M., et al., *The preparation of label-free electrochemical immunosensor based on the Pt-Au alloy nanotube array for detection of human chorionic gonadotrophin.* Clinica Chimica Acta, 2011. **412**(7-8): p. 550-555.

[36] Yang, H., et al., *Electrochemical immunosensor for human chorionic gonadotropin based on horseradish peroxidase-functionalized Prussian blue-carbon nanotubes/gold*

nanocomposites as labels for signal amplification. Electrochimica Acta, 2011. **56**(5): p. 1973-1980.

[37] Yang, H., et al., *Electrochemically deposited nanocomposite of chitosan and carbon nanotubes for detection of human chorionic gonadotrophin.* Colloids and Surfaces B-Biointerfaces, 2011. **82**(2): p. 463-469.

[38] Campbell, J.L.E. and G. Davis, *Reducing interference from leukocytes in analyte immunoassay, involves contacting biological sample containing leukocytes with magnetic sacrificial beads opsonized to leukocytes under specific conditions, and retaining beads*, Abbott Point of Care Inc.

[39] Wang, J., et al., *A novel immunosensor based on gold nanoparticles and poly-(2,6-pyridinediamine)/multiwall carbon nanotubes composite for immunoassay of human chorionic gonadotrophin.* Biochemical Engineering Journal, 2010. **51**(3): p. 95-101.

[40] Chikae, M., et al., *Highly Sensitive Method for Electrochemical Detection of Silver Nanoparticle Labels in Metalloimmunoassay with Preoxidation/Reduction Signal Enhancement.* Electrochemistry, 2010. **78**(9): p. 748-753.

[41] Mao, L., et al., *A new electrochemiluminescence immunosensor based on Ru(bpy)(3)(2+)-doped TiO2 nanoparticles labeling for ultrasensitive detection of human chorionic gonadotrophin.* Sensors and Actuators B-Chemical, 2010. **149**(1): p. 226-232.

[42] Yang, H., et al., *Electrochemical immunoassay for human chorionic gonadotrophin based on Pt hollow nanospheres and silver/titanium dioxide nanocomposite matrix.* Journal of Chemical Technology and Biotechnology, 2010. **85**(4): p. 577-582.

[43] Takoh, K., et al., *Label-free Immunosensor Using a Gold Electrode Covered with Conductive Self-assembled Monolayer*, in *2010 Ieee Sensors*. 2010. p. 411-414.

[44] J. Pignatello, D.L., P. Huston, Environ. Sci. Technol., 1999. **33**: p. 1832.

[45] R.H. Bradley et al., *Surface studies of hydroxylated multi-wall carbon nanotubes.* Applied Surface Science 258 (2012) 4835-4843.

[46] E. Bauer, *Phänomenologische Theorie der Kristallabscheidung an Oberflächen. II.* Zeitschrift für Kristallographie, (1958).

[47] S. Kono, C.S. BFadley, N.F.T. Hall, Z. Hussain, *Azimuthal Anisotropy in Core-Level X-Ray Photoemission from c (2× 2) Oxygen on Cu (001): Experiment and Single-Scattering Theory.* Physical review letters 41(2) (1978) 117.

[48] M.P. Seah, and W.A. Dench, *Quantitative electron spectroscopy of surfaces: A standard data base for electron inelastic mean free paths in solids.* Surface and Interface Analysis 1(1) (1979) 2-11.

[49] D. Lee et al., *Raman spectra of epitaxial graphene on SiC and of epitaxial graphene transferred to SiO2.* Nano letters 8(12) (2008) 4320-4325.

[50] S.D. Collyer, F. Davis, A. Lucke, J.M.C. Stirling and S.P.J. Higson, *The Electrochemistry of the Ferri/Ferrocyanide couple at a Calix[4]resorcinarenetetrathiol modified Gold Electrode as a study of novel electrode modifying coatings for use within Electro-analytical Sensors.* . Journal of Electroanalytical Chemistry 549 (2003) 119-127.

[51] Camara, N., Tiberj, A., Jouault, B., Caboni, A., Jabakhanji, B., Mestres, N., Godignon, P., & Camassel, J. (2010) Current status of self-organized epitaxial graphene ribbons on the C face of 6H--SiC substrates. *Journal of Physics D: Applied Physics* 43, 374011.

[52] P. Huang, H. Zhu, L. Jing, Y. Zhao & X. Gao, *Graphene covalently binding aryl groups: conductivity increases rather than decreases.* ACS nano 5 (2011) 7945-7949.

[53] W.A. Heer, C. Berger, X. Wu, M. Sprinkle, Y. Hu, M. Ruan, J.A. Stroscio *Epitaxial graphene electronic structure and transport.* Journal of Physics D: Applied Physics, 43 (2010) 374007.

[54] N. Mohanty, and V. Berry, *Graphene-Based Single-Bacterium Resolution Biodevice and DNA Transistor: Interfacing Graphene Derivatives with Nanoscale and Microscale Biocomponents.* Nano letters 8 (2008) 4469-4476.

[55] B. Kumar, M. Kyoungmin, M. Bashirzadeh, A.B. Farimani, M.H. Bae, D. Estrada, Y.D. Kim, P. Yasaei, Y.D. Park, E. Pop, N.R. Aluru, A. Salehi-Khojin, *The role of external defects in chemical sensing of graphene field-effect transistors.* Nano Lett, 13(5) (2013) 1962-1968.

[56] N. Camara, A. Tiberj, B. Jouault, A. Caboni, B. Jabakhanji, N. Mestres, P. Godignon, & J. Camassel, *Current status of self-organized epitaxial graphene ribbons on the C face of 6H--SiC substrates.* journal of Physics D: Applied Physics 43 (2010) 374011.

[57] Peters, A., *The Diagnosis of Pregnancy.* Glob. libr. women's med., 2008.

[58] M. Tao et al., *The preparation of label-free electrochemical immunosensor based on the Pt-Au alloy nanotube array for detection of human chorionic gonadotrophin.* Clinica chimica acta; international journal of clinical chemistry 412(7-8) (2011) 550-555.

CHAPTER 5

"I walk slowly, but I never walk backward"

Abraham Lincoln (1809-1865), 16th President of the USA

Nanocomposites of chitosan and gold nanoparticles cast on graphene and bound to antibodies for label-free human chorionic gonadotropin detection

The next three chapters describe a variety of techniques used to develop SPE graphene and CNT's sensors. The techniques use an intermediate layer to which antibody bioreceptor were attached.

5.1 Introduction

Immunosensors are analytical techniques that can detect a wide range of analytes, including pathogens [1], drugs [2], bacteria [3], toxins [4], biomarkers [5] using antigen - antibody interactions. Immunoassays and immunosensors based on antibodies have been used over thirty years and are still among the most important diagnostic tools, which are widely used in medical diagnostics, environmental analysis, forensic medicine [6, 7]. Antibodies are used as probes in immunosensors [8, 9]. The major type of immunosensor relies on the ability of an immobilized antibody to recognize and to bind its associated target, which is known as an antigen. Recently, electrochemical impedance spectroscopy (EIS) [10] has been used for the direct monitoring of antigen-antibody interactions. The efficient immobilization of an antibody on the solid surface of assay chips is an essential step in the preparation of these biosensors [11]. Physical adsorption proves to be the easiest immobilization method, but often suffers from random orientation and denaturation of immobilized antibodies, yielding poor reproducibility. More-stable immobilization of antibodies is obtained by covalent attachment. Furthermore, this immobilization method yields better sensor reproducibility. To develop an immunosensor with high performance, oriented immobilization of antibodies is preferable [12]. The advantages of

oriented immobilization are 2-8 times higher antigen-binding capacity, which results in higher sensitivity of immunosensors and in many cases increased stability [13].

One of the best ways to achieve oriented immobilization of antibody molecules is their immobilization on a sublayer consisting of Fc-binding receptors, which specifically bind the F_c-part of antibody molecules [14, 15]. The current standard method of immobilizing antibodies to surfaces involves noncovalent physical adsorption to a detection surface through nonspecific hydrophobic interactions (physical adsorption method) [16-18]. This method, however, results in randomly oriented antibody molecules on the detection surface and yields ~90% antibody that has an inactive orientation due to steric blocking of the antigen binding sites [10, 19]. A common alternate method involves nonspecific chemical immobilization to amine reactive surfaces by utilizing the lysine side chain amino groups present on the surface of antibodies (ε-NH^{3+} method) [20, 21]. An essential task for the development of amperometric immunosensors is the efficient and effective immobilization of biomolecules [22].

Chitosan (CS) (Figure 5.1), a natural polymer product, is derived from chitin via deacetylation with alkali. Its excellent film forming and adhesion ability, together with non-toxicity and biocompatibility makes it a promising matrix for biomaterial immobilization [23]. The electrodeposition method is simple, controllable and reproducible for film Chitosan preparation [25]. Moreover, other substances such as gold nanoparticles (AuNPs), MWNTs and even enzymes can be effectively entrapped within CS to form biocomposites during the deposition process [24, 26]. At a constant electrodeposition potential, protons are consumed at the cathode, resulting in a pH gradient established in the vicinity of the surface. Another advantage of this new hybrid material is the widely present amino groups in chitosan molecules, thus, providing a hydrophilic environment which is compatible with biomolecules [25].

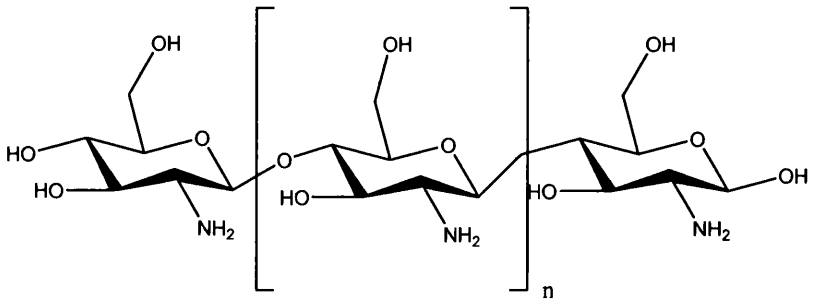

Figure 5.1 - Chemical structure of chitosan.

Electrochemical immunosensors using advances in nanomaterials are increasingly being used for biosensing applications [27]. In this context, carbon-based nanomaterials are gaining interest as an alternative to gold electrodes. Different carbon nanostructures, with different inherent electrical properties have been used in electrochemical immunosensors including CNTs [28, 29] and more recently (since 2005) graphene [30]. Graphene displays a combination of interesting properties, such as large surface area, high electrical conductivity and biocompatibility [31-38]. Heterogeneous electron transfer (the transfer of electrons between graphene and molecules in solution, necessary for the oxidation/reduction of said molecule) occurs at the edges of the graphene or at defects in the basal plane [39]. Additional defects are also introduced by functionalization, required to immobilize biomolecules, including antibodies, on to graphene. The antibodies act as biological receptors in immunosensors.

5.2 Experimental Section

5.2.1 Materials and Reagents

All chemicals used were of analytical grade and water was de-ionized. Potassium hexacyanoferrate III (K3[Fe(CN)6]) and potassium hexacyanoferrate II (K4[Fe(CN)6]) trihydrate and magnesium chloride were obtained from Riedel Haen; Chitosan and AuNPs were obtained from Sigma. Acetic acid was obtained from Carlo Erba. N-Hydroxysuccinimide (NHS) and creatinine was obtained from Fluka; N-(3-Dimethylaminopropyl)-N'-ethylcarbodiimide hydrochloride (EDAC) and Bovine serum albumin (BSA) were obtained from Sigma; Phosphate Buffered Saline (PBS) Tablets were obtained from Amresco. hCG protein was purchased from Abcam (UK). Anti-hCG antibody was supplied by Ig Innovations. Ammonium chloride and calcium chloride were obtained from Merck. Sodium dihydrogen phosphate was obtained from Scharlau. Potassium sulphate and sodium chloride were obtained from Panreac.

Firstly, a 1% (v/v) acetic acid solution was prepared in D. I. Water. Chitosan was then added to obtain 0.1% (w/w) solution. Finally, AuNPs were also added to obtain a 1% (v/v) solution. PBS solution was prepared by dissolution of 1 tablet of PBS in 100mL of D.I. Water. EDAC, NHS and antibody solutions were prepared in this buffer. Synthetic urine was prepared with creatinine ($5.3x10^{-6}$M), magnesium chloride ($9.8x10^{-7}$M), calcium chloride ($6.80x10^{-7}$M), sodium dihydrogen phosphate ($3.2x10^{-6}$M), ammonium chloride ($3.3x10^{-6}$M), potassium sulphate ($3.94x10^{-6}$M) and sodium chloride ($6.52x10^{-6}$M).

5.2.2 Apparatus

Electrochemical measurements were conducted with a potentiostat/galvanostat from Metrohm Autolab PGSTAT302N (Figure 5.2), with Frequency Response Analysis (FRA) module, controlled by Nova software. Graphene-SPEs were purchased from DropSens (DRP-110GPH), having a counter electrode of Platinum (Pt), a reference electrode of Ag/AgCl, and a working electrode of printed graphene of 4 mm diameter. The Graphene-SPEs were interfaced with the potentiostat/galvanostat via a switch box (Figure 5.3), also from DropSens (DRP-DSC). Fourier transform infrared spectroscopy (FTIR) measurements were performed using a Thermo Scientific Smart iTR Nicolet iS10, coupled to the Attenuated Total Reflectance (ATR) smart accessory, from Thermo Scientific.

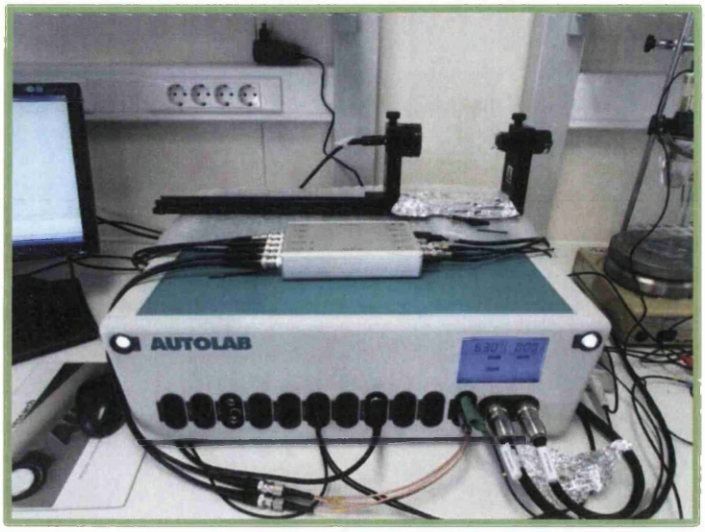

Figure 5.2 - Autolab PGSTAT302N.

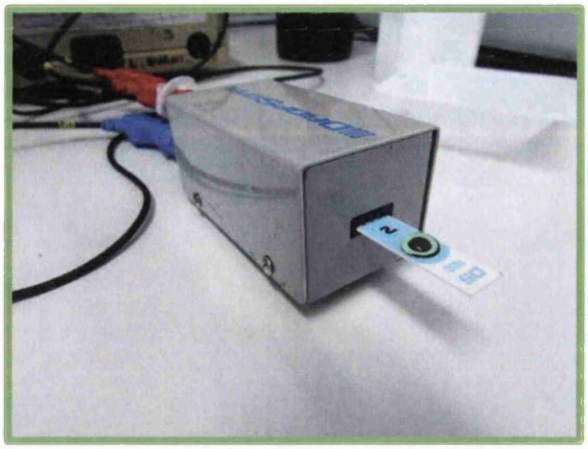

Figure 5.3 - Switch box.

5.2.3 Procedures for immunosensor assembly

The chitosan (CS) film was obtained by electrodeposition of chitosan on the graphene-SPE surface using chrono amperometry (CA). The three-electrodes of the SPE were covered by a solution of 0.1% of chitosan and 1% of AuNPs. A potential of -2.5V was applied for 120 sec.

In parallel, an antibody solution of 200µg/mL was mixed with 25mmol/L EDAC, and 50mmol/L of NHS, for 2 hours at room temperature. A drop of this resulting solution was then placed on the CS-AuNPs/graphene-SPE surface. After 2 hours at room temperature, the electrode was rinsed and a drop of BSA solution (0.5mg/mL in PBS buffer) was added for 30 minutes. The immunosensor was then washed with PBS buffer.

5.2.4 hCG Binding

hCG binding to the antibody on the immunosensor was achieved by placing a drop of the hCG solution on the sensor surface. Different concentration of hCG solutions, ranging from 0.01 to 100ng/mL, were prepared by dilution of the 250ng/mL standard hCG solution in PBS or synthetic urine. hCG was also detected in real urine samples from pregnant woman. A period of 20 minutes was allowed for antigen/antibody binding. This was followed by PBS washing prior to redox probe EIS measurements.

5.2.5 Electrochemical assays

CV measurements were conducted in 5.0mmol/L of $[Fe(CN)6]^{3-/4-}$, prepared in PBS buffer, pH 7.4. In CV assays the potential was scanned from -0.7V to +0.7V, at 50mV/s. All assays were conducted in triplicate.

EIS assays were also conducted in triplicate with the same redox couple $[Fe(CN)6]^{3-/4-}$ at a standard potential of +0.10 V, using a sinusoidal potential perturbation with amplitude of 100mV and a frequency equal to 50Hz, logarithmically distributed over a frequency range of 100000Hz-0.1Hz. The impedance data were fitted to a R(RC) circuit equivalent to a Randles circuit using the Nova Software. The Randles equivalent circuit, R(RC), is one of the simplest and most commom equivalent circuit models. It includes a solution resistance (R_Q), a double layer capacitor (C_{dl}) or a constant phase element (*CPE*), and a charge transfer (R_{CT}) or a polarization resistance (R_p). This model assumes that the double layer capacitance is in parallel with the charge transfer resistance. In addition to being a useful model in its own right, the simplified Randles equivalent circuit is often the starting point for other more complex models. The Nyquist plot for a simplified Randles equivalent circuit is always a semicircle. The solution resistance (R_Q) can be found by reading the real axis value at the high frequency intercept. This is the intercept near the origin of the plot. The real axis value at the other intercept is the sum of the solution resistance and the charge transfer resistance ($R_Q + R_{CT}$). The diameter of the semicircle is therefore equal to the charge transfer resistance [40].

The immunosensor response to varying hCG concentrations was assessed by EIS measurements. The hCG solutions ranged from 0.01 to 100ng/mL in concentration, and were prepared either in PBS buffer pH 7.4 or in synthetic urine. The limit of detection (LOD) was calculated using the interception of the linear range slope with the non-linear range.

5.3 Results and discussion

5.3.1 Immunosensor assembly

Surface modification was achieved by an electrochemical oxidation followed by an electrodeposition of chitosan with AuNPs on a graphene electrode (Figure 5.4 and 5.5A and B), thus yielding surface amine groups on the CS/AuNPs-graphene electrode. These amine groups are used to bind the anti-hCG to the modified graphene SPE.

The next stage was antibody binding to the amine-terminated surface. An antibody is a protein that has many functional groups capable of adsorbing to an amine-terminated surface, meaning that the antibody solution could simply be placed above this layer. However, this procedure would lead to a random position of the antibodies over the surface, which in turn would implicate that many antibodies had been deactivated or partially deactivated through stereochemical constrains for antigen binding. Antibodies were first activated by EDAC and NHS chemistry. The reaction of –COOH with EDAC formed a highly reactive O-acylisourea unstable intermediate that reacted later with NHS to produce a more stable active ester [41]. This ester underwent nucleophilic substitution reaction with any amine group on the protein, resulting in the formation of an amide bond between antibody and amine-terminated surface. This layer was washed with PBS pH 7.4 in order to remove unbound protein from the surface (Figure 5.5C).

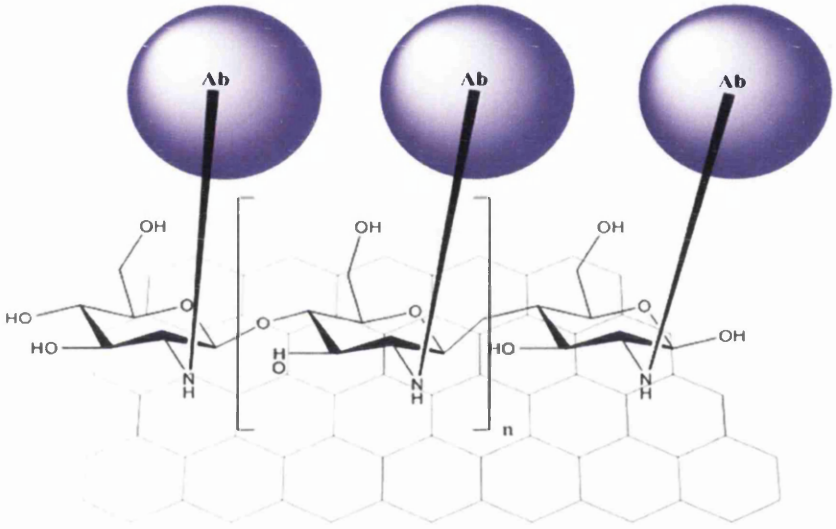

Figure 5.4 - Illustration of Graphene coated with an antibody-modified chitosan layer.

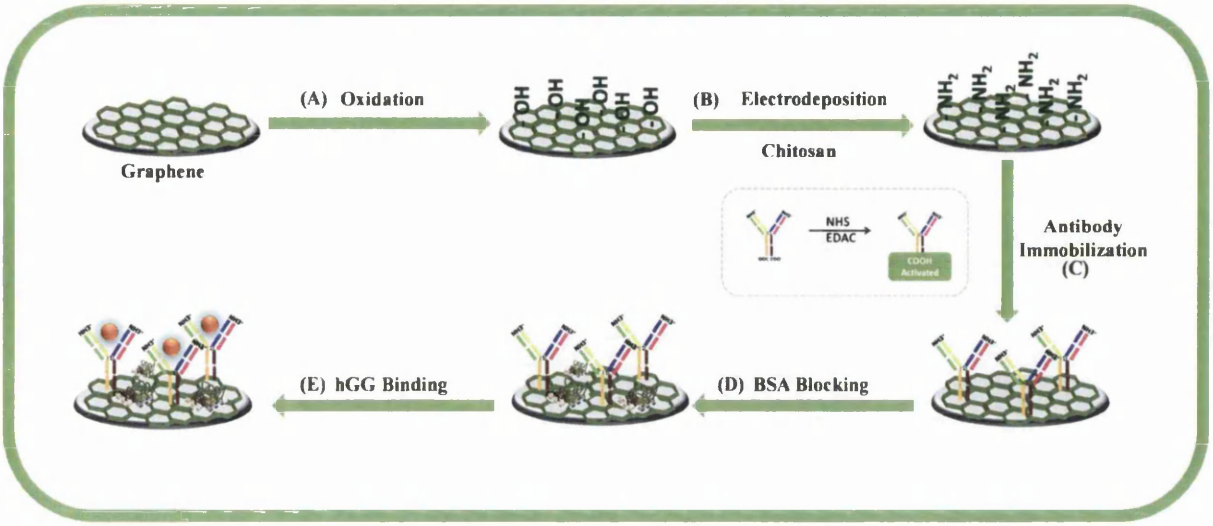

Figure 5.5 - Schematic illustration of the immunosensor assembly.

The final stage of the assembly was devoted to blocking any free amine sites which could otherwise allow non-specific binding to biomolecules other than hCG. Amino groups were blocked by adding BSA (Figure 5.5D), a simple and low-cost protein, to the sensor surface. BSA adsorbed to regions of non-specific protein binding, preventing subsequent binding of the compounds different than HCG. At the same time, this reaction deactivated the carboxylic functions that remained active after antibody binding, also contributing to eliminate side-responses from the immunosensor.

5.3.2 Electrochemical follow-up of the immunosensor

The chemical modifications taking place at graphene surface were monitored using CV and EIS (Figure 5.6), characterising changes in electron transfer properties against the redox probe [42]. The EIS data were analyzed by Nyquist plots. Nyquist plots showed the frequency response of the electrode/electrolyte system and area plot of the imaginary component (Z``) of the impedance against the real component (Z`). The charge-transfer resistance (Rct) at the electrode surface is given by the semicircle diameter obtained in EIS and can be used to define the interface properties of the electrode. The graphene surface showed a small semicircle at the Nyquist plot, which indicated the presence of a very fast electron-transfer process.

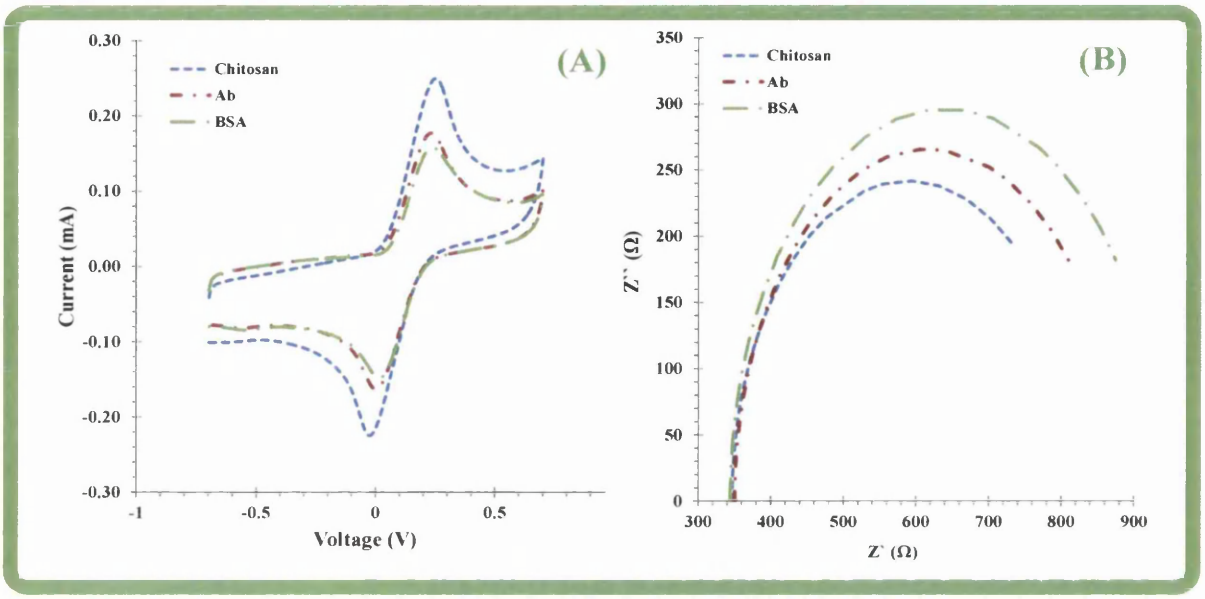

Figure 5.6 - CV data taken at each stage of the assembly of the immunosensor (A) and EIS spectra of each stage (B). **(A)** CV record after modification of Chitosan/AuNPs/Graphene-SPE with antibody and BSA; **(B)** Nyquist plots of BSA/anti-hCG/CS/Graphene-SPE sensor, obtained in 5.0 mM $[Fe(CN)6]^{3-/4-}$ PBS buffer pH 7.4.

CV analysis of the formation of a CS/AuNPs layer on graphene, via electrodeposition, yielded an increase in current (Figure 5.6A). Electrochemical data, obtained by using an iron redox probe with the newly formed CS/AuNPs layer, showed Nyquist plots where the R_{ct} increased compared to unmodified graphene. This is in agreement with the EIS data (Figure 5.6B).

Subsequent Antibody and BSA binding (both proteins) promoted substantial increases in the barrier to the redox probe accessing the CS/AuNPs/graphene-SPE surface, thus leading to additional increases in R_{ct}. CV assays supported the results of EIS studies (Figure 5.6B), with decreased current peaks after protein binding and an increase in the peak-to-peak potential separation.

The CS/AuNPs composition gives superior sensitivity to the CS graphene sensor without AuNPs. The reasons for the superior sensitivity are currently not certain but the following suggestions are presented as possible explanations: 1) increased conductivity of the composite layer compared with CS layer (however this seems to be unlikely since a conductive film would intrinsically have a lower impedance. 2) Due to the charge transfer between graphene and adsorbed molecules from the AuNPs to the graphene layer, the surface enhancement typically comes from a chemical mechanism based on a charge transfer between the molecule and the substrate. It is a short-range effect which usually requires the molecule to be close enough to the

substrate. This contributes to the overall enhancement. Further work it is required for fully understands this mechanism.

5.3.3 Analytical performance of the sensor

Figure 5.7A shows the Nyquist plots of the immunosensor Ab/CS/AuNPs/graphene-SPE against increasing hCG concentrations. The concentration range of hCG used for calibration was 0.1 and 25ng/mL and these solutions were prepared in PBS. The corresponding calibration curve was plotted as R_{ct} (extracted from the Nyquist plots) against the logarithm of the hCG concentration (inset of Figure 5.7A). Figure 5.7A (inset) shows, R_{ct} increases logarithmically over the 0.1 to 25ng/mL concentration range. The average slope of the R_{ct} versus log[hCG] was 0.129kΩ/decade hCG with an R^2 correlation coefficient of 0.95. The limit of detection (LOD) was determined as 0.1ng/mL.

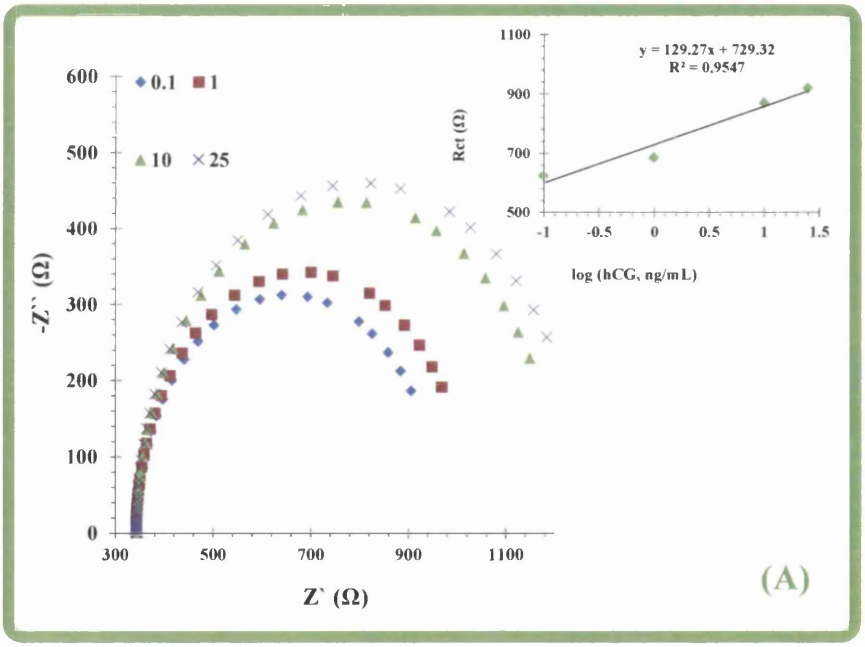

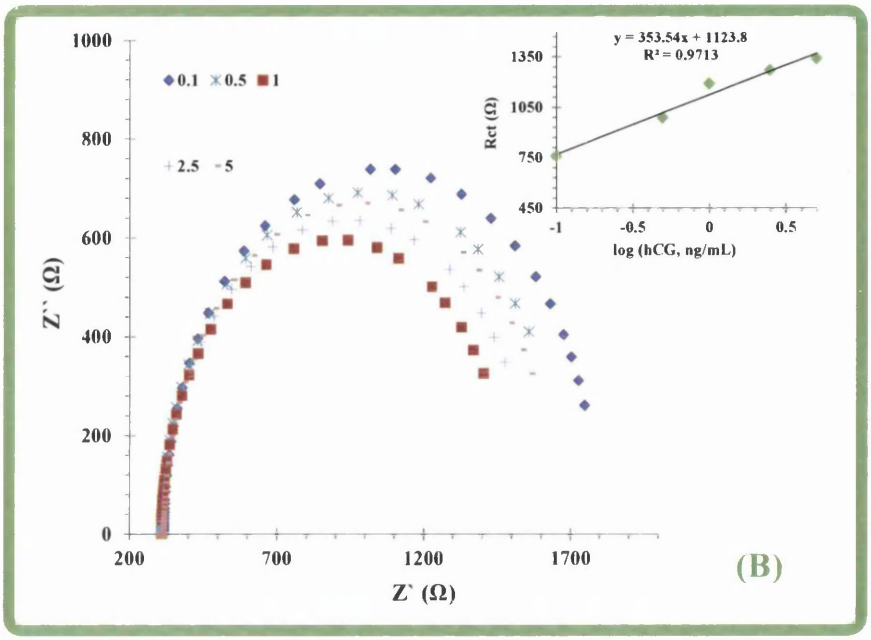

Figure 5.7 - Calibration curve of the immunosensor. (A): Nyquist plots of BSA/anti hCG/Chitosan/Graphene-SPE sensor, in 5.0 mM $[Fe(CN)6]^{3-/4-}$ PBS buffer pH 7.4, previously incubated in increasing concentrations of hCG. (B): Nyquist plots of BSA/anti-hCG/Chitosan/Graphene-SPE sensor, in 5.0 mM $[Fe(CN)6]^{3-/4-}$ synthetic urine buffer pH 6.5, previously incubated in increasing concentrations of hCG.

5.3.4 Selectivity of the sensor

Typically, selectivity is assessed by evaluating the effect of compounds present in the test solution, other than the target analyte (hCG), on the analytical response of a sensor device. To simulate the effect of real biological conditions, and ascertain the effect of urine on the performance of the sensor, the immunosensor was exposed to solutions of synthetic urine spiked with hCG. The selectivity of the sensor was thus investigated by monitoring its response to the synthetic urine. The synthetic urine was prepared according to recipes from [43] and contained creatinine, magnesium chloride, calcium chloride, sodium dihydrogen phosphate, ammonium chloride, potassium sulphate and sodium chloride.

Figure 5.7B shows the Nyquist plots obtained by calibrating the immunosensor in increasing concentrations of hCG prepared in synthetic urine. Linear responses were observed from log [0.01 to 5 (ng/mL)], with a slope of 0.353kΩ/[hCG, ng/mL]. Comparing the calibration in PBS, the sensitivity was slightly decreased and the LOD was superior, but the upper concentration limit was higher. Overall, the analytical response of the immunosensor was slightly changed, although

the overall performance was unexpectedly enhanced. No interference in the sensor was observed, suggesting its successful application in real urine samples.

5.3.5 Application to urine samples

The values of hCG in real urine samples were determined by EIS measurements after calibration of the Ab/CS/AuNPs/graphene-SPE device. The Nyquist plots obtained are shown in Figure 5.8, along with the corresponding calibration curve. The sensor exhibited linear behaviour from log [0.01 to 5 (ng/mL)], when the standard hCG solutions were prepared in urine of non-pregnant women. When another sensor Ab/CS/AuNPs/graphene-SPE was tested using urine of pregnant woman, the obtained concentration was 3.5ng/mL (17.4mIU/mL), which corresponded to a pregnancy period lying within 3 weeks to 5 weeks, which is also in agreement with the patients term of pregnancy status. The shape of the R_{ct} curve was similar to that of the standards (Figure 5.8), suggesting that the system was operating well when applied to real sample conditions.

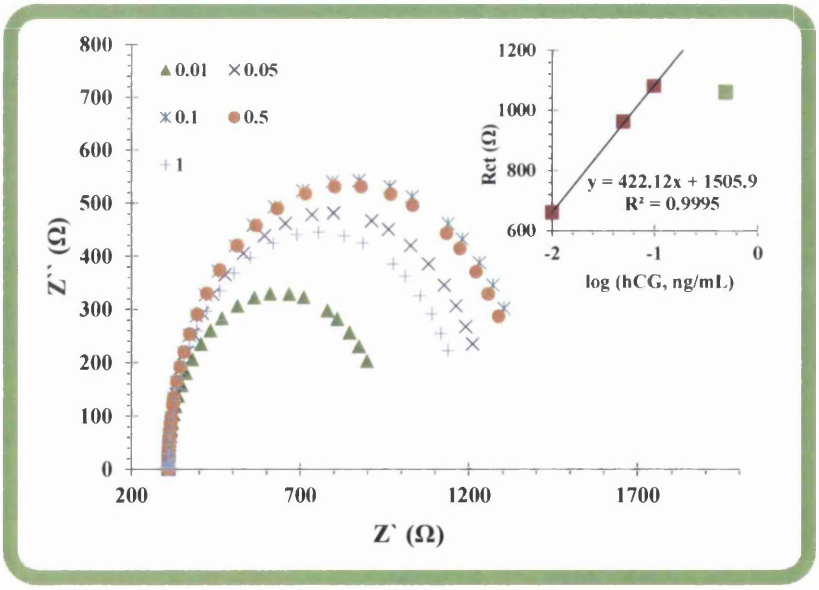

Figure 5. 8 - Calibration curve of the immunosensor in real urine. Rct values extracted from the Nyquist plots against log hCG concentration.

5.4 Conclusions

In summary, a new impedimetric biosensor for hCG was fabricated based on antibody–antigen binding to a CS-modified screen-printed graphene electrode. In this work, it was shown that CS was successfully deposited on graphene-SPE. The simple approach for antibody binding, enabled attachment of the antibody to the sensing layer, and provided excellent reproducibility and stability. The electrode impedance increased linearly with increasing log hCG protein concentration and was not significantly affected by interference from chemical components present in synthetic urine.

The sensor has been used to successfully detect hCG concentrations in the urine of pregnant women, which concurs with the pregnancy status. The presented results and the accuracy and precision of the analytical data from the Antibody/CS modified graphene sensors proposed in this work, suggest that these sensors may be used in POC diagnostics in a near future.

References

[1] Vaisocherová, H., et al., *Surface plasmon resonance biosensor for direct detection of antibody against Epstein-Barr virus.* Biosensors & bioelectronics, 2007. **22**(6): p. 1020-1026.

[2] Conneely, G., et al., *Development of an immunosensor for the detection of testosterone in bovine urine.* Analytica chimica acta, 2007. **583**(1): p. 153-160.

[3] Delibato, E., et al., *Development of SYBR-Green Real-Time PCR and a Multichannel Electrochemical Immunosensor for Specific Detection of Salmonella enterica.* Analytical Letters, 2006. **39**.

[4] Romanazzo, D., et al., *ELIME (enzyme linked immuno magnetic electrochemical) method for mycotoxin detection.* Journal of visualized experiments : JoVE, 2009(32).

[5] Li, Y., H. Lee, and R. Corn, *Detection of protein biomarkers using RNA aptamer microarrays and enzymatically amplified surface plasmon resonance imaging.* Analytical chemistry, 2007. **79**(3): p. 1082-1088.

[6] Saerens, D., et al., *Antibody Fragments as Probe in Biosensor Development.* Sensors, 2008. **8**.

[7] Suzuki, M., et al., *Miniature surface-plasmon resonance immunosensors--rapid and repetitive procedure.* Analytical and bioanalytical chemistry, 2002. **372**(2): p. 301-304.

[8] Kurtinaitiene, B., et al., *Amperometric immunosensor for diagnosis of BLV infection.* Biosensors & bioelectronics, 2008. **23**(10): p. 1547-1554.

[9] Ramanavicius, A., et al., *Conducting polymer based fluorescence quenching as a new approach to increase the selectivity of immunosensors.* Biosensors & bioelectronics, 2007. **23**(4): p. 499-505.

[10] Kausaite-Minkstimiene, A., et al., *Comparative study of random and oriented antibody immobilization techniques on the binding capacity of immunosensor.* Analytical chemistry, 2010. **82**(15): p. 6401-6408.

[11] Lee, J., et al., *Direct immobilization of protein g variants with various numbers of cysteine residues on a gold surface.* Analytical chemistry, 2007. **79**(7): p. 2680-2687.

[12] Byung-Keun, O., et al., *Immunosensor for detection of Legionella pneumophila using surface plasmon resonance.* Biosensors and Bioelectronics, 2003. **18**.

[13] Turková, J., *Oriented immobilization of biologically active proteins as a tool for revealing protein interactions and function.* Journal of chromatography. B, Biomedical sciences and applications, 1999. **722**(1-2): p. 11-31.

[14] Hoffman, W.L.O.S.D.J., *Site-specific immobilization of antibodies by their oligosaccharide moieties to new hydrazide derivatized solid supports.* J. Immonol. Methods, 1988. **112**(11): p. 113-120.

[15] Gaurav, G.M., Sugimoto; Yoshikazu, Matsui; Jun Kondoh, *Use of a low refractive index prism in surface plasmon resonance biosensing.pdf.* Sensors & Actuactors:B Chemical, 2008. **130**(2): p. 689-695.

[16] Xiong, Q.G.F., *Identification and evaluation of a panel of serum biomarkers for predicting response to thalidomide in multiple myeloma patients.* Expert Rev Proteomics, 2011. **8**(4): p. 439-442.

[17] McNulty, C., P. Lehours, and F. Mégraud, *Diagnosis of Helicobacter pylori Infection.* Helicobacter, 2011. **16 Suppl 1**: p. 10-18.

[18] Moelans, C., et al., *Current technologies for HER2 testing in breast cancer.* Critical reviews in oncology/hematology, 2011. **80**(3): p. 380-392.

[19] J.E. Butler, L.N., W.R. Brown, K.S. Joshi, J. Chang, B. Rosenberg, E.W. Voss Jr, *The immunochemistry of sandwich elisas—VI. Greater than 90% of monoclonal and 75% of polyclonal anti-fluorescyl capture antibodies (CAbs) are denatured by passive adsorption.* Molecular Immunology, 1993. **30**(13): p. 1165-1175.

[20] Byeon, J.-Y., F. Limpoco, and R. Bailey, *Efficient bioconjugation of protein capture agents to biosensor surfaces using aniline-catalyzed hydrazone ligation.* Langmuir : the ACS journal of surfaces and colloids, 2010. **26**(19): p. 15430-15435.

[21] Chan, F.S.a.W.C.W., *Principles of conjugating quantum dots to.pdf.* Nanotechnology, 2011. **22**: p. 494006 (7pp).

[22] Dempsey, E., D. Diamond, and A. Collier, *Development of a biosensor for endocrine disrupting compounds based on tyrosinase entrapped within a poly(thionine) film.* Biosensors & bioelectronics, 2004. **20**(2): p. 367-377.

[23] Miao, Y. and S.N. Tan, *Amperometric hydrogen peroxide biosensor with silica sol–gel/chitosan film as immobilization matrix.* Analytica chimica acta, 2001. **437**.

[24] Rebecca, A.Z., et al., *Electrochemical study of chitosan films deposited from solution at reducing potentials.* Electrochimica Acta, 2006. **51**.

[25] Solanki, H., et al., *Development of microencapsulation delivery system for long-term preservation of probiotics as biotherapeutics agent.* BioMed research international, 2013. **2013**: p. 620719.

[26] Kumar, M., et al., *Chitosan chemistry and pharmaceutical perspectives.* Chemical reviews, 2004. **104**(12): p. 6017-6084.

[27] Sánchez, S., et al., *Toward a fast, easy, and versatile immobilization of biomolecules into carbon nanotube/polysulfone-based biosensors for the detection of hCG hormone.* Analytical chemistry, 2008. **80**(17): p. 6508-6514.

[28] Jie, W., et al., *Biomedical and clinical applications of immunoassays and immunosensors for tumor markers.* TrAC Trends in Analytical Chemistry, 2007. **26**.

[29] Song, L. and G. Xuefeng, *Carbon nanomaterials field-effect-transistor-based biosensors.* NPG Asia Materials, 2012. **4**.

[30] Martin, P., et al., *Graphene for electrochemical sensing and biosensing.* TrAC Trends in Analytical Chemistry, 2010. **29**.

[31] Yueming, L., T. Longhua, and L. Jinghong, *Preparation and electrochemical performance for methanol oxidation of pt/graphene nanocomposites.* Electrochemistry Communications, 2009. **11**.

[32] Li, J., et al., *High-sensitivity determination of lead and cadmium based on the Nafion-graphene composite film.* Analytica chimica acta, 2009. **649**(2): p. 196-201.

[33] Li, X., et al., *Highly conducting graphene sheets and Langmuir-Blodgett films.* Nature nanotechnology, 2008. **3**(9): p. 538-542.

[34] Qin, W., et al., *Multifunctional mesoporous silica nanoparticles as sensitive labels for immunoassay of human chorionic gonadotropin.* Sensors and Actuators B: Chemical, 2011. **153**.

[35] McCreery, R., *Advanced carbon electrode materials for molecular electrochemistry.* Chemical reviews, 2008. **108**(7): p. 2646-2687.

[36] Li, M., et al., *Electrochemical and optical biosensors based on nanomaterials and nanostructures: a review.* Frontiers in bioscience (Scholar edition), 2011. **3**: p. 1308-1331.

[37] Yuyan, S., et al., *Graphene Based Electrochemical Sensors and Biosensors: A Review.* Electroanalysis, 2010. **22**.

[38] Kuila, T., et al., *Recent advances in graphene-based biosensors.* Biosensors & bioelectronics, 2011. **26**(12): p. 4637-4648.

[39] Martin, P., *Graphene in biosensing.* Materials Today, 2011. **14**.

[40] Mansfeld, F., *Electrochemical impedance spectroscopy (EIS) as a new tool for investigating methods of corrosion protection.* Electrochimica Acta, 1990. **35**(10): p. 1533-1544.

[41] Jiang, K., Schadler, L.S., Siegel, R.W., Zhang, X., Zhang, H., Terrone, M., Journal of Materials Chemistry, 2004. **14**: p. 37-39.

[42] Daniels, J. and N. Pourmand, *Label-Free Impedance Biosensors: Opportunities and Challenges.* Electroanalysis, 2007. **19**(12): p. 1239-1257.

[43] H. Haddad, *Synthetic urine for use in urine assay kits used for medical identification of illness or drug abuse, comprises a synthetic urine formulation and a heat activator,* Patent Number: US2004077106-A1 (2004); US7109035-B2 (2006).

CHAPTER 6[3]

"Experiments are the only means of knowledge at our disposal. The rest is poetry, imagination"

Max Planck (1858-1947), German Theoretical Physicist

Label-free human chorionic gonadotropin detection at picogram levels using oriented antibodies bound to graphene screen printed electrodes

The immunosensor development reported in this chapter is simpler than the others sensors devices developed in this thesis, produced via modification of a disposable graphene-SPE surface with an amine layer polyaniline (PANI), which preserves the chemical structure of graphene and allows subsequent binding of the bioreceptor antibody, anti-hCG to this layer. The amine layer is obtained by *in situ* electropolymerization of aniline on the graphene - SPE electrode. The amine groups of the PANI can react with the –COOH groups at the F_c region of the antibody, activated by carbodiimide chemistry, to ensure successful antibody binding. The antibody is bound to the PANI through its F_c terminal (thus allowing the paratope regions free to bind to the antigen epitopes) (see Chapter 2, section 2.4.1). The resulting biosensor has been evaluated using EIS, and utilised in the detection of hCG in biological samples.

[3] S Teixeira, S Conlan, O Guy, MGF Sales, Label-free human chorionic gonadotropin detection at picogram levels using oriented antibodies bound to graphene screen printed electrodes, Journal of Materials Chemistry B, 2014, 2,1852-1865.

6.1 Introduction

Immunoassay techniques using a specific molecular interaction between antibody and antigen have become the dominant clinical test methods for antigen detection. Alternative immunoassay detection methods include radioimmunoassay, enzyme-linked immunosorbent assay (ELISA), fluoroimmunoassay, chemiluminescent immunoassay, and electrochemiluminescent immunoassay [1]. Despite their sensitivity, precision and selectivity, these techniques suffer from several drawbacks that include radiation hazards, long test times, high costs, the need for qualified personnel and sophisticated instrumentation to perform the assays. Furthermore, existing diagnostic tests (e.g., microtiter-plate ELISAs) may not be sensitive enough for screening a wide range of proteins at low concentrations, with optical detection suffering from interference from other luminescence molecules. Also, single-analyte immunoassays are not fast enough for high-volume throughput [1]. New immunoassay systems for sensitive, selective, low-cost, multi-analyte and high-throughput immunoassay have therefore attracted considerable interest, leading to the integration of immune-reactions into electrochemical biosensors.

In electrochemical immunosensing, direct detection of antibody-antigen recognition is usually not possible and electrochemically redox couples are often employed [2]. Colloidal gold/silver, semiconductor nanoparticles, and marker loaded nanocarriers (carbon nanotubes, apoferritin, silica nanoparticles, and liposome beads) have all been used as labels [3]. However, this is a complex and quite expensive procedure.

In contrast, electrochemical impedance spectroscopy (EIS) can be used to directly measure the effect of the antigen binding on the resistance to charge-transfer across the electrode surface.

Electrochemical immunosensors using advances in nanomaterials are increasingly being used for biosensing applications [4]. In this context, carbon-based nanomaterials are gaining interest as an alternative to gold electrodes. Different carbon nanostructures, with different inherent electrical properties, have been used in electrochemical immunosensors including CNTs [5] and more recently (since 2005) graphene [6].

Graphene displays a combination of interesting properties, such as large surface area, high electrical conductivity and biocompatibility [7-14]. Heterogeneous electron transfer (the transfers of electrons between graphene and molecule in solution (necessary for the oxidation/reduction of said molecule) occurs at the edges of the graphene or at defects in the basal plane [2]. Additional defects are also introduced by functionalization, required to immobilize biomolecules, including antibodies, on to graphene. The antibodies act as biological receptors in immunosensors. Direct functionalization can affect the performance of the graphene electrode – by significantly reducing

the carrier mobility in the graphene. Overall, graphene is employed within a quite complex chemistry to produce specific composite nanomaterials. These nanomaterials are in turn involved in the assembly of immunosensors including several consecutive layers, increasing the risk of device failure in routine testing. Furthermore, chemically modified positions in graphene may hinder the excellent electronic transfer ability of this carbon matrix for changing the carbon hybridization from sp^2 to sp^3, thereby interrupting the path of conjugated π electrons.

An alternative way of attaching the bioreceptor antibodies to the sensor electrode is through grafting to an intermediate layer such as pyrene [15] or polyaniline which is deposited on top of the graphene electrode [16]. This avoids the introduction of defects into the graphene substrate and preserves graphene's electrical characteristics [17]. Intermediary pyrene or polyaniline layers allow efficient electron transfer to the graphene electrode. Correct orientation of the antibody on the PANI-graphene support is crucial, to ensure that the two binding sites in each antibody are free for antigen binding and that antibody activity is preserved after grafting.

Thus, this work proposes a new immunosensor set-up, where the antibody is directly attached to a PANI-modified screen-printed graphene electrode, and used to detect human chorionic gonadotrophin (hCG) using label-free EIS measurements.

At present, conventional methods for determining hCG are immunoradiometric assays (IRMA) and enzyme-linked immunosorbent assays (ELISA) [18]. IRMA is extremely sensitive, but involves radiation hazards, complicated washing procedures and is expensive, while the ELISA is less sensitive but time-consuming. Various electrochemical immunosensors for hCG measurements have also been reported recently, but only few of these use graphene [19-22]. The detailed process involved in the assembly of these immunosensors and the relevant chemical course/data for hCG determination have been resumed in table 1 in Chapter 2. Finally, the overall processes for hCG detection is especially complex when labeled nanomaterials are employed, requiring as well longer times for reaching a response.

6.2 Experimental Section

6.2.1 Materials and Reagents

All chemicals used were analytical grade and water was de-ionized. Potassium hexacyanoferrate III ($K_3[Fe(CN)_6]$) and potassium hexacyanoferrate II ($K_4[Fe(CN)_6]$) trihydrate were obtained from Riedel Haen; N-Hydroxysuccinimide (NHS) was obtained from Fluka; N-(3-Dimethylaminopropyl)-N'-ethylcarbodiimide hydrochloride (EDAC), bovine serum albumin

(BSA), and aniline were obtained from Sigma; phosphate buffered saline (PBS) tablets were obtained from Amresco. The hCG protein was purchased from Abcam (UK). The anti-hCG antibody was supplied by Ig Innovations.

A 0.1M aniline solution was prepared in 2.5M H_2SO_4. PBS solution was prepared by dissolution of 1 tablet (1814.5 - 2005.5mg/tab) of PBS in 200mL of D.I. Water. EDAC, NHS and antibody solutions were prepared in this buffer. Synthetic urine was prepared with creatinine ($5.3x10^{-6}$M), magnesium chloride ($9.8x10^{-7}$M), calcium chloride ($6.80x10^{-7}$M), sodium dihydrogen phosphate ($3.2x10^{-6}$M), ammonium chloride ($3.3x10^{-6}$M), potassium sulphate ($3.94x10^{-6}$M) and sodium chloride ($6.52x10^{-6}$M).

6.2.2 Apparatus

Electrochemical measurements were conducted with a potentiostat/galvanostat from Metrohm Autolab PGSTAT302N, with Frequency Response Analysis (FRA) module, controlled by Nova software. Graphene-SPEs were purchased from DropSens (DRP-110GPH), having a counter electrode of Platinum (Pt), a reference electrode of Ag/AgCl, and a working electrode of printed graphene of 4mm diameter. The Graphene-SPEs were interfaced with the potentiostat/galvanostat via a switch box, also from DropSens (DRP-DSC). Raman measurements were performed using a Thermo Scientific DXR Raman microscope system with a 100 mW 532 nm excitation laser, and spectra were recorded using 5 mW power and 50μm pinhole aperture. Fourier transform infrared spectroscopy (FTIR) measurements were performed using a Thermo Scientific Smart iTR Nicolet iS10, coupled to the Attenuated Total Reflectance (ATR) smart accessory, also from Thermo Scientific.

6.2.3 Procedures for immunosensor assembly

The polyaniline (PANI) film was obtained by electropolymerization of aniline on the graphene-SPE surface using cyclic voltammetry (CV). The three-electrodes of the SPE were covered by a solution of 0.1M aniline and a potential sweep applied from –0.1V to 1.2V, at a sweep rate of 50mV/s, for 20 cycles.

An antibody solution of 200μg/mL was mixed with 25mmol/L EDAC, and 50mmol/L of NHS, to activate the antibody, and a drop of this resulting solution was then placed on the PANI/graphene-SPE surface for 2 hours. After 2 hours at room temperature, the electrode was

rinsed and a drop of BSA solution (0.5mg/mL in PBS buffer) was added for 30 minutes. The immunosensor was then washed with PBS buffer.

6.2.4 hCG binding

hCG binding to the antibody on the immunosensor was achieved by placing a drop of the hCG solution on the sensor surface. Different concentration hCG solutions, ranging from 0.01 to 5ng/mL, were prepared by dilution of the 25ng/mL standard hCG solution in PBS or synthetic urine. hCG was also detected in real urine samples from pregnant woman. A period of 15 minutes was allowed for antigen/antibody binding. This was followed by PBS washing prior to redox probe EIS measurments.

6.2.5 Electrochemical assays

CV measurements were conducted in 5.0mmol/L of $[Fe(CN)6]^{3-/4-}$, prepared in PBS buffer, pH 7.4. In CV assays the potential was scanned from -0.7V to +0.7V, at 50mV/s. All assays were conducted in triplicate.

EIS assays were also conducted in triplicate with the same redox couple $[Fe(CN)6]^{3-/4-}$ at a standard potential of +0.10V, using a sinusoidal potential perturbation with amplitude of 100mV and a frequency equal to 100Hz, logarithmically distributed over a frequency range of 10Hz–0.001Hz. The impedance data were fitted to a Randles equivalent circuit using the Nova Software.

The immunosensor response to varying hCG concentrations was assessed by EIS measurements. The hCG solutions ranged from 0.01 to 5ng/mL, and were prepared either in PBS buffer pH 7.4 or in synthetic urine pH 6.5. The limit of detection (LOD) was calculated using $3\sigma/S$, where S was the slope of the linear calibration plot and σ the standard deviation.

6.3. Results and discussion

6.3.1 Immunosensor assembly

A schematic of the functionalization process for the immunosensor assembly can be seen in Figure 6.1. The first stage in the sensor fabrication was modification of the screen-printed graphene electrode with a thin film of polyaniline, thus yielding surface amine groups on the

PANI-graphene electrode (Figure 6.1ii). These amine groups are used to bind the anti-hCG to the modified graphene SPE. A PANI film was formed on the graphene SPE via coating the electrode in a solution of aniline and subsequent electropolymerization of aniline to form a conductive polymer layer over the nanostructured graphene support [23-25]. This PANI layer is electrically conductive and is able to transfer electrical carriers to the graphene SPE [26]. Of the several conductive polymers that have been employed in electrochemical applications, PANI was selected because of its simple synthesis and good stability [27]. The requirement for graphene oxidation prior to electropolymerization of aniline was investigated [28] and no significant differences were observed between standard and oxidised PANI/ graphene-SPE.

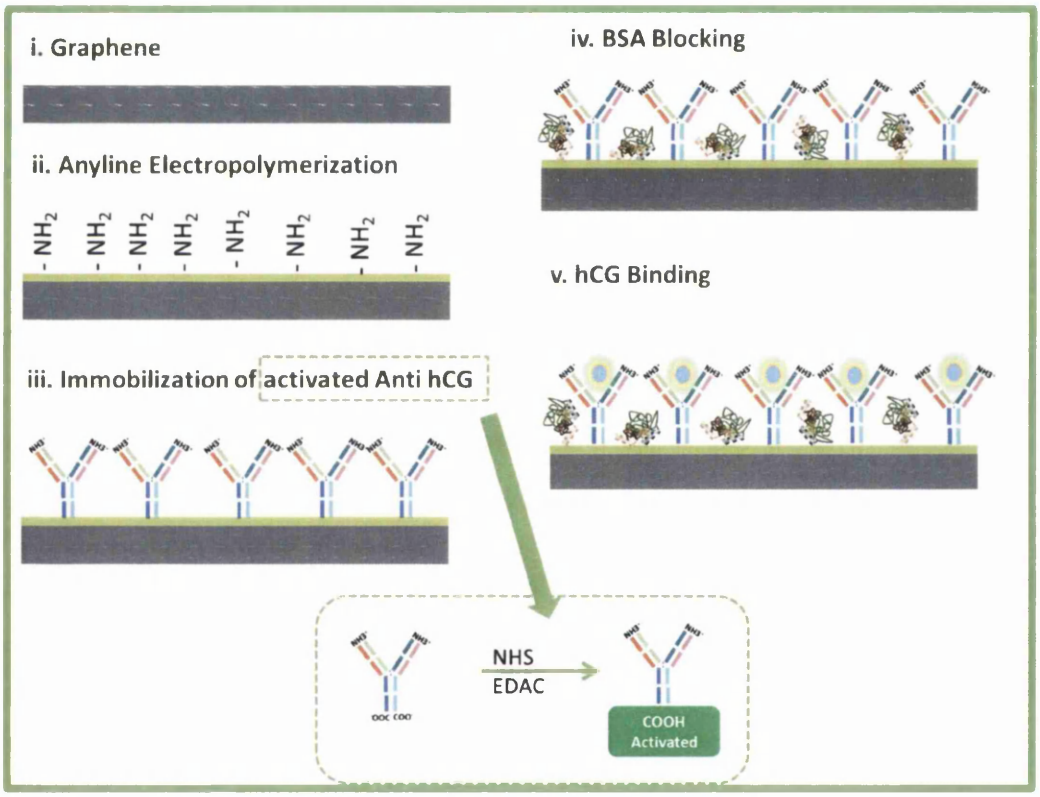

Figure 6.1 - Schematic illustration of the immunosensor assembly.

The next stage of the sensor fabrication was antibody binding to the PANI layer. Antibodies have several functional groups that facilitate adsorption to PANI, meaning that the antibody solution could simply be deposited on this layer. However, this procedure would lead to a random positioning of the antibodies on the surface. Consequently, many antibodies could be deactivated or partially deactivated with respect to antigen binding through stereochemical constraints.

Thus, covalent binding of the antibody to the PANI-graphene SPE was performed in order to achieve a more stable and homogenous orientation of the antibodies. This covalent binding can be accomplished through the –COOH terminated F_c site of the antibody. Attachment via the F_c site ensures that both F_{ab} sites are free for subsequent antigen binding. Antibodies were first activated by EDAC/NHS chemistry, forming a highly reactive *O*-Acylisourea intermediate that reacted rapidly with NHS to produce a stable succinimydyl ester [29]. This ester then undergoes a nucleophilic substitution reaction with the amine groups on the PANI, leading to the formation of an antibody grafted PANI layer (Figure 6.1iii).

The final stage of the assembly was devoted to blocking any free amine sites on surface which could otherwise allow non-specific binding of biomolecules other than hCG. Amino groups were blocked by adding BSA, a simple and low-cost protein, to the sensor surface. BSA adsorbed to regions of non-specific protein binding, preventing subsequent binding of the compounds other than hCG. At the same time, this reaction deactivated the carboxylic functions that remained active after antibody binding, this eliminating any potential side-responses from non-specific binding in the immunosensor.

6.3.2 Electrochemical follow-up of the immunosensor

The chemical modifications taking place at graphene surface were monitored using CV and EIS (Figure 6.2), characterising changes in electron transfer properties against the redox probe [30]. The EIS data were analyzed by Nyquist plots. Nyquist plots showed the frequency response of the electrode/electrolyte system and area plot of the imaginary component (Z``) of the impedance against the real component (Z`). The charge-transfer resistance (R_{ct}) at the electrode surface is given by the semicircle diameter obtained in EIS and can be used to define the interface properties of the electrode. The graphene surface showed a small semicircle at the Nyquist plot, which indicated the presence of a very fast electron-transfer process. This process had no diffusion limited step, which suggests a Faradaic process.

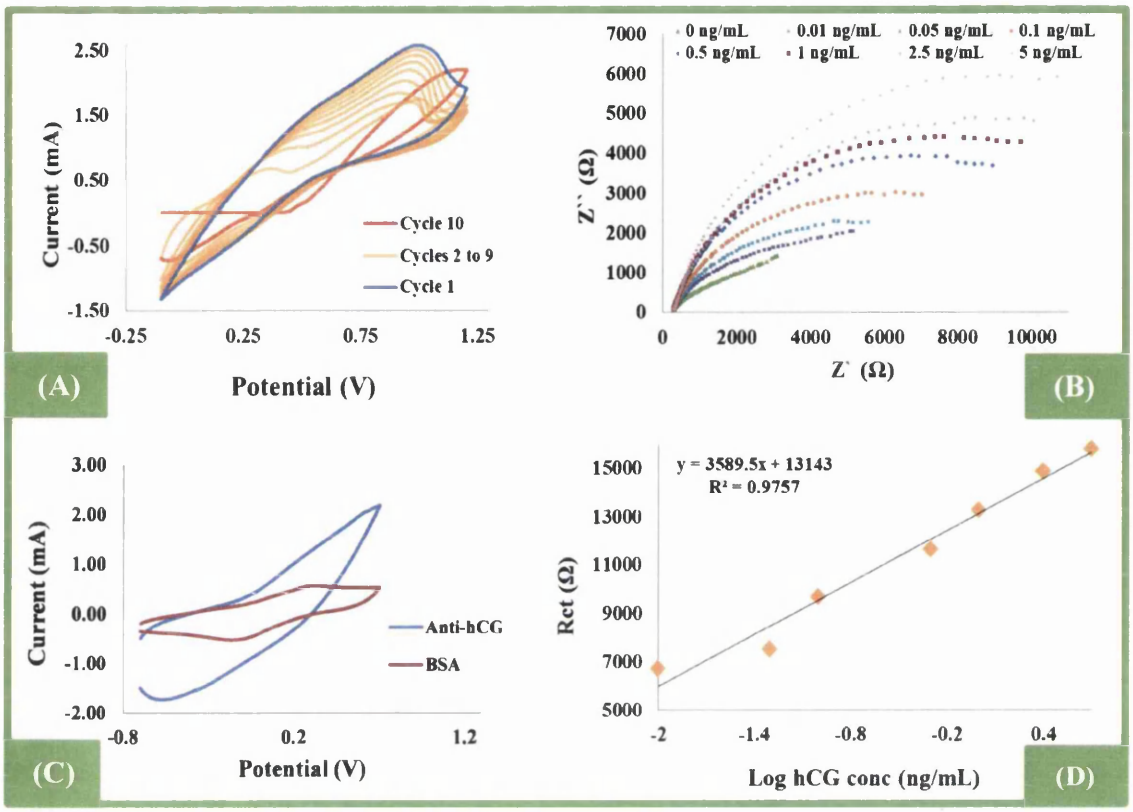

Figure 6.2 - CV data taken during the assembly of the immunosensor (A and C) and EIS spectra of calibration (B) along with its calibration plot (D). **(A)** Synthesis of polyaniline on Graphene-SPE electrode (10 cycles performed with a scan rate of 50mV/s; **(B)** Nyquist plots of BSA/anti-hCG/PANI/Graphene-SPE sensor, incubated in increasing concentrations of hCG, obtained in 5.0 mM $[Fe(CN)6]^{3-/4-}$ PBS buffer pH 7.4; **(C)** CV records after modification of PANI/Graphene-SPE with antibody and BSA; **(D)** The R_{ct} values of the previous calibration plotted against log hCG concentration.

CV analysis of the formation of a PANI layer on graphene, via electropolymerization, yielded a decrease in current with an increasing number of cycles (Figure 6.2A). After 10 cycles, the current density of the oxidation peak was greatly reduced, thus confirming the formation of a PANI film. Electrochemical data, obtained by using an iron redox probe with the newly formed PANI layer, showed Nyquist plots where the R_{ct} increased relative to the unmodified graphene which was in agreement with the CV data obtained at the electropolymerization stage.

Subsequent Antibody and BSA binding (both proteins) promoted substantial increases in the barrier to the redox probe accessing the PANI/graphene-SPE surface, thus leading to additional increases in R_{ct}. CV assays supported the results of EIS studies (Figure 6.2B), with decreased current peaks after protein binding and an increase in the peak-to-peak potential separation.

6.3.3 Qualitative analysis of the immunosensor surface

Figure 6.3 shows the FTIR spectra of the Graphene-SPE before any modification (A) and after coating the electrode through electropolymerisation to form the PANI/Graphene-SPE (B). The Graphene-SPE spectrum acted here as control reference spectrum, from which changes related to the PANI layer in the FTIR spectrum of the PANI-Graphene-SPE can clearly be distinguished.

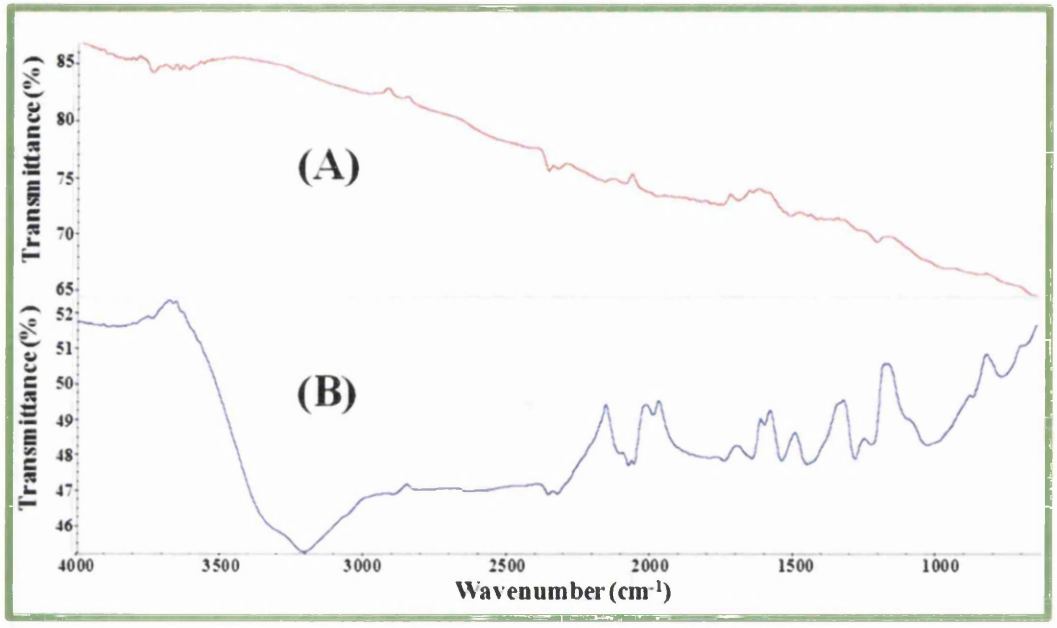

Figure 6.3 - FTIR spectra of modified Graphene-SPE before **(A)** and after electrodeposition of aniline to yielded polyaniline **(B)**.

Overall, the introduction of the PANI film on graphene gave rise to a wide range of absorption bands/peaks not present in the control sample spectrum, thus confirming the presence of the PANI layer. The presence of two bands in the vicinity of 1500cm^{-1} and 1600cm^{-1} were assigned to the 6 carbon stretching modes of the bezenoid (B) and quinoid (Q) rings, respectively [31,32]. The peaks in the vicinity of 1250 and 750cm^{-1} were assigned to vibrations associated with the C-N stretching vibration of aromatic amine and C-H vibrations [33]. The absorption peak near 1150cm^{-1} could be assigned to B–NH–B and δ(C–H) vibrations [34].

Raman spectroscopic measurements (Figure 6.4) were also performed after each stage of the immunosensor functionalization process. The spectra of the control graphene-SPE showed three Raman bands at 1350, 1600 and 2700 cm^{-1} that were assigned to the well-documented D, G and 2D bands in standard chemically graphene. The G peaks represent the in-plane bond-stretching

vibrations of sp^2-hybridized carbon atoms, while D peak is related to the vibrations of the carbon atoms of dangling bonds or sp^3-hybridised carbon atoms of disordered and / or defected graphite [35]. The intensity ratio of I_G/I_D bands is typically used for quantifying the defect density in graphene, and the small ratio extracted from Figure 6.4 indicates significant disorder, arising from structural defects, despite recent evidence that the I_G intensity increases with increasing laser excitation energy [36,37]. Since the intensity of the G band increases almost linearly as the graphene thickness increases, the ratio of I_G/I_{2D} could be used to determine the number of layers in the graphene [38,39]. The ratio of I_G/I_{2D} obtained was ~0.4, this showing the graphene is just a few layers thick (less than 5).

After electrochemical polymerization of aniline, all of the Raman spectra showed distinct bands attributable to PANI [37], which overlap the characteristic bands of standard graphene (at 1300 and 1600 cm^{-1}). The sp^3 peak of graphene becomes more intense and broad after PANI deposition, [28].

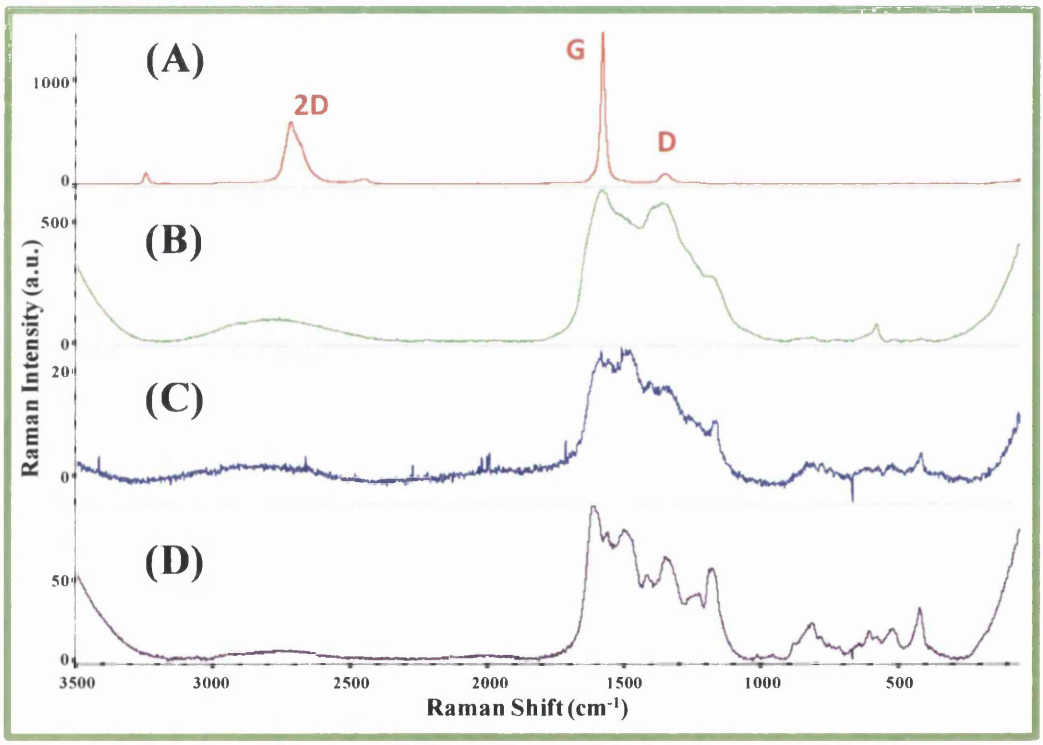

Figure 6.4 - Raman spectra of **(A)** Graphene-SPE, **(B)** PANI/Graphene-SPE, **(C)** anti hCG/PANI/Graphene and **(D)** BSA/anti-hCG/PANI/Graphene-SPE.

Compared with Graphene, the sp^3 peak of PANI showed a slight shift to higher frequencies, probably due to the electrostatic interaction between aniline monomers and Graphene-SPE, both

displaying aromatic features. Overall, the obtained Raman spectra indicated the successful modification of the Graphene-SPE, which implied the formation of a PANI film.

Subsequent antibody and BSA binding introduced an additional increase in the Raman intensity, related to fluorescence generation produced by the residues in the protein structure. This implied the need for specific fluorescence correction, which is detrimental to the quality of the resulting spectra.

6.3.4 Polyaniline and Antibody coverage

The antibody coverage of the electrode surface was assessed by mapping a 610×500 μm area of the PANI/graphene-SPE and Anti-hCG/PANI/graphene-SPE device with the Raman Spectrometer coupled to Confocal Microscopy and automated XY stage.

Figure 6.5 shows a typical colour coverage distribution map after graphene PANI electropolymerization (A). This is a spatial map of the intensity of the PANI-related Raman peak at 1663cm^{-1}and indicates that 83% of the analysed area was covered with PANI, considering that each spectrum entering this calculation displayed Raman shift at 1663 cm^{-1} of PANI spectra with Raman intensity higher than 90 (a.u.). This region was completely different from that of unmodified Graphene-SPEs.

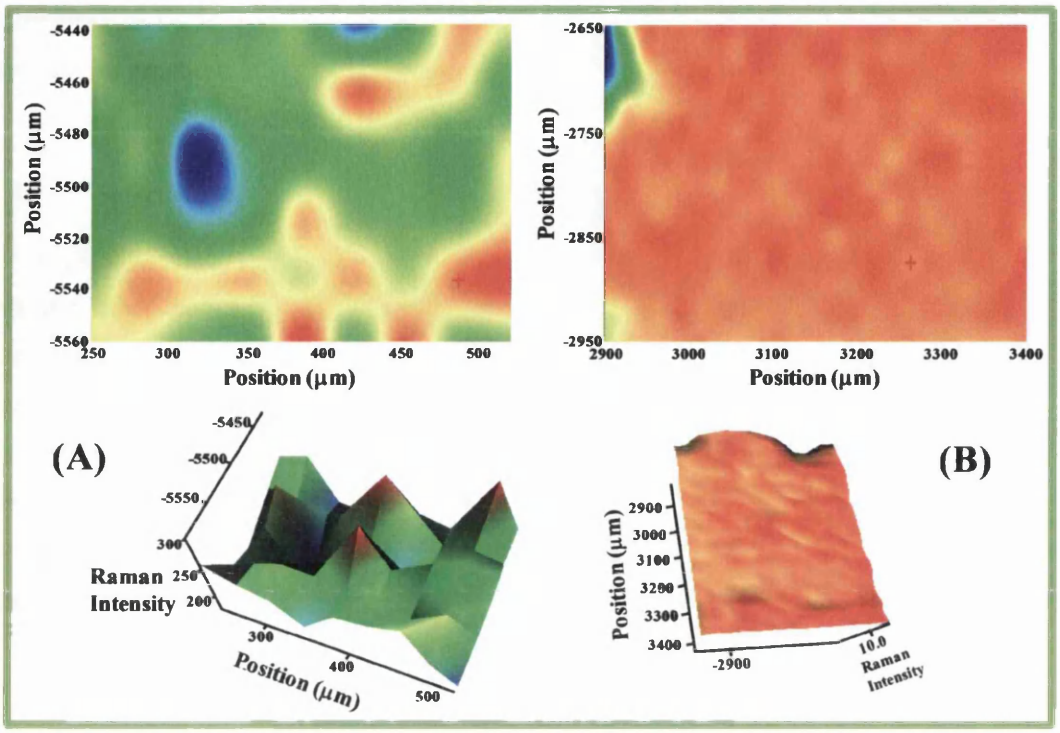

Figure 6.5 - Raman spectra mapping of the **(A)** PANI/Graphene-SPE and **(B)** anti-hCG/PANI/Graphene-SPE, along with the corresponding surface spatial distribution (bottom 3D graphics).

The colour coverage distribution map of Anti-hCG/PANI/graphene-SPE (B) was obtained in a similar way, considering this time the intensities of Raman peaks at 1484cm^{-1}, because this was not present in graphene. The anti-hCG coverage of the surface was 97%, extracted by spectral mapping of the Raman peaks at 1484cm^{-1} with intensities greater than 27%.

6.3.5 Analytical performance

Figure 6.2B shows the Nyquist plots of the immunosensor Ab/PANI/graphene-SPE against increasing hCG concentrations, while Figure 6.2D shows the corresponding EIS calibration curve, plotting Rct Ab/PANI/graphene-SPE against logarithm hCG concentration. The concentration range of hCG used for calibration was 0.01 and 5ng/mL. No diffusion-controlled effect was observed in EIS spectrum, and the diameter of the semicircle increased with increasing hCG concentrations.

The R_{ct} in the Nyquist plot, increased linearly with the increase of the logarithm of hCG concentration. This is as expected because protein structures bound to the surface of an electrode, typically act as barrier to electrical transfer. The average slope of the R_{ct} versus log[hCG] was 3.6kΩ/[hCG, ng/mL] with an R^2 correlation coefficient of 0.98. The limit of detection (LOD) was

determined as 0.286pg/mL. This represents a significantly lower detection limit than previously reported for graphene and anti-hCG sensors.

6.3.6 Selectivity of the sensor

Typically, selectivity is assessed by evaluating the effect of compounds present in the test solution, other than the target analyte (hCG), on the analytical response of a sensor device. To simulate the effect of real biological conditions, and ascertain the effect of urine on the performance of the sensor, the immunosensor was exposed to solutions of synthetic urine spiked with hCG. The selectivity of the sensor was thus investigated by monitoring its response to the synthetic urine. The synthetic urine was prepared according to recipes from [38] and contained creatinine, magnesium chloride, calcium chloride, sodium dihydrogen phosphate, ammonium chloride, potassium sulphate and sodium chloride.

The EIS calibration curve of the immunosensor in response to increasing concentrations of hCG in synthetic urine (Figure 6.6), was very similar to that of the sensor in PBS (Figure 6.2). Thus, no interference to the sensor, related to synthetic urine, was observed. This suggests that the sensor would be capable of selective and specific detection of hCG in real urine samples. The calibration curve was made for hCG concentrations ranging from 0.001 to 100ng/mL, showing a linear dependence with log[hCG] from 0.001 to 50ng/mL, with a slope of 14.8kΩ/[hCG, ng/mL].

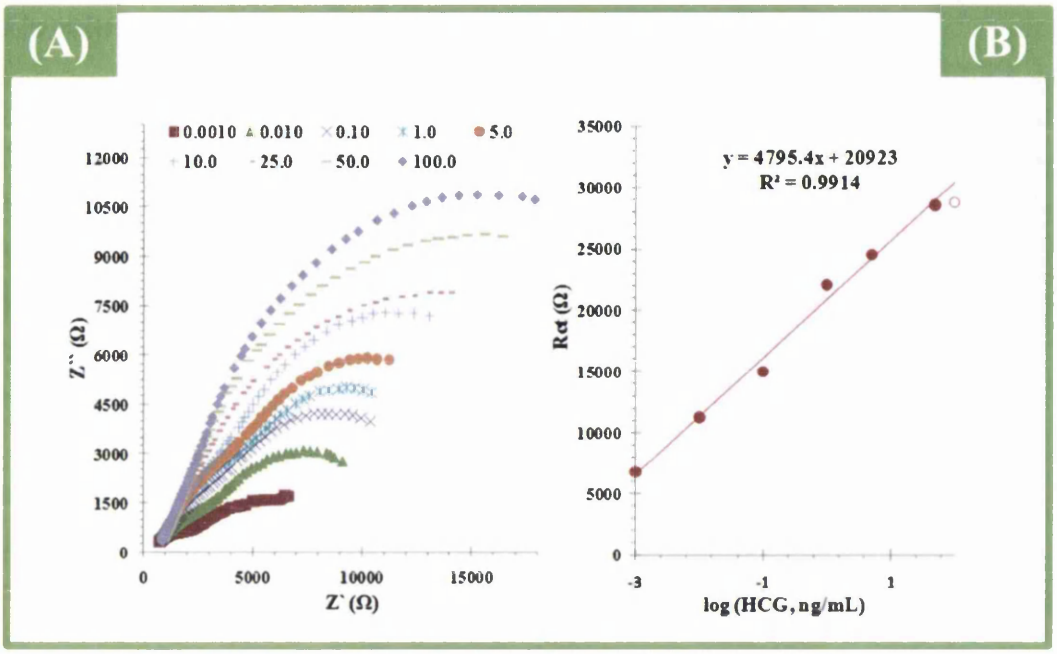

Figure 6.6 - Calibration curve of the immunosensor in real urine. **(A)**: Nyquist plots of BSA/anti-hCG/PANI/Graphene-SPE sensor, in 5.0 mM $[Fe(CN)_6]^{3-/4-}$ synthetic urine pH 6.5, previously incubated in increasing concentrations of hCG. **(B)**: R_{ct} values extracted from the Nyquist plots, against log hCG concentration.

6.3.7 Application to urine samples

The values of hCG in real urine samples were determined by EIS measurements after calibration of the Ab/PANI/graphene-SPE device. The Nyquist plots obtained are shown in Figure 6.6 A, along with the corresponding calibration curve (Figure 6.6B). The sensor exhibited linear behaviour from log [0.001 to 100 (ng/mL)], when the standard hCG solutions were prepared in urine of non-pregnant women. When identical sensor Ab/PANI/graphene-SPE was tested using urine of pregnant woman, the obtained concentration was 63ng/mL (315mIU/mL), which corresponded to a pregnancy period lying within 4 weeks to 5 weeks, which is also in agreement with the patients term of pregnancy status. The format of the R_{ct} curve was close to that of the standards (Figure 6.6A), suggesting that the system was operating well when applied to real sample conditions.

6.4. Conclusions

In summary, a new impedimetric biosensor for hCG has been fabricated based on antibody–antigen binding to a PANI-modified screen-printed graphene electrode. In this work, it has been shown that polyaniline was successfully deposited on graphene-SPE. The simple approach for antibody binding, enabled attachment of the antibody to the PANI sensing layer, and provided excellent reproducibility and stability. The electrode impedance increased linearly with increasing log hCG protein concentration and was not significantly affected by interference from chemical components present in synthetic urine.

Overall, PANI modified graphene may also be a promising sensing platform for assembling other immunosensing devices for detection of other biomarkers. The sensor has been used to successfully detect hCG concentrations in the urine of pregnant women, the results of which concur with the pregnancy status. The presented results the accuracy and precision of the analytical data from the Antibody/PANI modified graphene sensors proposed in this work, suggest that these sensors may be used in POC diagnostics in the near future.

References

[1] J. Wu, Z. Fu, F. Yan and H. Ju, *TrAC Trends Anal. Chem.*, 2007, **26**, 679–688

[2] P. Martin, *Materials Today*, 2011, **14**, 308-315.

[3] G. Liu, Y. Lin, *Talanta*, 2007, **74**, 308-317.

[4] S. Sánchez, M. Roldán, S. Pérez and E. Fàbregas, *Anal. Chem.*, 2008, **80**, 6508–6514.

[5] N. Liu and X. Guo, NPG Asia Materials, 2012, **4**, e23, doi:10.1038/am.2012.42.

[6] A. Plume, *Research Trends*, 2010, **18**, 5-7.

[7] Y. Li, L. Tang, J. Li, *Electrochem. Commun.*, 2009, **11**, 846-849.

[8] J. Li, S. Guo, Y. Zhai, E. Wang, *Electrochem. Commun.*, 2009, **11**, 1085–1088.

[9] D. Li, M. B. Muller, S. Gilje R. B., Kaner and G. G. Wallace, *Nat. Nanotechnol.*, 2008, **3**, 101-105.

[10] Q. Wei, R. Li, B. Du, D. Wu, Y. Han, Y. Cai, Y. Zhao, X. Xin, H. Li and M. Yang, *Sens. Actuat. B-Chem,* 2011, **153**, 256-260.

[11] R. McCreery, *Chemical reviews*, 2008, **108**, 2646-2687.

[12] M. Li, R. Li, C. Li and N. Wu, *Front. Biosci.* , 2011, **3**, 1308-1331.

[13] Y. Shao, J. Wang, H. Wu, J. Liu, I. A. Aksay and Y. Lin, *Electroanal.*, 2010, **22**, 1027-1036.

[14] T. Kuila, S. Bose, P. Khanra, A. Mishra, N. Kim and J. Lee, *Biosens Bioelectron.*, 2011, **26**, 4637-4648.

[15] F. Zhang, X. Chen, R. A. Boulos, F. Md Yasin, H. Lu, C. Raston and H. Zhang, *Chem. Commun.*, 2013, **49**, 4845-4847.

[16] H. K. Hassan, N. F. Atta and A. Galal, *Int. J. Electrochem. Sci*, 2012, **7**, 11161-11181.

[17] Y. Wang, Z. Li, J. Wang, J. Li and Y. Lin, *Trends Biotech.*, 2011, **29**, 205-212.

[18] T. K. Lim and T. Matsunaga, *Biosens. Bioelectron.*, 2001, **16**, 1063-1069.

[19] J. Lu, S. Liu, S. Ge, M. Yan, J. Yu,, X. Hu, *Biosens. Bioelectron.*, 2012, **33**, 29-35.

[20] Q. Wei, R. Li, B. Du, D. Wu, Y. Han, Y. Cai, Y. Zhao, X. Xin, H. Li, M. Yang, *Sens. Actuat B*, 2011, **153,** 256-260.

[21] D. Wu, Y. Zhang, L. Shi, Y. Cai, H. Ma, B. Du, Q. Wei, *Electroanal.* 2013, **25**, 427 – 432.

[22] R. Li, D. Wu, H. Li, C. Xu, H. Wang, Y. Zhao, Y. Cai, Q. Wei, B. Du, *Anal. Biochem.*, 2011, **414**, 196–201.

[23] S. Bhadra, N. K. Singha and D. Khastgir, *J. Chem. Eng. Mat. Sci.*, 2011, **2**, 1-11.

[24] Z. L. Wang, R. Guo, G. R. Li, H. L. Lu, Z. Q. Liu, F. M. Xiao, M. Zhang and Y. X. Tong, *J. Mat. Chem.*, 2012, **22**, 2401-2404.

[25] D. Li, J. Huang and R. Kaner, *Accounts Chem. Res.*, 2009, **42**, 135-145.

[26] Z. Zheng, Y. Du, Q. Feng and Z. Wang and Chunming Wang, *J. Mol. Cat. A-Chem.*, 2012, **353-354**, 80-86.

[27] H. D. Tran, D. Li and R. B. Kaner, *Adv.Mat.*, 2009, **21**, 1487-1499.

[28] Y. Liu, R. Deng, Z. Wang andH. Liu, *J. Mater. Chem.*, 2012, **22**, 13619-13624.

[29] K. Jiang, L.S. Schadler, R. W. Siegel, X., Zhang, H. Zhang and M. Terrone, *J. Mat. Chem.*, 2004, **14**, 37-39.

[30] J. Daniels and N. Pourmand, *Electroanal.*, 2007, **19**, 1239-1257.

[31] S. S. Srinivasan and P. C. Sharma, Development of Novel Polymer Nanostructures and Nanoscale Complex Hydrides for Reversible Hydrogen Storage, Chapter 1 in *Hydrogen Storage*, J. Liu Editor, ISBN 978-953-51-0731-6, InTech, 2012 2012.

[32] N. Carrillo, U. León-Silva, T. Avalos, M. Nicho, S. Serna, F. Castillon, M. Farias and R. Cruz-Silva, *J. Colloid Interf. Sci.*, 2012, **369**, 103-110.

[33] J. Chen, J. Yang, X. Yan, Q. Xue, *Synthetic Met.*, 2010, **160**, 2452-2458.

[34] M. Trchová and A. J. Stejskal, *Pure Appl. Chem.*, 2011, **83**, 1803-1817.

[35] D. C. Elias, R. R. Nair, T. M. G. Mohiuddin, S. V. Morozov, P. Blake, M. P. Halsall, A. C. Ferrari, D. W. Boukhvalov, M. I. Katsnelson, A. K. Geim, K. S. Novoselov, *Science*, 2010, **323**, 610-613.

[36] J. Ding, M. Wang, X. Yan, X. Zhang, C. Ran, H. Chen, X. Yao, *J. Colloid Interf. Sci.*, 2013, **395**, 40-44.

[37] E. B. Barros, K. Sato, G. G. Samsonidze, A. G. Souza Filho, M. S. Dresselhaus, and R. Saito, *Phys. Rev. B*, 2011, **83**, 245435, pp. 8, DOI: 10.1103/PhysRevB.83.245435.

[38] H. Haddad, *Synthetic urine for use in urine assay kits used for medical identification of illness or drug abuse, comprises a synthetic urine formulation and a heat activator,* Patent Number: US2004077106-A1 (2004); US7109035-B2 (2006).

CHAPTER 7[4]

"What distinguishes us from others is not what we are given, is what we can do with what we have"

Nelson Mandela (1918-2013), South African Politician

SWCNT Screen-printed electrode as immunosensor for human chorionic gonadotropin

This work reports electrochemical oxidation procedures for CNTs, yielding hydroxyl functional groups and the subsequent attachment of APTES followed by oriented Ab attachment. This is applied herein to hCG detection, by using an anti-hCG antibody as a biological receptor. Several immunosensing devices for hCG have been reported in the literature so far [1-5] but simple and low cost procedures are still needed for the routine POC determination of this biomarker. Considering that an immunosensor is not reusable and that the antibodies are expensive and need special storage conditions, it is very important to establish simple, low cost and rapid detection procedures, both at the stage of biosensor development.

The electrochemical analytical approach selected was EIS, because it enabled label-free, low cost and quick analytical measurements. EIS detection method was used to plot the calibration curve for CNT sensor. These curves were than used for determination of the detection limit range and selectivity of the sensor. The sensor device has been used to successfully detect hCG in the urine of pregnant women.

[4] Sofia Teixeira, Robert Steven Conlan, O. J. Guy, M. Goreti F. Sales, SWCNT Screen-printed electrode as an immunosensor for human chorionic gonadotropin, Electrochimica Acta, under review.

7.1 Introduction

Immunosensors are widely used in clinical applications and consist of an Ab, immobilized on a suitable support, which is capable of selective detection of a specific antigen. In general, a gold support coupled with an electrochemical transduction detection method is the most common format for electrochemical immunosensors reported in the literature [6]. Carbon nanostructured materials are also employed over the gold layer, mostly in the form of carbon nanotubes [7-15]. This may consist of single-wall (SWCNTs) or multiwall (MWCNTs) compositions [7-10]. CNTs are biocompatible with natural biomolecules [16], have lower cost than gold and display excellent electronic properties [10, 11]. The use of CNTs as electrode support is not however a common choice - with relatively few reports of CNT based biosensor [6, 7, 17, 18], due to the highest complexity of the process. Despite this, advantages in terms of electrical response would be expected for CNT electrodes compared with gold – related to the increased surface area of such electrodes.

In addition to the sensor electrode, the Ab is also a critical component of an immunosensor. It is a naturally produced protein, composed of four chains: two identical "heavy" and two identical "light" polypeptide chains, which together form a "Y-shaped" conformation. The arms of the Y-shaped molecule are the antigen binding fragments (F_{ab}), and the vertical portion is called the fragment-crystallisable (F_c) region. When an Ab is randomly attached to a conductive support, it may adopt four possible orientations: F_c attached to the support, F_{ab} attached to the support, one F_c and one F_{ab} attached to the support, or all three fragments attached to the support [19] (see Chapter 2 section 2.4.1). The actual orientation of the antibodies on the surface may indeed comprise of a combination of these four positions. As the active sites of the antibody are on the F_{ab} segment, the ideal orientation of the immobilized antibody is when the F_c fragment binds to the adsorbent substrate surface and the F_{ab} is oriented so that it is exposed to the analyte solution [19]. Thus, this oriented Ab immobilization is expected to yield an analytical improvement of the final immunosensor over sensors using randomly oriented Abs.

There are few reported strategies related to the oriented immobilization of antibodies to solid supports. Feng *et al.* reported an affinity ligand fused to the N/C-terminus of chimeric antigen for site-oriented immobilization, which resulted in significant enhancement of the analytic signal [20]. Rosales-Rivera *et al.* reported the oriented immobilization of antibodies on surfaces of gold, achieved using a carboxylic-terminated bipodal alkanethiol that is covalently linked with amino groups of the antibody's F_{ab} fragments [21].

Here binding an activated Ab to a carbon support requires that the support is modified to yield an amine terminated surface. The use of amine terminated organosilanes as amine-surface

modifiers is among the most common approaches to amination [22-24]. Here, the silane group binds to silicon or glass substrates [25] where vicinal hydroxyl groups may be found. In practice, CNTs are not normally hydroxyled, but these hydroxyl groups may exist as defects in the carbon matrix or may be intentionally added by chemical or electrochemical modification.

3-triethoxysilylpropylamine (APTES) is the most commonly used organosilane for producing amine terminated surfaces and immobilizing different entities of biological interest on various substrates [30-37]. APTES has a terminal primary amine and three ethoxy groups *per* molecule bonded to the Si atom. These ethoxy groups can polymerize in the presence of water, which can give rise to different surface coverages: covalent attachment, two-dimensional self-assembly (horizontal polymerization), and multilayers (vertical polymerization). The resulting structure and coverage of the layers are highly dependent on several experimental parameters, including temperature [38] and humidity [36, 39]. The simplest route yields a single aminopropylsilane layer having amine-terminal groups on the modified surface (Figure 7.1).

Figure 7.1 – APTES functionalization reaction.

7.2 Experimental Section

7.2.1 Materials and Reagents

All chemicals used were of analytical grade and water was de-ionized. Potassium hexacyanoferrate III ($K_3[Fe(CN)_6]$) and potassium hexacyanoferrate II ($K_4[Fe(CN)_6]$) trihydrate and magnesium chloride were obtained from Riedel Haen; 3-Triethoxysilylpropylamine (APTES) was obtained from VWR; N-Hydroxysuccinimide (NHS) and creatinine was obtained from Fluka; *N*-(3-Dimethylaminopropyl)-*N'*-ethylcarbodiimide hydrochloride (EDAC) and Bovine serum albumin (BSA) were obtained from Sigma; Phosphate Buffered Saline (PBS) Tablets were obtained from Amresco. hCG protein was purchased from Abcam (UK). Anti-hCG antibody was supplied by Ig Innovations. Ammonium chloride and calcium chloride were

obtained from Merck. Sodium dihydrogen phosphate was obtained from Scharlau. Potassium sulphate and sodium chloride were obtained from Panreac.

A solution of 0.5% (v/v) APTES (0.021M) prepared in D. I. water was employed. PBS solution was prepared by dilution of 1 tablet (1814.5-2005.5mg/tab) of PBS in 200mL of D. I. water. EDAC, NHS and antibody solutions were prepared in this buffer. Synthetic urine was prepared with creatinine ($5.3x10^{-6}$M), magnesium chloride ($9.8x10^{-7}$M), calcium chloride ($6.80x10^{-7}$M), sodium dihydrogen phosphate ($3.2x10^{-6}$M), ammonium chloride ($3.3x10^{-6}$M), potassium sulphate ($3.94x10^{-6}$M) and sodium chloride ($6.52x10^{-6}$M).

7.2.2 Apparatus

Electrochemical measurements were conducted using a potentiostat/galvanostat from Metrohm (Autolab PGSTAT302N), with Frequency Response Analysis (FRA) module, controlled by Nova software. CNT-SPEs were purchased from DropSens (DRP-110SWCNT), having a counter electrode of Platinum (Pt), a reference electrode of Ag/AgCl, and a 4 mm diameter CNT working electrode. The CNT-SPEs were interfaced with the potentiostat/galvanostat equipment by a switch box, also from DropSens (DRP-DSC). Raman measurements were performed using a Thermo Scientific DXR Raman microscope system with a 100 mW 532 nm excitation laser. Spectra were recorded using a 5mW power and 50μm pinhole aperture.

7.2.3 Surface modification

The surface of the CNT-SPE was modified first by electrochemical oxidation. The three-electrodes of the SPE were immersed in 0.5M of H_2SO_4 and cyclic voltammetry (CV) was performed by sweeping the potential from –0.2V to 1.5V, at a sweep rate of 50mV/s, for 20 cycles.

The CNT working electrode at the SPE was subsequently amine terminated, by reaction with 0.021mol/L of APTES in water. This reaction was performed at different temperatures (ambient and 120°C). In parallel, an antibody solution of 200μg/mL was mixed with 25mmol/L EDAC, and 50mmol/L NHS, for 2 hours. A drop of this solution was then placed on the amine-terminated SPE surface. After 2 hours at room temperature, the SPE was washed and exposed to Bovine Serum Albumin (BSA) solution (0.5mg/mL in PBS buffer), for 30 minutes. The immunosensor was subsequently washed with PBS buffer to remove any unbound BSA. The

resulting CNT surface is covered with the Ab and any amine sites unoccupied by the Ab are blocked with BSA.

7.2.4 hCG Binding

hCG binding to the antibody functionalised immunosensor was performed by placing a drop of hCG solution on to the Ab functionalized SPE sensor surface. Solutions of different concentrations of hCG were prepared by dilution of a standard hCG solution (25ng/mL) in PBS or synthetic urine, to yield solutions with concentrations ranging from 0.01 to 100ng/mL. In addition, a sample of real urine from a pregnant volunteer was tested for its hCG content. A period of 15 minutes was allowed for antigen/antibody binding. This was followed by PBS washing prior to redox probe EIS measurements.

7.2.5 Electrochemical assays

CV measurements were conducted in 5.0mmol/L of $[Fe(CN)6]^{3-/4-}$, prepared in PBS buffer (pH 7.4). In CV assays a potential sweep from -0.7V to +0.7V, at 50mV/s was used. All assays were conducted in triplicate.

EIS assays were also conducted in triplicate with the same redox couple $[Fe(CN)6]^{3-/4-}$ at a standard potential of +0.10V, using a sinusoidal potential perturbation with an amplitude of 100mV and a frequency equal to 50Hz, logarithmically distributed over a frequency range of 100000Hz-0.1Hz. The impedance data were fitted to a Randles equivalent circuit using the Nova Software.

The immunosensor response to varying hCG concentrations was assessed by EIS measurements after incubating the biosensor in hCG solutions for 15 minutes, with hCG concentrations ranging from 0.01 to 100ng/mL, prepared either in PBS buffer pH 7.4 or in synthetic urine pH 6.8. The limit of detection (LOD) was calculated using the interception of the linear range slope with the non-linear range.

7.3 Results and discussion

7.3.1 Principle of the immunosensor

The CNT surface of the working electrode was first modified by an electrochemical oxidation. This procedure is intended to generate hydroxyl groups (Figure 7.2A), although it may also produce carbonyl and carboxylic functions. Hydroxyl groups are produced in the initial stages of carbon oxidation and only these are relevant for this work as they are involved in the covalent binding to silane groups.

The next stage of the CNT functionalisation was the silanization with APTES (Figure 7.2B), where the ethoxy groups of APTES was expected to react with the hydroxyl groups within the oxidized CNT matrix. This reaction yielded a covalent bond (C – Si) between APTES and the CNTs.

The next stage in the immunosensor fabrication was Ab binding to the amine-terminated surface (Figure 7.2C). The Ab was bound to the CNT support, only after activating the carboxylic functions located at the F_c terminal via EDAC and NHS chemistry (see Chapter 2, section 2.4.1.1). The initial step of this transformation was the reaction of the F_c carboxylic group with the carbodiimide function of EDAC, thereby forming an O-acylisourea intermediate. This intermediate is formed rapidly and subsequently reacts with the surface amine to form an amide bond [40]. Unbound Ab was later removed from the SPE working area by thorough washing with PBS pH 7.4.

The above chemical activation of the Ab contributed to its ordered orientation on the CNT sensing surface. Thus, the Ab was attached to the CNT material through its F_c region, leading to free F_{ab} sites projected towards the aqueous solution. However, because all –COOH groups on the Ab were exposed to the reagents EDAC/NHS, all –COOH groups at the external surface of the Ab protein may have been activated. Consequently, it is not possible to ensure that all Ab proteins were bound through the F_c terminal, but the probability of achieving the desired F_c attached orientation using this approach, is significantly higher than with random Ab adsorption. In addition, covalent binding is also more stable than adsorption, especially considering that the final surface will be incubated in complex solutions for a significant amount of time (more than 10 minutes).

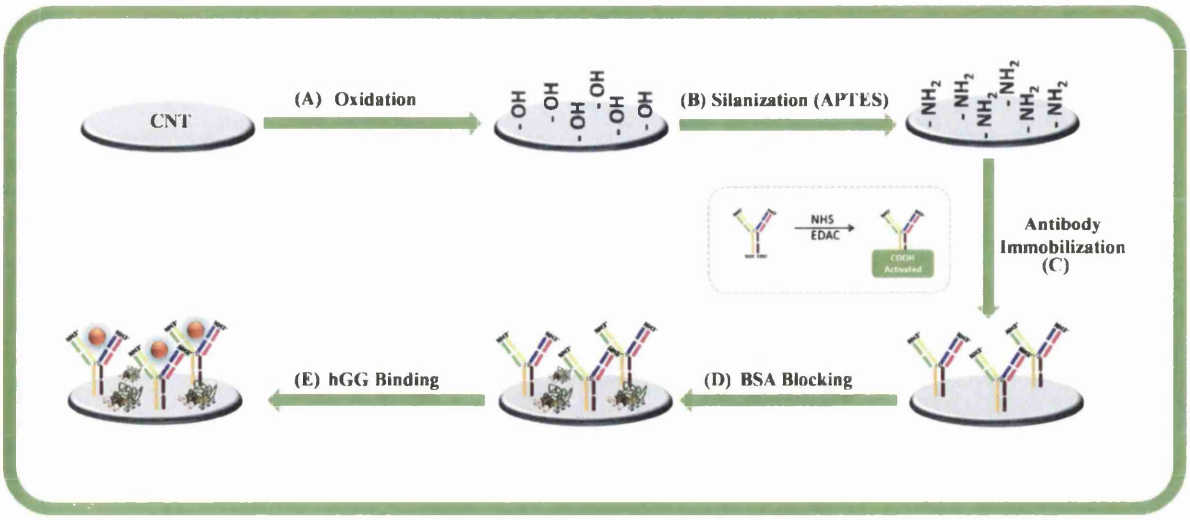

Figure 7.2 - Fabrication of the immunosensor assembly.

The final stage of the assembly consisted in blocking non-specific binding sites, such as free surface amine groups and carboxylic functions that remained activated. This was done by adding a simple and low-cost protein (BSA) to the sensor surface (Figure 7.2D). Overall, this procedure contributed to enhance the selectivity/specificity of the biosensor, eliminating its non-specific responses.

7.3.2 Control of the surface modification by voltammetry and impedance measurements

The chemical modification of the CNT-SPE was controlled by measuring the changes in the electron transfer properties of the SPE relative to a $[Fe(CN)6]^{3-/4-}$ redox probe. This was characterised using CV and EIS experiments (Figure 7.3).

The typical CV data obtained at every stage of chemical modification process is shown in Figure 7.3A. In general, each step of CNT-SPE modification increased the potential separation of the $Fe^{3+/2+}$ redox probe. This increase in peak-to-peak potential separation was correlated to a decrease in the reversibility of the iron oxidation/reduction, which accounted for an increased resistance to the charge-transfer process across the CNT-SPE. This behaviour was expected, as each new layer binding to the conductive electrode surface limits electron transfer accross the non-modified CNT. The more layers or the thicker the layer, the more limited the electron transfer will be.

The EIS spectra corresponding to each stage of chemical modification are shown in Figure 7.3B. All EIS plots contain a semicirclar portion lying on the real axis at higher frequencies that tends to become almost a constant value at lower frequencies. This is the typical behaviour of a

Randle's equivalent circuit, composed of the resistance of the solution phase (R_S), the capacitance of the double layer (C_{dl}), the charge-transfer resistance (R_{ct}) and the Warburg diffusion element (W) from the bulk solution to the electrode interface. The diameter of the semicircle equals R_{ct}, and this resistance controls the electron transfer kinetics of the redox probe at the electrode interface [41]. In general, the resistance to charge transfer increased after each chemical modification, which was fully consistent with the CV data.

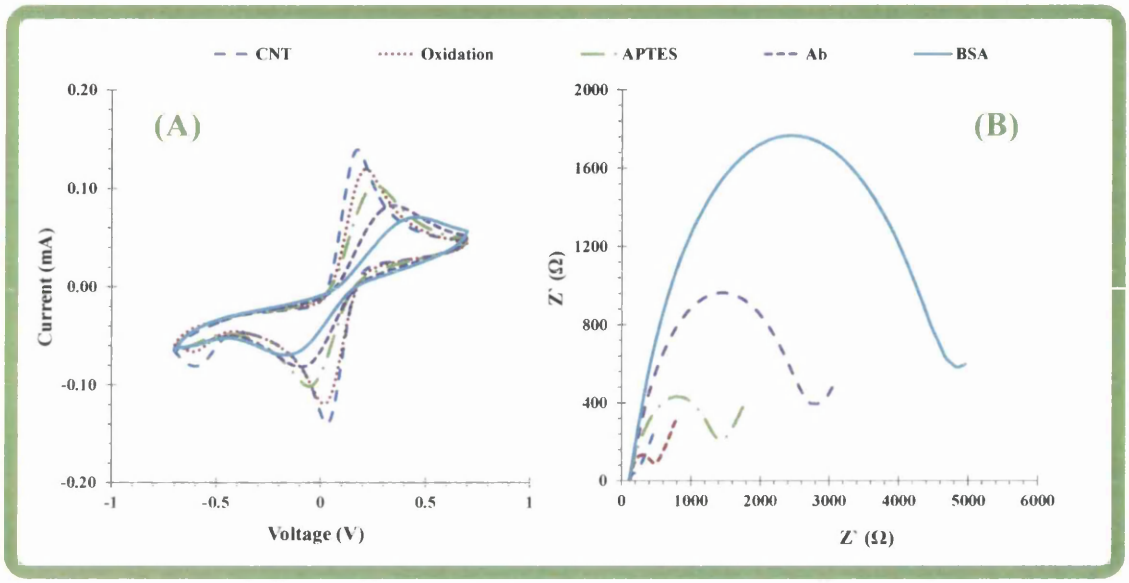

Figure 7.3 - (A) CV records after modification of APTES/CNT-SPE with antibody and BSA; **(B)** Nyquist plots of BSA/anti-hCG/APTES/CNT-SPE sensor obtained in 5.0 mM $[Fe(CN)6]^{3-}$/5.0 mM $[Fe(CN)6]^{4-}$/PBS buffer pH 7.4;

7.3.3 Raman analysis

Raman spectroscopic assays were performed after each stage of the immunosensor assembly. The Raman spectra of clean SPE-CNT, SPE-CNT/APTES and SPE-CNT/APTES/Ab are presented in Figure 7.4.

The spectra of the CNT area showed three Raman bands at 1350, 1590 and 2670 cm^{-1} that were assigned to D, G and G` bands, commonly present in the Raman spectra of CNTs. The D band indicates disorder, corresponding to sp^3-hybidized carbon atoms, while the G band reflects the structural integrity of the sp^2-hybridized carbon atoms of the nanotubes, corresponding to the stretching mode in the graphite plane [42]. The ratio between the Raman intensity of D and G bands is thus a good indicator of the extent of carbon-containing defects among the CNTs [42].

Comparing the SPE-CNT and SPE-CNT/APTES spectra, a slight increase was observed in the intensity of the D peak compared to that of the G peak of the APTES modified CNT, accounting for the introduction of structural defects to the carbon electrode. The corresponding ratios IG/ID were 0.62 and 0.67, respectively. The observed ratio change was not very significant, but the surface of the CNT electrode was modified, while the Confocal Raman analysed all the CNT material present at the electrode. Comparing the SPE-CNT/APTES and SPE-CNT/APTES/Ab spectra, a similar observation was found because the IG/ID ratio was 0.67 and 0.5 respectively.

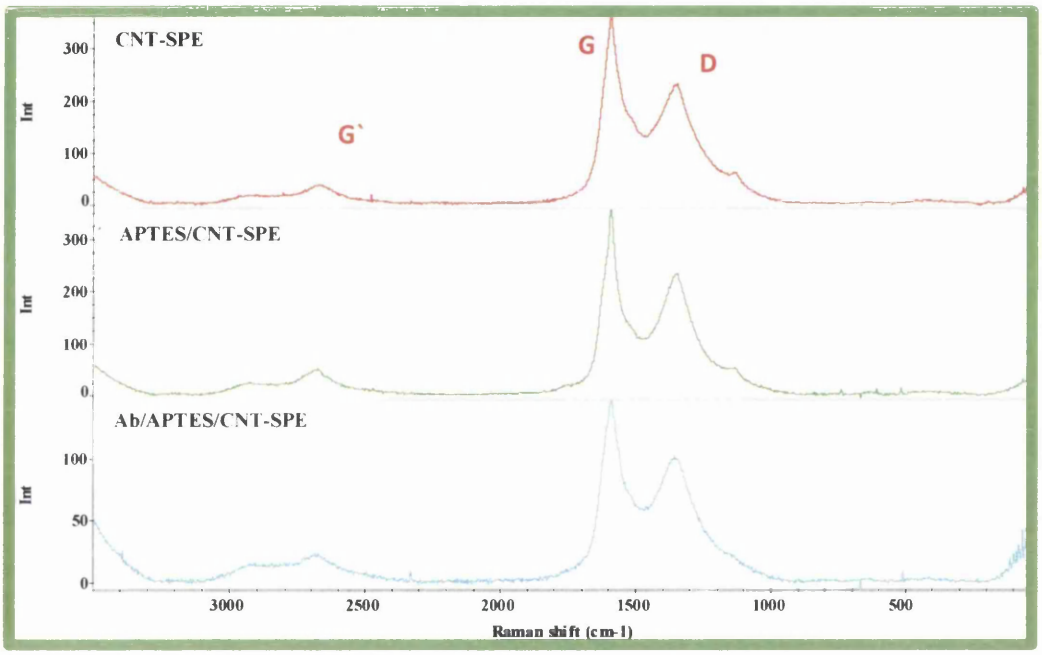

Figure 7.4 - Raman spectra of CNT-SPE, APTES/CNT-SPE, and anti-hCG/APTES/CNT-SPE.

Overall, the intensity changes within the Raman spectra of clean CNT and modified CNT were small, but confirmed the increased chemical disorder of the carbon sp^2 matrix, due to chemical modification of the carbon layer with APTES and anti-hCG.

7.3.4 Analytical performance of the sensor

Figure 7.5A shows the Nyquist plots of the immunosensor SPE-CNT/APTES/Ab incubated in increasing concentrations of hCG. The solutions of hCG used for calibrating the immunosensor ranged from 0.01 to 100ng/mL and these solutions were prepared in PBS. The corresponding calibration curve was plotted as R_{ct} (extracted from the Nyquist plots) against the

logarithm of the hCG concentration (inset of Figure 7.5A). From Figure 7.5A (inset), Rct increases linearly with the logarithm of concentration, over the 0.01 to 100ng/mL range. The average slope was 0.96kΩ/decade of hCG concentration and the square of the correlation coefficient was 0.9826, with a limit detection of 0.01ng/mL. For concentrations higher than 25ng/mL, the impedance became constant, indicating saturation.

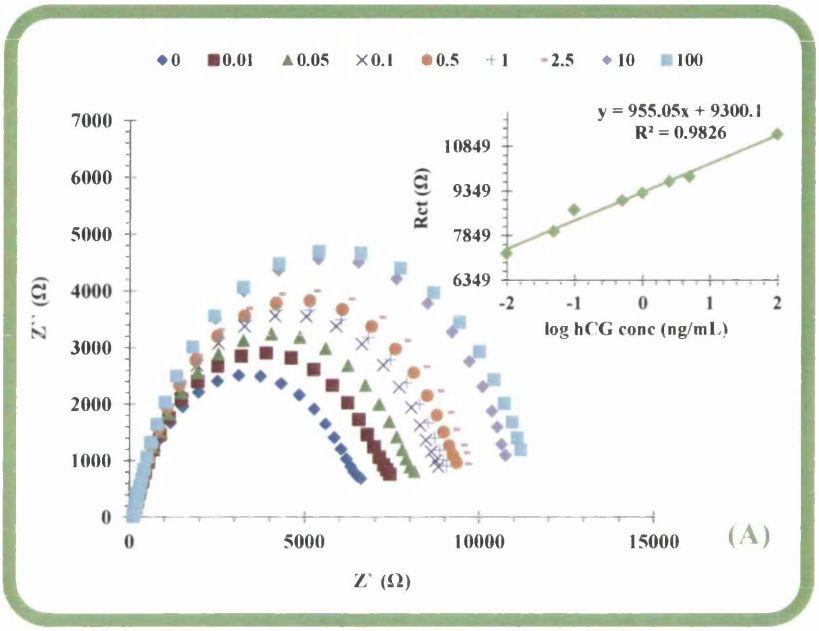

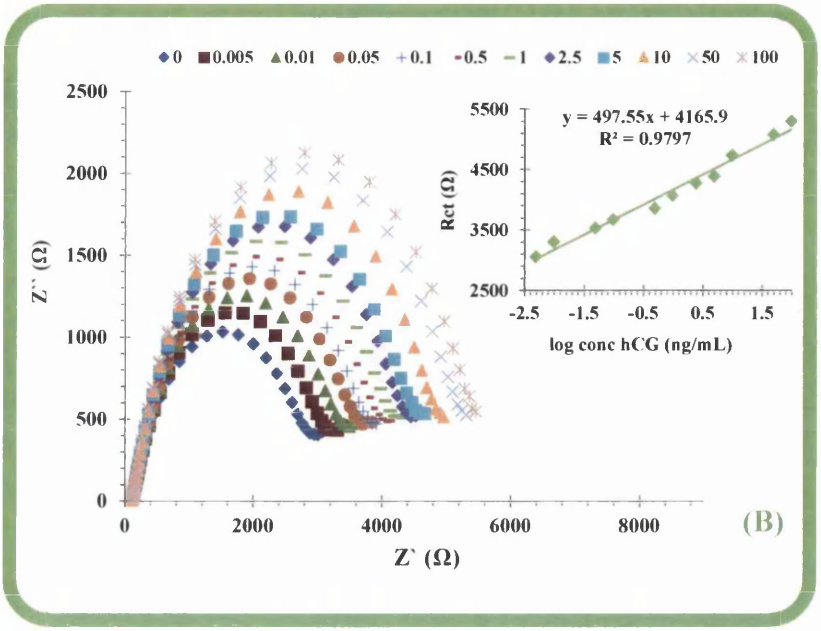

Figure 7.5 - Calibration curve of the immunosensor in PBS **(A)** and in synthetic urine **(B)**. Nyquist plots correspond to BSA/anti-hCG/APTES/CNT-SPE sensor, in 5.0 mM $[Fe(CN)6]^{3-/4-}$ PBS buffer pH 6.5, previously incubated in increasing concentrations of hCG. Inset is the Rct values extracted from the Nyquist plots against log hCG concentration.

7.3.5 Selectivity of the sensor

The selectivity of the immunosensor was investigated by assessing its response to hCG in a synthetic urine background. This approach of using a complex mixture of potentially interfering compounds was performed in order to determine the taken sensor's selectivity to hCG and study non-specific binding in a realistic biological environment. The synthetic urine used in this study was prepared as indicated in [43] and contained creatinine, magnesium chloride, calcium chloride, sodium dihydrogen phosphate, ammonium chloride, potassium sulphate and sodium chloride. Concentrations of each component used were similar to those found in real urine.

Figure 7.5B shows the Nyquist plots obtained by calibrating the immunosensor in increasing concentrations of hCG prepared in synthetic urine. Linear responses were observed from log [0.005 to 100 (ng/mL)], with a slope of 0.497kΩ/decade hCG concentration. Compared to the calibration in PBS, the sensitivity in synthetic urine was slightly decreased, but the Limit of Detection and the upper concentration limit improved. No interference in the sensor was observed, suggesting its successful application in real urine samples.

7.3.6 Application to urine samples

Values of hCG in real urine samples were determined by EIS measurements after calibration of a new SPE-CNT/APTES/Ab device with solutions of hCG prepared in real urine without hCG (nonpregnant women). This provided a calibration procedure very close to the real conditions in which a commercial sensor would be used. The resulting Nyquist plots showed a linear behaviour from log [0.01 to 1.0 (ng/mL)], as indicated in Figure 7.6, with a slope of 0.129kΩ/decade hCG concentration.

The analysis of real urine samples from the pregnant volunteer used a new biosensor prepared under identical conditions to the calibration sensor. The calibration sensor itself cannot be used as the electrical response to the calibration procedure was a result of irreversible antigen/Ab binding – thus consuming this particular sensor. The analysis of urine from pregnant woman generated Nyquist plots with similar profiles to those generated with standard solutions prepared in PBS or synthetic urine. The hCG concentration extracted from the measurement on the real urine of the pregnant volunteer was 1.0ng/mL (5mIU/mL), which is indicative of pregnancy of between 3 to 4 weeks. This was in agreement with pregnancy status of the patient.

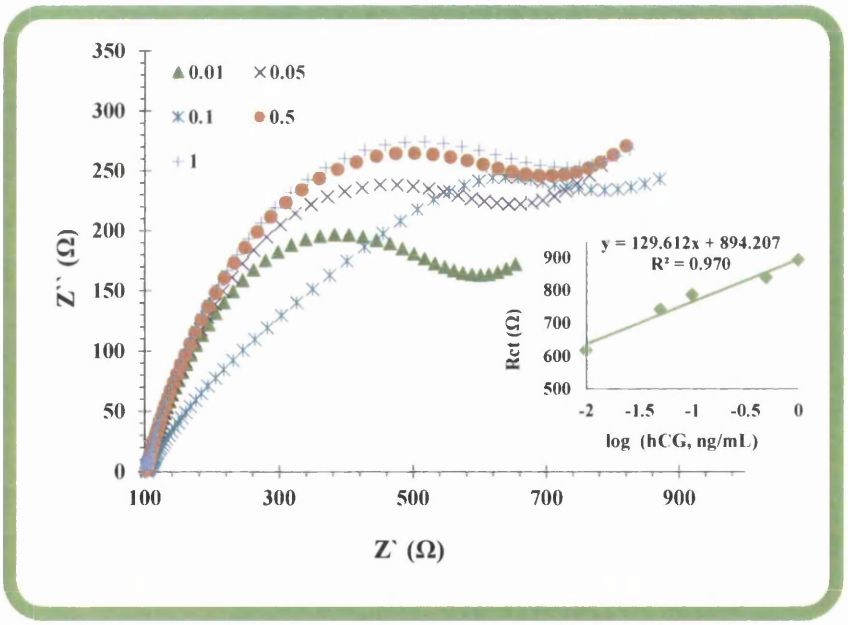

Figure 7.6 - Calibration curve of the immunosensor in real urine. Rct values extracted from the Nyquist plots against log hCG concentration.

7.4 Conclusions

A new immunosensor for hCG has been fabricated, based on Ab/antigen binding to an APTES modified SPE electrode of CNT layer. It uses a simple approach for oriented antibody binding, yielding a sensor with a limit of detection of 0.01ng/mL.

The sensitivity of the biosensor decreased marginally in the presence of a complex background solution in the order (PBS > synthetic urine > real urine). However, non-specific binding effects were negligible and the background solution had little impact on the sensor's feasibility as an hCG diagnostic. The biosensor was used to successfully detect hCG concentrations in the urine of a pregnant volunteer, with similar performance to hCG detection in standard solutions of PBS or in synthetic urine. Overall, the analytical performance of the biosensor suggests its successful application as a point-of-care diagnostic.

References

[1] Teixeira, S., et al., *Epitaxial graphene immunosensor for human chorionic gonadotropin.* Sensors and Actuators B: Chemical, 2014. 190.

[2] Yang, H., et al., *Electrochemically deposited nanocomposite of chitosan and carbon nanotubes for detection of human chorionic gonadotrophin.* Colloids and surfaces. B, Biointerfaces, 2011. 82(2): p. 463-469.

[3] Truong, L., et al., *Labelless impedance immunosensor based on polypyrrole-pyrolecarboxylic acid copolymer for hCG detection.* Talanta, 2011. 85(5): p. 2576-2580.

[4] Tao, M., et al., *The preparation of label-free electrochemical immunosensor based on the Pt-Au alloy nanotube array for detection of human chorionic gonadotrophin.* Clinica chimica acta; international journal of clinical chemistry, 2011. 412(7-8): p. 550-555.

[5] Chai, R., et al., *Amperometric immunosensors based on layer-by-layer assembly of gold nanoparticles and methylene blue on thiourea modified glassy carbon electrode for determination of human chorionic gonadotrophin.* Talanta, 2008. 74(5): p. 1330-1336.

[6] Huang, K.-J., et al., *A disposable electrochemical immunosensor for carcinoembryonic antigen based on nano-Au/multi-walled carbon nanotubes-chitosans nanocomposite film modified glassy carbon electrode.* Analytica chimica acta, 2010. 659(1-2): p. 102-108.

[7] Arben, M., et al., *New materials for electrochemical sensing VI: Carbon nanotubes.* TrAC Trends in Analytical Chemistry, 2005. 24.

[8] Rivas, G., et al., *Carbon nanotubes for electrochemical biosensing.* Talanta, 2007. 74(3): p. 291-307.

[9] Agüí, L., P. Yáñez-Sedeño, and J. Pingarrón, *Role of carbon nanotubes in electroanalytical chemistry: a review.* Analytica chimica acta, 2008. 622(1-2): p. 11-47.

[10] Gregory, G.W., et al., *Chemically Modified Carbon Nanotubes for Use in Electroanalysis.* Microchimica Acta, 2005. 152.

[11] Banks, C. and R. Compton, *Exploring the electrocatalytic sites of carbon nanotubes for NADH detection: an edge plane pyrolytic graphite electrode study.* The Analyst, 2005. 130(9): p. 1232-1239.

[12] Carla, G.-C., P. Rasa, and M.A.B. Christopher, *Development of electrochemical oxidase biosensors based on carbon nanotube-modified carbon film electrodes for glucose and ethanol.* Electrochimica Acta, 2008. 53.

[13] Guang-Chao, Z., et al., *Direct electrochemistry of cytochrome c on a multi-walled carbon nanotubes modified electrode and its electrocatalytic activity for the reduction of H2O2.* Electrochemistry Communications, 2005. 7.

[14] Yajing, Y., et al., *Immobilization and direct electrochemistry of cytochrome c at a single-walled carbon nanotube-modified electrode.* Journal of Solid State Electrochemistry, 2006. 11.

[15] Qiang, Z., G. Zhenhai, and Z. Qiankun, *Electrochemical Sensors Based on Carbon Nanotubes.* Electroanalysis, 2002. 14.

[16] Smart, S.K., et al., *The biocompatibility of carbon nanotubes.* Carbon, 2006. 44.

[17] Sánchez, S., et al., *Toward a fast, easy, and versatile immobilization of biomolecules into carbon nanotube/polysulfone-based biosensors for the detection of hCG hormone.* Analytical chemistry, 2008. 80(17): p. 6508-6514.

[18] Lu, J., et al., *Ultrasensitive electrochemical immunosensor based on Au nanoparticles dotted carbon nanotube-graphene composite and functionalized mesoporous materials.* Biosensors & bioelectronics, 2012. 33(1): p. 29-35.

[19] Wan, Y., et al., *Development of electrochemical immunosensors towards point of care diagnostics.* Biosensors & bioelectronics, 2013. 47C: p. 1-11.

[20] Bo, F., et al., *Site-oriented immobilization of fusion antigen directed by an affinity ligand, and its validation in an immunoassay.* Surface and Interface Analysis, 2011. 43.

[21] Rosales-Rivera, L., et al., *Electrochemical immunosensor detection of antigliadin antibodies from real human serum.* Biosensors & bioelectronics, 2011. 26(11): p. 4471-4476.

[22] Mansur, H., et al., *Biomaterial with chemically engineered surface for protein immobilization.* Journal of materials science. Materials in medicine, 2005. 16(4): p. 333-340.

[23] Murphy, A., P. St John, and D. Kaplan, *Modification of silk fibroin using diazonium coupling chemistry and the effects on hMSC proliferation and differentiation.* Biomaterials, 2008. 29(19): p. 2829-2838.

[24] Mansur, H., et al., *Surface functionalization of porous glass networks: effects on bovine serum albumin and porcine insulin immobilization.* Biomacromolecules, 2000. 1(4): p. 789-797.

[25] Kathryn, L.B., et al., *Direct oriented immobilization of F(ab') antibody fragments on gold.* Analytica chimica acta, 2003. 496.

[30] Smith, E. and W. Chen, *How to prevent the loss of surface functionality derived from aminosilanes.* Langmuir : the ACS journal of surfaces and colloids, 2008. 24(21): p. 12405-12409.

[31] Howarter, J. and J. Youngblood, *Optimization of silica silanization by 3-aminopropyltriethoxysilane.* Langmuir : the ACS journal of surfaces and colloids, 2006. 22(26): p. 11142-11147.

[32] Pasternack, R., S. Rivillon Amy, and Y. Chabal, *Attachment of 3-(Aminopropyl)triethoxysilane on silicon oxide surfaces: dependence on solution temperature.* Langmuir : the ACS journal of surfaces and colloids, 2008. 24(22): p. 12963-12971.

[33] El-Ghannam, A., et al., *Model surfaces engineered with nanoscale roughness and RGD tripeptides promote osteoblast activity.* Journal of biomedical materials research. Part A, 2004. 68(4): p. 615-627.

[34] Kim, J., et al., *Formation, structure, and reactivity of amino-terminated organic films on silicon substrates.* Journal of colloid and interface science, 2009. 329(1): p. 114-119.

[35] Weng, Y.J., et al., *Immobilization of bovine serum albumin on TiO2 film via chemisorption of H3PO4 interface and effects on platelets adhesion.* Applied Surface Science, 2008. 254.

[36] Lapin, N. and Y. Chabal, *Infrared characterization of biotinylated silicon oxide surfaces, surface stability, and specific attachment of streptavidin.* The journal of physical chemistry. B, 2009. 113(25): p. 8776-8783.

[37] Kim, J., et al., *Investigations of chemical modifications of amino-terminated organic films on silicon substrates and controlled protein immobilization.* Langmuir : the ACS journal of surfaces and colloids, 2010. 26(4): p. 2599-2608.

[38] Robert, H.B., et al., *Surface studies of hydroxylated multi-wall carbon nanotubes.* Applied Surface Science, 2012. 258.

[39] Oliver, S., et al., *Control and stability of self-assembled monolayers under biosensing conditions.* Journal of Materials Chemistry, 2011. 21.

[40]Jiang, K., Schadler, L.S., Siegel, R.W., Zhang, X., Zhang, H., Terrone, M., Journal of Materials Chemistry, 2004. 14: p. 37-39.

[41] Panagopoulou, M., et al., *Impedimetric biosensor for the assessment of the clotting activity of rennet.* Analytical chemistry, 2010. 82(20): p. 8629-8636.

[42] Costa, S., et al., *Characterization of carbon nanotubes by Raman spectroscopy.* Mater Sci Poland, 2008. 26(2): p. 433-441.

[43] Haddad, H., *Synthetic urine for use in urine assay kits used for medical identification of illness or drug abuse, comprises a synthetic urine formulation and a heat activator.*

CHAPTER 8

"After climbing a great hill, one only finds that there are many more hills to climb. I have taken a moment here to rest, to steal a view of the glorious vista that surrounds me, to look back on the distance I have come. But I can rest only for a moment, for with freedom comes responsibilities, and I dare not linger, for my long walk is not yet ended. "

Nelson Mandela (1918-2013), South African Politician

8.1 Conclusions and future perspectives

In this chapter general conclusions about this research and future perspectives for further development of this research area, are presented.

8.1.1 Conclusions

This thesis has presented new biosensing materials and platforms that may open new horizons for medical diagnostics, for non-invasive or minimally-invasive early screening of chronic diseases and rapid-screening in POC applications.

Electrochemical techniques used in this thesis are easily adaptable for diagnostic screening purposes, enabling simple and inexpensive detection of biomolecules, providing specific readings at low concentrations and using low sample volumes. Furthermore, the sensors developed offer portable detection, enabling tests at POC.

The work presented in this thesis was an investigation of the fabrication of a graphene device able to detect the presence of hCG. This fabrication involved a study of the epitaxial growth of graphene on 4H-SiC, a study of the surface functionalization, and electrical characterisation of the device. Note that these results are from a DC-I(V) measurements.

Table 8.1 – Epitaxial graphene results.

Sensor	Sensitivity kΩ/[hCG, ng/mL]	Range [hCG, ng/mL]	R^2	LOD [hCG, ng/mL]
Epitaxial graphene	0.142	0.62 - 5.62	0.9754	0.62

Epitaxial-graphene devices show clinical relevant detection capability and high specificity. These sensors could be optimized even further by using different attachment chemistry and improved device design (channel dimensions) and FET design, rather than a simple resistor.

To complement the study, other sensors using SPE were tested for hCG detection.

Electrochemical functionalized amine-terminated surfaces were subsequently used to attach anti-hCG. Using CV, EIS, I-V, Raman, FTIR, SEM, AFM and XPS, it was confirmed, that the anti-hCG antibody was covalently attached to the amine functional group.

An electrochemical sensor for hCG, an indicator of pregnancy – also linked to an increased risk factor for cancer – was fabricated using these functionalised graphene SPEs. Several approaches were used to functionalize and biofunctionalize graphene. The main results for each type of sensor are presented in the table below.

These results are provided by EIS, as opposed to the I(V) measurements performed on the epitaxial-graphene sensors. Therefore a direct comparison is not possible between the sensitivity/LOD.

Table 8.2 – Main experimental results of all the SPEs sensors.

Sensor	Sensitivity kΩ/log[hCG,ng/mL]	Range [hCG, ng/mL]	R^2	LOD [hCG, ng/mL]
Graphene-SPE/CS/AuNPs	0.129	0.1 - 25	0.9547	0.1
Graphene-SPE/PANI	3.58	0.001 - 5	0.9757	0.0003
CNTs	0.955	0.01 - 100	0.9826	0.01

All the developed sensors showed a good capacity to detect hCG and were revealed to be at least 30 times more sensitive than an ELISA test performed under the same conditions. Overall,

the analytical performance of the biosensors suggests its successful application as a point-of-care diagnostic for hCG.

Graphene-SPE/PANI showed the highest sensitivity and also the lowest LOD. This is suggested to be related to more efficient electron/charge transfer between the PANI and the graphene electrode – related to the π-π coupling of the aromatic rings of the PANI coupling with those of the graphene.

Graphene-SPE/CS/AuNPs is the least sensitive of the SPEs. This could be related to the fact that the preparation of this electrode involves an oxidation step – partially converting graphene to graphene oxide. This step is used to provide better adhesion of the chitosan to the graphene/graphene oxide. However, oxidation of graphene to graphene oxide would degrade the electrical performance of the SPE sensor and it is suggested that this may be the origin of the inferior sensitivity of the graphene-SPE/CS/AuNPs sensor relative to the PANI and CNT sensors.

CNTs also performed well with low LOD and a good range of detection. It is suggested that the CNT SPEs operate in a similar way to the graphene SPEs – with enhanced performance over carbon electrodes – due to the increased surface area.

The functionalization process for Graphene-SPE/PANI proved to be the simplest of the three SPE sensors.

This work introduced new technical innovations in the development of biosensors, both in terms of chemical (functionalization techniques) system configuration and assembly of the recognition element (attachment of antibodies to the graphene electrodes) for biomarker detection at POC. Further developments may be achieved for instance by modifying the detection antibody – in order to detect several other biomarkers.

8.1.2 Future perspectives

As with any kind of research work, a large number of questions and paths remain unanswered and unexplored. Based on the results presented herein and in recent literature regarding immunosensors, some recommendations for future work are suggested in this section.

One potentially existing development is the replacement of the Ab receptor with Molecular imprinted polymers (MIPs) that are polymeric structures designed to resemble natural antibodies. Enhancement of the selectivity of standard antibodies may be assessed by imprinting biomarkers using polymer chemistries and imprinting "plastic" antibodies compatible with

physiological conditions in order to preserve the appropriate protein conformation. They combine the high specificity and affinity of the antibodies with the robustness, low cost, long term stability, and reusability of the synthetic materials. For a successful MIP design, several variable parameters need to be optimized, such as the selection of the monomers, solvents, temperature and reaction time. The selection of suitable monomers is a critical step for the good performance of the imprint approach in terms of selectivity and specificity. The specificity depends of the exposed surface area of the MIP, its functionality and charge. This concept could be successfully applied to detection of a biomarker of clinical significance.

Furthermore, the developed biosensing devices, offering good analytical response, could be used to develop multi-analyte tests (multiplexing experiments to identify two or more different target biomarkers at the same time on the same sample).

Multiplex sensors and integrated detection of different biomarkers with micro-fluidics – in a point-of-care device performance is another area for development.

Response time and life time[5] of the sensors should also be studied in order to completely characterise the devices.

[5] Response time is defined as the time for a sensor to respond from zero concentration to a step change in concentration. Life time is defined as the length of time over which the sensor will operate.